Manipulation and Motion of Organelles and Single Molecules in Living Cells

Norregaard, Kamilla; Metzler, Ralf; Ritter, Christine M. ; Berg-Sørensen, Kirstine; Oddershede, Lene B.

Published in:
Chemical Reviews

Link to article, DOI:
10.1021/acs.chemrev.6b00638

Publication date:
2017

Document Version
Publisher's PDF, also known as Version of record

CHEMICAL REVIEWS

Review

pubs.acs.org/CR

Manipulation and Motion of Organelles and Single Molecules in Living Cells

Kamilla Norregaard,[†] Ralf Metzler,[‡] Christine M. Ritter,[¶] Kirstine Berg-Sørensen,[§] and Lene B. Oddershede*[,¶]

[†]Cluster for Molecular Imaging, Department of Biomedical Science and Department of Clinical Physiology, Nuclear Medicine and PET, Rigshospitalet, University of Copenhagen, 2200 Copenhagen, Denmark

[‡]Institute for Physics & Astronomy, University of Potsdam, 14476 Potsdam-Golm, Germany

[¶]Niels Bohr Institute, University of Copenhagen, 2100 Copenhagen, Denmark

[§]Department of Physics, Technical University of Denmark, 2800 Kgs. Lyngby, Denmark

ABSTRACT: The biomolecule is among the most important building blocks of biological systems, and a full understanding of its function forms the scaffold for describing the mechanisms of higher order structures as organelles and cells. Force is a fundamental regulatory mechanism of biomolecular interactions driving many cellular processes. The forces on a molecular scale are exactly in the range that can be manipulated and probed with single molecule force spectroscopy. The natural environment of a biomolecule is inside a living cell, hence, this is the most relevant environment for probing their function. In vivo studies are, however, challenged by the complexity of the cell. In this review, we start with presenting relevant theoretical tools for analyzing single molecule data obtained in intracellular environments followed by a description of state-of-the art visualization techniques. The most commonly used force spectroscopy techniques, namely optical tweezers, magnetic tweezers, and atomic force microscopy, are described in detail, and their strength and limitations related to in vivo experiments are discussed. Finally, recent exciting discoveries within the field of in vivo manipulation and dynamics of single molecule and organelles are reviewed.

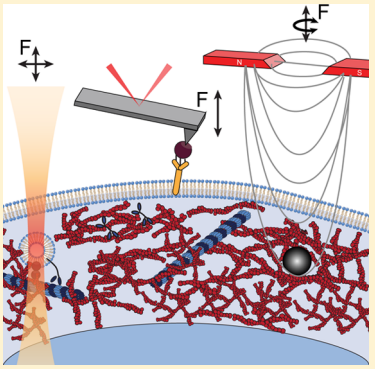

CONTENTS

Received: September 16, 2016
Published: February 3, 2017

DOI: 10.1021/acs.chemrev.6b00638
Chem. Rev. 2017, 117, 4342−4375

1. INTRODUCTION

To understand the basics of life, it is essential to study the construction and function of single molecules. Action−reaction mechanisms at the single molecule level provide information that can be up-scaled to explain functional properties of organelles, the entire cell, and even of the whole organism. Also, as many diseases originate from failure at the single molecule level, for instance by the malfunction of a misfolded protein, a deeper understanding of action−reaction mechanisms might help deciphering the origin of the disease. Despite the great knowledge obtained from in vitro experiments on dynamics of single molecules, it has become evident that to fully uncover their behavior, single molecules must also be studied under natural conditions, as their function often is highly regulated by their local environment. Hence, to increase the biological relevance of single molecule manipulation and force probing, the experimental stage must be brought inside the living cells.

1.1. The Cell

The living cell is a highly complex organism with numerous regulatory pathways and action−reaction mechanisms that are strictly coordinated (Figure 1). First of all, the cell is surrounded by a cell wall that protects the cytoplasm from the exterior. In the cell wall, there are certain transmembrane proteins and receptors constituting channels and transport systems which allow for controlled passage across the cell membrane. Inside the cell the cytoskeleton is responsible for mechanical tasks, for instance for maintaining cell shape, for transportation, for the dynamics related to cell division, and for cell movement. The cytoskeleton consists of a variety of biopolymers of which the most abundant are microtubule, actin, and spectrin. Typical locations of these cytoskeletal elements are illustrated in Figure 1. The most common mean of transport inside the cell is probably diffusion; however, it is not

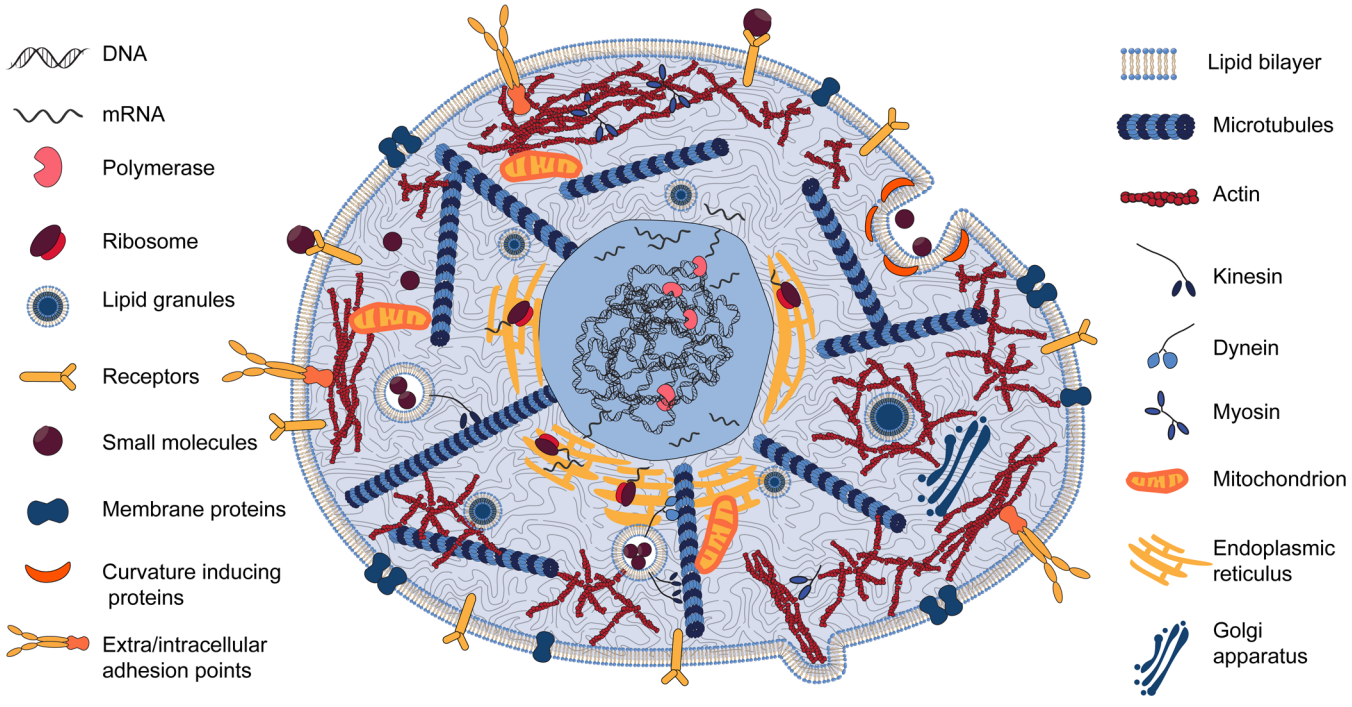

Figure 1. Illustration of the content of the highly crowded cytoplasm of a normal living cell. Force spectroscopy and manipulation have been used to investigate the mechanical and dynamic properties of, for example, membrane components and proteins, molecular motors, assembly of the cytoskeleton, cell division, DNA transcription machinery, cell adhesion, and signaling pathways.

DOI: 10.1021/acs.chemrev.6b00638
Chem. Rev. 2017, 117, 4342−4375

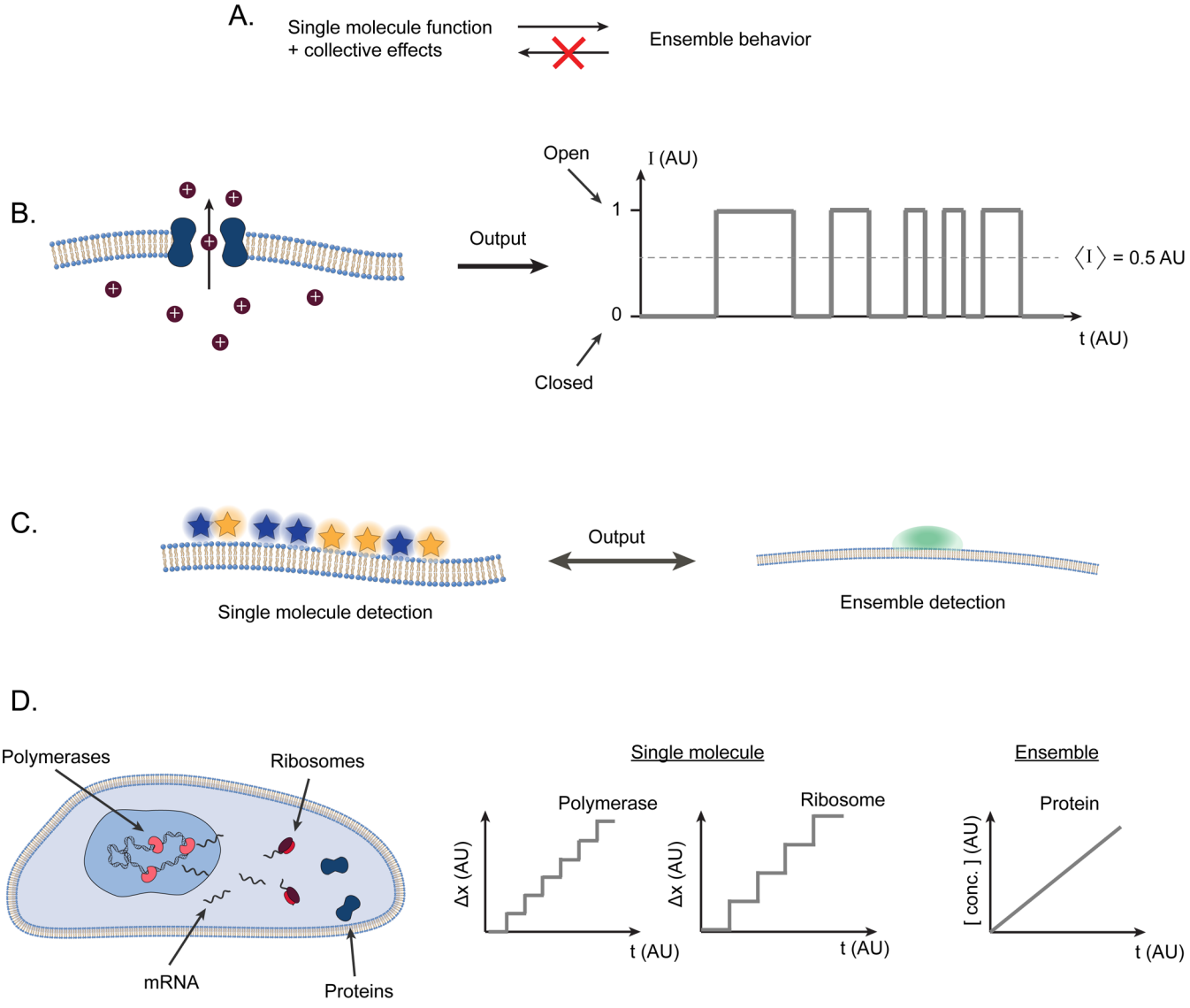

Figure 2. (A) Illustrations of how information on single molecule behavior can predict ensemble behavior, however, that the opposite is not true. (B) The fundamental behavior of a channel that can be either closed or open, allowing charges to pass, cannot be deciphered by ensemble measurements. (C) The fluorescence signal from a mix of fluorophores emitting blue and yellow light, respectively, will appear green if observed on an ensemble level. (D) The stepping nature of the DNA replicating machinery (polymerases and ribosomes) is hidden in ensemble measurements that typically evaluate protein production when replication efficiency is studied.

very effective for larger objects in the crowded cytoplasm. A more effective mode of transportation is by means of molecular motors (e.g., kinesin and dynein), which move their cargo in a processive manner along microtubules. The nucleus contains the DNA, which is transcribed by the polymerase in the making of mRNA (see Figure 1). mRNA is transported out of the nucleus where the ribosomes, located in the endoplasmic reticulum, translate the information stored in the mRNA into proteins. These above-mentioned cellular parts and processes have been highlighted here as their mechanical properties and dynamics are some of the most common action points studied using single molecule manipulation and force spectroscopy.

1.2. Single Molecule versus Ensemble Measurements

A good hallmark of high-quality single molecule experimentation is if the behavior obtained on the single molecule level on average is the same as in ensemble measurements. In other words, one can deduce the ensemble properties from single molecule measurements provided that collective effects are also understood. The opposite is, however, not true as the dynamics of individual molecules are hidden in ensemble experiments. This is illustrated in the following relevant examples sketched in Figure 2: consider a membrane channel through which charges can pass in a selective manner (Figure 2B). The channel is either open or closed and hence allows a current of either 0 or 1 (arbitrary units, AU) to pass through the channel. If the channel is closed exactly half of the time, the average current through the channel will be 0.5 (AU). Without other evidence, this readout could indicate that the channel is always halfway open. This conclusion is obviously wrong as the channel is never half-open, it is either fully closed or fully open. The only way to uncover the correct function of the channel is to observe the current through a single channel over a certain timespan. A second example, illustrated in Figure 2C, is the observation of fluorescence from a mixture of two fluorophores emitting blue and yellow light, respectively. An ensemble observation of the light emitted will show green light. However, by picking up

DOI: 10.1021/acs.chemrev.6b00638
Chem. Rev. 2017, 117, 4342−4375

light from each fluorophore individually, one would observe emitted light from two distinct populations. The third relevant example, illustrated in Figure 2D, regards the process of protein synthesis. The information stored in DNA is transcribed into mRNA by the polymerase, which moves along the DNA in a steplike fashion with a step size of 3.4 Å.[1,2] The mRNA is then translated into a nascent protein by the ribosome, which also moves in a steplike fashion with a step-size of 1 codon.[3] Measuring the production rate of proteins in cells by, for example, Western blotting, returns a continuous process that will not bear any traces of the steplike motion of the two molecular motors involved. In contrast, measuring the mechanical function of the polymerase and the ribosome using, for example, optical tweezers, returns the kinetic properties (i.e., stepsize and velocity) of these motors that are hidden in the ensemble measurements.

1.3. Technological Breakthroughs

A window to the dynamics of the smallest entities of the living world appeared with the evolution of novel techniques capable of monitoring or even influencing single molecules and organelles inside living cells. The first report on manipulation of single molecules was published in 1969, where Nicklas & Koch investigated the role of tension on the reorientation of mal-oriented chromosomes by direct micropipette manipulation of chromosomes inside a living cell.[4] Soon after this pioneering study, Arthur Ashkin demonstrated in the early 1970's that micron-sized particles could be stably trapped by the radiation pressure from two counter propagating laser beams.[5] This work paved the way for optical manipulation of atoms and living organisms, and during the next decade optical tweezers were significantly refined. Optical trapping of individual living micro-organisms such as yeast and *Escherichia coli* was demonstrated in 1987.[6] Here, the micro-organisms were shown to tolerate trapping by a near-infrared laser, and they even appeared physiologically healthy as they proliferated while in the optical trap.[7] Optical tweezers can not only spatially restrict trapped objects but also perform force and distance measurements in regimes relevant for single molecule movement, namely in the pico-Newton and nanometer regimes. This was demonstrated in 1990 when Ashkin and co-workers performed the first quantitative measurements of the force generated by a microtubulus-associated molecular motor inside the giant amoeba *Reticulomyxa*, which was found to be 2.6 pico-Newtons.[8] Optical tweezers are probably the technique which has found the most widespread use for quantifying forces generated by molecular motors both in vitro and in vivo. This is aided by the fact that optical tweezers are the only nanotool capable of operating inside a living cell or a living organism without perforating the cellular membrane and without the need for inserting artificial handles.

The atomic force microscope (AFM) was invented in the 1980's.[9] In contrast to the scanning tunneling microscope, the AFM has the advantage with respect to handling living specimen that it does not require a conductive sample and it does not require a vacuum. An AFM can be operated in an aqueous environment, in a physiological relevant temperature range, and it is capable of measuring forces and distances of high relevance for the molecular and cellular level. The AFM is probably the single molecule technique that has found the largest commercial market, also for its capabilities to scan and image surfaces with molecular resolution. In particular, AFMs have proven extremely useful for probing and mapping out cell surface receptors, thereby assessing their function and binding kinetics.[10]

Magnetic tweezers resemble optical tweezers, however, utilize a magnetic field to generate forces instead of an optical field.[11,12] Magnetic tweezers can relatively easily rotate a magnetizable particle attached to a probed molecule and also manipulate a large number of particles in parallel within a sample. Because of magnetic tweezers' ability to induce a controlled tension through rotation of a handle, they have been particularly useful for obtaining information on the physical properties of DNA and on the dynamics of DNA associating enzymes.[12]

In parallel with the emergence of single molecule manipulation techniques came development and refinement of microscopy. In the 1980's, the group of Gelles demonstrated how the position of beads attached to single molecules could be determined with a resolution down to tens of nanometers by the use of clever image analysis.[13] With the development of super-resolution imaging modalities, for instance STED (stimulated emission depletion),[14,15] STORM (stochastic optical reconstruction microscopy),[16] and PALM (photo-activated localization microscopy),[17] Abbe's criterion for the smallest distinguishable distance between two objects was bypassed, and the window to the single molecule world became even wider. Besides direct tracking of the dynamics of objects inside living organisms, these imaging modalities can often readily be combined with single molecule force spectroscopy techniques, thereby allowing visualization simultaneously with manipulation.

1.4. Why Go in Vivo

The in vitro setting has several advantages (e.g., the influence of a single parameter can often be isolated), and the experiments and their interpretation are typically less complex than in vivo. Hence, many spectacular discoveries of the function and dynamics of single molecules such as kinesin,[18] polymerase,[1,19] and the ribosome[3] obtained in vitro have been published. However, results obtained in vitro often face critique from the life science community because the investigated molecules are in an artificial environment instead of in their natural one. Therefore, to fully uncover and understand the natural functions of single molecules, they must be studied while in their natural environments as well. One example of a molecule whose properties appear to vary from in vitro to in vivo is the ribosome; while overall translation rates of 1 codons/second or less were reported from in vitro single molecule experiments,[3] the in vivo rates were observed to be between 4.2 and 21.6 codons/second dependent on sequence.[20] Another example is myosin, where the velocity of the motor in vivo was found to be faster (710 ± 50 nm/s) than in vitro (500 ± 30 nm/s), and myosin was also found to stay on the track significantly longer in vivo than in vitro.[21] These observations appear somewhat counterintuitive considering the crowded nature of the cytoplasm, and they definitely show that there are important mechanisms at play in vivo which are not reproduced in vitro. These interesting "hidden in vivo mechanisms" have been termed "the Dark Matter of Biology" in a recent review by J. Ross[22] comparing the hidden players inside living cells with the dark matter in gravitational physics.

There are, however, many challenges related to in vivo manipulation and in vivo measurements involving single molecules and organelles.[23] First, the molecule should remain in its natural environment, and efforts should be made to label

DOI: 10.1021/acs.chemrev.6b00638
Chem. Rev. 2017, 117, 4342−4375

or handle only the molecule of interest and only one such molecule. Second, the living cell or whole organism must be kept viable. To keep the cell(s) viable, it is necessary to control e.g., the temperature of the sample chamber and possibly the atmosphere too. Also, the techniques should preferably be noninvasive, which none of the above-mentioned techniques truly are, even the microscopy techniques involve photons which interact with the sample. However, the techniques focused on in this review can be operated in a nearly noninvasive manner and thereby reliably probe the system.

This review first provides a description of theoretical tools useful for analyzing single molecule dynamics and an overview of the most well-established models relevant for in vivo dynamics. This is followed by two experimental sections outlining the state-of-the-art with respect to single molecule visualization and manipulation covering the most promising and widely used techniques. Then we present the exciting and most recent results on in vivo dynamics obtained through visualization and manipulation of single molecules and organelles inside a living cell, also with a focus on the collective effects. The review ends with an outlook on future possibilities.

2. THEORY ON DYNAMICS INSIDE LIVING CELLS

A colloidal particle in water experiences random collisions with the vicinal water molecules. While on average these collisions are isotropic and thus balance out, on sufficiently short time scales, a colloidal particle performs a zigzagging path. This type of motion is called Brownian motion and was reported already by Jan Ingenhousz in 1785,[24] and Robert Brown in 1828.[25] Mathematically, Brownian motion is described by the same laws as the random motion of individual molecules such as sugar molecules in a cup of tea or individual proteins in a dilute aqueous solution. In these cases, the squared width of the distance traveled by the observed particle scales linearly with time. Modern experiments on biological systems have, however, shown clear deviations from the laws of Brownian motion, where instead, the motion is described by a power law or more complex mathematical expressions, capturing the live biological processes.

2.1. Single Particle Tracking

There exist several experimental techniques to measure the motion of microscopic particles inside the cytoplasm of living cells or within cellular membranes. Diffusion of fluorescently labeled molecules can, for example, be determined by methods such as fluorescence correlation spectroscopy (FCS),[26] fluorescence recovery after photo bleaching (FRAP),[27] or Förster resonant energy transfer (FRET).[28] While these methods have many advantages and can measure the motion of quite small and mobile tracers, they have the intrinsic disadvantage that the quantity they report is not the particle position but averages over the position in terms of correlation functions. The signatures of these generally provide less precise information than the full particle trajectory.

As an alternative to these ensemble-based methods, the trajectory $\mathbf{r}(t)$ of a particle can be directly measured using single particle tracking by light-based microscopy modalilties, detailed in section 3, that provide direct information on the particle's spatiotemporal behavior. Tracer particles such as artificial beads of typical size >0.5 μm or endogenous granules of several hundred nanometers in size can be directly recorded by digital cameras mounted on modern microscopes. Smaller particles can be observed by fluorescent tagging for hundreds of seconds at millisecond time resolution and at spatial accuracy down to some tens of nanometers. Within the relatively large volume of eukaryotic cells, molecules down to the size of single and dimeric green fluorescent proteins (GFPs) can now be successfully tracked[29] as well as single lipid molecules in lipid membranes.[30] Apart from imaging by means of cameras, the motion of a tracer can also be directly obtained through (weak) optical trapping which provides better temporal and spatial resolution of the trajectory, cf. section 4.

Single particle tracking (of larger objects) in fact has a long tradition. In 1828, Robert Brown reported the erratic motion of small granules of 1/4000th to 1/5000th of an inch extracted from larger pollen grains as well as of milled stones from the Sphinx.[25] Since then, more systematic single particle tracking methods were developed by Louis Georges Gouy[31] and, most notably, by Jean Perrin in his seminal studies to determine the Avogadro number from measured diffusion coefficients.[32] Modern single particle tracking combined with new evaluation methods for single particle traces was originally conceived by Ivar Nordlund at the University of Uppsala.[33] Combining a moving photographic plate with a clock pendulum triggered stroboscopic "central shutter", he managed to produce time series of small mercury droplets of 10 to 15 s in length (see Figure 3).

2.2. Mean Squared Displacement

In his work from 1908, Perrin used the theory of Brownian motion developed by Einstein[34] and von Smoluchowski[35] to analyze the particle motion in terms of the mean squared displacement (MSD)

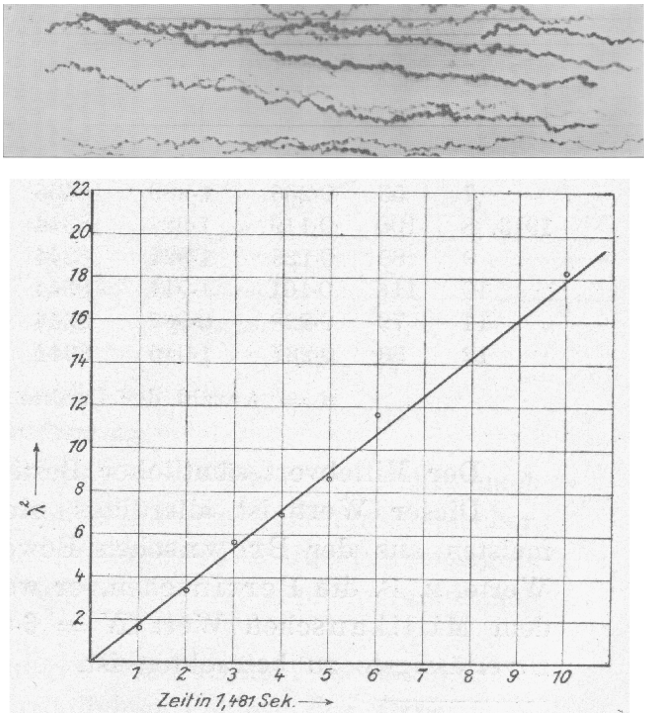

Figure 3. (Top) Motion of small mercury droplets during sedimentation measured by Ivar Nordlund with his moving photographic plate technique.[33] The jittery Brownian motion of the droplets on top of the deterministic sedimentation is distinct. (Bottom) Plot of the purely diffusive motion $\langle x^2(t)\rangle - \langle x(t)\rangle^2$ spanning some 15 s. Reproduced with permission from ref 33. Copyright 1914 Akademische Verlagsgesellschaft Geest & Portig.

DOI: 10.1021/acs.chemrev.6b00638
Chem. Rev. 2017, 117, 4342−4375

$$\langle \mathbf{r}^2(t)\rangle = \int \mathbf{r}^2(t)P(\mathbf{r}, t)\, dV \cong K_1 t \tag{1}$$

where the diffusion coefficient K_1 is of physical dimension length^2/ time. As indicated in equation 1, the MSD is constructed from the spatial average denoted by angular brackets of the squared particle position, weighted by the probability density function $P(\mathbf{r},t)$ to find the particle at position $\mathbf{r}$ at time t. As this quantity can only be obtained by measuring an ensemble of tracer particles, it is called the ensemble averaged MSD.[36,37] In contrast to Perrin's approach, Nordlund quantified his measurements based on the information provided by individual trajectories and determined the time-averaged MSD. In modern single particle tracking literature, the time averaged MSD, denoted by an overline, is typically evaluated as[36,37]

$$\overline{\delta^2(\Delta)} = \frac{1}{T-\Delta}\int_0^{T-\Delta} (\mathbf{r}(t+\Delta) - \mathbf{r}(t))^2\, dt \tag{2}$$

where T is the length of the measured trajectory and Δ is called the lag time. In the calculation of equation 2, the information on the entire time series $\mathbf{r}(t)$ is used for any lag time. For a random walk process, defined in detail in section 2.3.1, the number of discrete spatial dislocations, hereafter referred to as "jumps", within the time period Δ, is given by the ratio Δ/τ, where τ is the typical time for a single jump. The expression in the integral in equation 2 is then just given by $\langle \delta x^2\rangle \Delta/\tau$, where $\langle \delta x^2\rangle$ is the variance of the jump lengths of this random walk process. The final result is

$$\overline{\delta^2(\Delta)} \simeq K_1 \Delta \tag{3}$$

where $K_1 = \langle \delta x^2\rangle/[2\tau]$ in the standard random walk sense.[37] For an ergodic system in the sense of Boltzmann, the time average of an observable should converge to the corresponding ensemble average at sufficiently long observation times T:[36,37]

$$\lim_{T\to\infty} \overline{\delta^2(\Delta)} = \langle \mathbf{r}^2(\Delta)\rangle \tag{4}$$

The laws of equation 1 and equation 3 thus demonstrate the ergodic nature of Brownian motion.

In actual analysis of data, results are often smoothened by averaging equation 2 over a number N of single trajectories i, producing the mean time averaged MSD

$$\left\langle \overline{\delta^2(\Delta)} \right\rangle = \frac{1}{N}\sum_{i=0}^{N} \overline{\delta_i^2(\Delta)} \tag{5}$$

In Figure 4, the ensemble averaged MSD of a simulated Brownian motion is shown together with the corresponding time averaged MSD from both individual trajectories (50000 steps) and an ensemble of trajectories (1000 time averaged MSDs). Figure 4 demonstrates that even for relatively long trajectories, the time-averaged MSD shows quite disparate behavior. However, the mean time averaged MSD, averaged over a sufficient number of individual trajectories, becomes indistinguishable from the ensemble averaged MSD.

2.3. Anomalous Diffusion

Measurements of the trajectories of tracer particles in living cells reveal a different picture than the behavior shown in Figure 4. In living cells, anomalous diffusion of the form:

$$\langle \mathbf{r}^2(t)\rangle \simeq K_\alpha t^\alpha \tag{6}$$

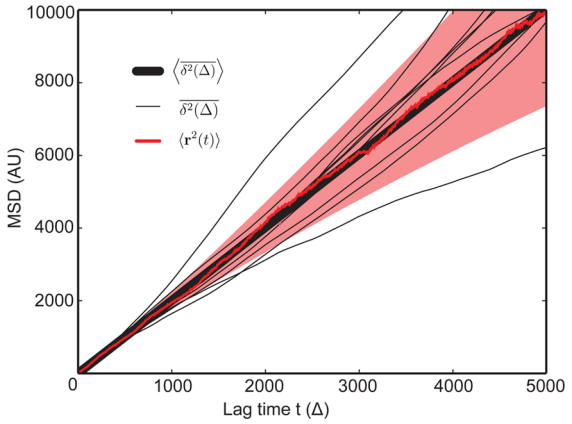

Figure 4. MSDs from simulated Brownian motion. The red line represents the ensemble averaged MSD from 1000 independent particles, showing some local variations around the linear law $\langle \mathbf{r}^2(t)\rangle \simeq t$. The thin black lines represent time averaged MSD $\overline{\delta^2(\Delta)}$ for individual trajectories of 50000 steps each, exhibiting quite pronounced deviations from the linear behavior. The thick black line represents $\left\langle \overline{\delta^2(\Delta)} \right\rangle$ averaged over 1000 individual trajectories. The shaded red interval is the variance calculated from 1000 individual $\overline{\delta^2(\Delta)}$.

is frequently observed.[37−39] In this case, the diffusion coefficient, K_α, is of physical dimension length^2/ time$^\alpha$. The anomalous diffusion exponent, α, measures the degree to which the particle motion deviates from Brownian motion where $\alpha = 1$. One distinguishes subdiffusion with $0 < \alpha < 1$ from superdiffusion with $\alpha > 1$.[40] Passive motion in living cells is typically subdiffusive, while superdiffusive motion occurs in the presence of active processes such as transport by molecular motors. As an example, in Figure 5 the ensemble averaged MSD is shown for granules performing anomalous diffusion inside living HUVEC cells.[41] A fit to the trajectories returns an exponent of $\alpha = 0.75$, meaning the granules show subdiffusive motion, probably due to the crowding in the cytoplasm of the cells.

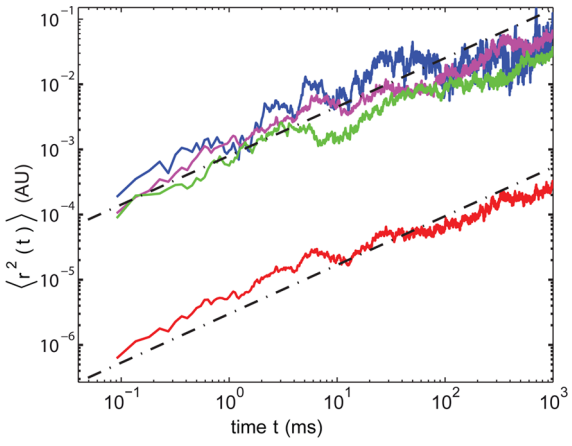

Figure 5. Ensemble-averaged MSD for anomalous diffusion. Blue, purple, and green traces are granule trajectories from inside a living cell. The color code represents the location of the granules, blue is in the nucleus, purple in the cytoplasm close to the nucleus, and green is at the cell's periphery. The red trace is an average of all trajectories and has artificially been shifted downward. The dotted lines represent a fit with a slope of $\alpha = 0.75$. Reproduced with permission from ref 41. Copyright 2012 Springer.

DOI: 10.1021/acs.chemrev.6b00638
Chem. Rev. 2017, 117, 4342−4375

In reality, anomalous diffusion defined by the power-law form of the MSD in equation 6 does not uniquely define the underlying mechanism causing it. In fact, there are many different scenarios leading to equation 6. Figure 6 shows a comparison of the behavior of Brownian motion with the two most widespread anomalous diffusion processes, continuous time random walks (CTRWs) and fractional Brownian motion (FBM).

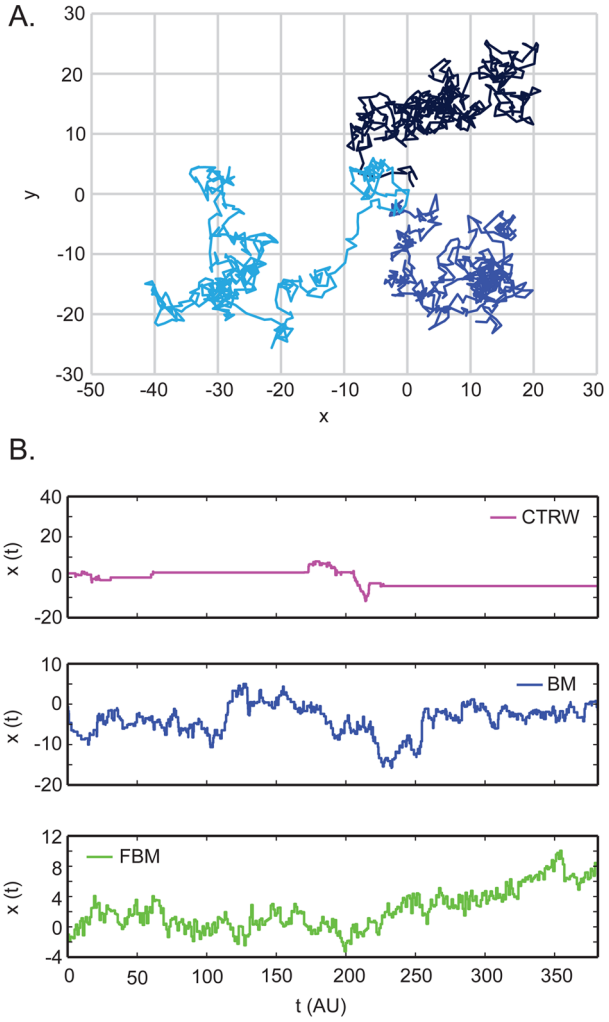

Figure 6. (A) Three trajectories of a two-dimensional Brownian motion. The trajectories of a subdiffusive CTRW would have looked similar, as the only difference is in the stopping times between individual jumps. (B) Comparison of the one-dimensional trajectories $x(t)$ for different diffusion processes. The upper panel shows a subdiffusive CTRW with $\alpha = 0.6$. Increasingly long trapping events occur, corresponding to the horizontal lines in $x(t)$. The middle panel shows a Brownian motion (BM), and the bottom panel an FBM with $\alpha = 0.6$.

2.3.1. Random Walks and Brownian Motion. The concept of random walks was originally introduced by Karl Pearson in his quest of modeling the mosquito infestation of newly created clearings in rain forests.[42] In his terms, imagine a drunkard trying to find home in a city built of square blocks. Each time he reaches an intersection, due to lack of memory he makes a random choice among the four possible directions for the next intersection. More abstract, imagine a particle moving on a lattice of spacing a in d spatial dimensions. During each time step τ, the particle moves randomly in any of the $2d$ directions (see two and one-dimensional trajectories in Figure 6, panels A and B, middle panel, respectively). For this process, it is straightforward to show that in the limit of many jumps, corresponding to times $t \gg \tau$, the probability density function $P(\mathbf{r},t)$ to find the particle at position $\mathbf{r}$ at time t is given by a Gaussian distribution

$$P(\mathbf{r}, t) = \frac{1}{(4\pi K_1 t)^{d/2}} \exp\left(-\frac{\mathbf{r}^2}{4K_1 t}\right) \tag{7}$$

as originally derived by Einstein.[34] The diffusion coefficient $K_1 = a^2/[2d\tau]$ is now composed of a and τ. It is easy to show that the MSD of the process follows equation 1, and the process itself is governed by the diffusion equation (Fick's second law).[43,44] An important step in this derivation is the long time limit of many jumps. In this limit, mathematically speaking, the central limit theorem enforces the rapid convergence to the Gaussian law (7).

2.3.2. Continuous Time Random Walks. CRTWs were originally conceived by Montroll and Weiss, and then generalized by Montroll, Scher, and Shlesinger.[45−47] In a CTRW, the random walker at each jump chooses a random jump distance $\mathbf{r}$ from a probability density $\lambda(\mathbf{r})$, symmetric or asymmetric, whereas in between any two jumps, the random walker becomes trapped for a random waiting time τ drawn from a probability density $\psi(\tau)$. Here, we concentrate on subdiffusive CTRWs for which the variance $\langle \delta \mathbf{r}^2 \rangle$ is finite, for example, it could equal the square of the fixed lattice spacing a. Notably, when a CTRW has a finite characteristic waiting time, $\langle \tau \rangle$, it can be shown that for many jumps, the waiting time distribution renormalizes to that of a constant, fixed waiting time $\tau^\star$,[48] that is the case of the Brownian motion. However, when the mean waiting time $\langle \tau \rangle$ diverges, the process becomes subdiffusive.[37,40,46,49,50] Scher and Montroll formulated the subdiffusive CTRW with a power-law waiting time density $\psi(\tau) \simeq (\tau^\star)^\alpha/\tau^{1+\alpha}$ where $0 < \alpha < 1$. The resulting trajectory $x(t)$ shows frequent jumps interspersed with pausing times of ever increasing durations. An example of a one-dimensional CTRW trajectory is displayed in Figure 6B, upper panel. Indeed, single particle tracking experiments have demonstrated the existence of power-law waiting time distributions with $0 < \alpha < 1$ for plastic microbeads in cross-linked actin meshes,[51] for functionalized microbeads moving along complementary functionalized surfaces,[52] and for the motion of potassium channels in the membrane of living human kidney cells.[53]

Ideal trajectories from simulations as the one in Figure 6B, upper panel, clearly show the stalling of the particle over certain periods in time as horizontal plateaus. In realistic systems, additional noise from the environment will at least partially preclude such clear immobilization events. To account for such additional noise, so-called noisy CTRW processes can be studied with respect to both their ensemble and time-averaged behavior.[54]

2.3.3. Viscoelastic Anomalous Diffusion and the Fractional Langevin Equation. A very different scenario from the jump-like processes of the CTRW family is the following: consider a long model polymer chain consisting of beads with a given mass connected by harmonic springs of given stiffnesses. The beads experience a viscous drag as well as a random Brownian force due to the thermal environment. Imagine one bead is being pushed slightly away from its position. It will then experience a hierarchy of restoring forces

DOI: 10.1021/acs.chemrev.6b00638
Chem. Rev. 2017, 117, 4342−4375

from its nearest neighbors, the next nearest neighbors, and so on. Each push in one direction is thus necessarily followed by a push in the opposite direction, an effect called antipersistence.[55] Thus, the motion of a single bead in the chain follows a regular Brownian motion but is coupled to the motion of all its peers. Consequently, the effective motion of this bead is governed by a generalized Langevin equation,[56−62] and the associated MSD is subdiffusive $\langle \mathbf{r}^2(t)\rangle \simeq K_\alpha t^\alpha$ with $0 < \alpha < 1$.

The motion of particles in a viscoelastic environment is naturally described by such a generalized Langevin equation.[60,61] For instance, it has been identified to govern the motion of various submicron tracer particles in living cells and complex liquids[63−67] or for the motion of lipid and protein molecules in simple lipid bilayer systems.[68−71] In the overdamped limit, the generalized Langevin equation motion is equivalent to fractional Brownian motion (FBM), exemplified by the trace in Figure 6B, lower panel. For this process, the associated MSD is again of the form of equation 6.[37] Generalized Langevin equation motion and FBM are mathematically quite intricate processes. In literature, they are therefore often modeled in terms of a diffusion equation with a time-dependent diffusion coefficient of the form $K(t) \simeq t^{\alpha-1}$. However, we stress that this is a completely different process called scaled Brownian motion,[72,73] and as long as the system is kept at a fixed temperature, we do not expect scaled Brownian motion to be a good description for the motion observed in a viscoelastic environment.

Further details about anomalous diffusion processes may be found in the reviews in refs 37, 39, 74, and 75.

2.4. Nonergodic Diffusion and Aging

2.4.1. Nonergodic Dynamics. As should be apparent from the above examples for anomalous diffusion, they show different faces. The common denominator of all processes is the ensemble averaged MSD, equation 1, however, the information on the ensemble averaged MSD is not sufficient to fully characterize the underlying physical process.[36,37] At longer times, the motion of larger tracers in the cellular cytoplasm, tracers in artificially crowded systems, and the motion of lipids in simple bilayer membranes most often display the characteristics of viscoelastic systems and ergodic processes, equation 4.[37,76−78] However, there exist several reports of systems in which ergodicity is broken whereby equation 4 is violated.[36,37] Typically, while the ensemble-averaged MSD still features the power law form of equation 1, the time-averaged MSD in such nonergodic cases follows a linear dependence of lag time[36,37,79]

$$\left\langle \overline{\delta^2(\Delta)} \right\rangle \simeq K_\alpha \frac{\Delta}{T^{1-\alpha}} \tag{8}$$

Examples of such nonergodic behavior are the motion of lipid granules in yeast cells on short time scales[64] and the motion of insulin lipids in MIN6 cells.[80] Similar ergodicity breaking is reported in the studies of diffusing proteins in the plasma membrane of living cells.[53,81] To make things even more complicated, the motion observed in refs 53 and 81 is composed of both ergodic and nonergodic motion, leading to power-law forms of both $\langle \mathbf{r}(t)\rangle$ and $\langle \delta^2(\Delta)\rangle$, which, however, have different scaling exponents. In all these cases, the analysis of the measured time series requires special care as the linear lag time dependence in equation 8 does not necessarily imply normal diffusion and the value of the time-averaged MSD from individual particle traces may significantly vary at a given lag time.[36,37,79] Figure 7 shows the time-averaged MSD of the tracked granules shown in Figure 5.[41] Notably, on short time scales, the time-averaged MSD trajectories are consistent with a value of $\alpha = 1$ that differs from that of the ensemble averaged MSD ($\alpha = 0.75$; Figure 5). This implies that the process is nonergodic for short time lags. The dashed line with scaling exponent $\alpha = 0.2$ at long lag times reflects the confinement of the particle due to the finite size of the cell and the laser trap used to monitor the motion.[37,64]

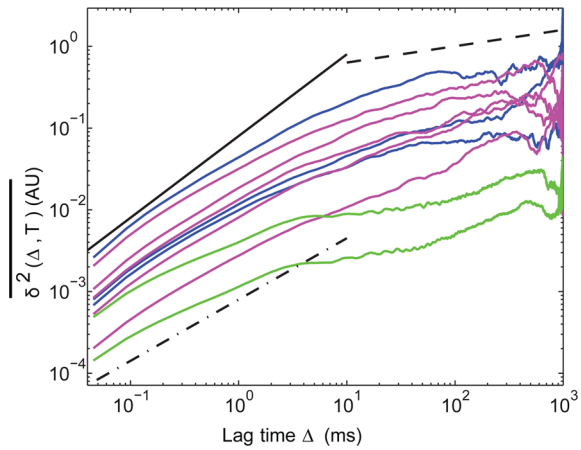

Figure 7. Time-averaged MSD for 10 different granule trajectories from inside a living cell (from same data set shown in Figure 5). The black lines represent guiding lines with a slope of $\alpha = 1$ (full), $\alpha = 0.75$ (dashed/dotted line), and $\alpha = 0.2$ (dashed line). The color coding represents the location of the granule: blue, in nucleus; purple, in cytoplasm close to the nucleus; and green, at the cell's periphery. Reproduced with permission from ref 41. Copyright 2012 Springer.

2.4.2. Aging. Another unusual phenomenon, that is often coupled with the violation of ergodicity, is referred to as aging.[36,37] Aging indicates the nonstationarity of a process, for instance that the effective mobility of an observed particle decreases as a function of time.[36,37,79] Aging can also appear in results where the measurements were started some (aging) time after the initial preparation of the system.[82−84] Aging may additionally induce a population splitting of particles into immobile and mobile fractions.[83,84] Aging has been observed in biological experiments, such as for the motion of protein channels in human cell walls[53,81] and of insulin granules in the cytoplasm of cells.[80] With the use of molecular dynamics simulations, it has recently been shown that aging effects can span as much as 13 decades in time for the internal dynamics of single protein molecules.[85] Figure 8 shows experimental measurements from potassium channels in the plasma membrane, exhibiting aging dynamics for different lag times.

2.5. Analyzing Anomalous Diffusion

2.5.1. Mean-Squared Displacements and Higher-Order Moments. The MSD corresponds to the second moment of the particle displacement. Additional information can be gained from higher-order moments. The non-Gaussianity parameter G provides a sensitive measure for the type of diffusion process under consideration. G involves higher-order moments and is defined in terms of the experimentally relevant time-averaged MSD as[39]

DOI: 10.1021/acs.chemrev.6b00638
Chem. Rev. 2017, 117, 4342−4375

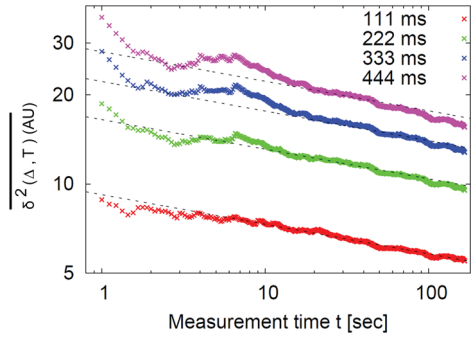

Figure 8. Time-averaged MSD for the motion of potassium channels in plasma membranes plotted as a function of measurement time at given lag times Δ = 111, 222, 333, and 444 ms. The time dependence shows that the process ages. The straight dashed lines represent fits with slope $\alpha - 1 = -0.10$, while the particle motion is represented with a CTRW. Reproduced with permission from ref 53. Copyright 2011 National Academy of Sciences.

$$G(\Delta) = \frac{d}{d+2} \times \frac{\left\langle \overline{\delta^4(\Delta)} \right\rangle}{\left\langle \overline{\delta^2(\Delta)} \right\rangle^2} - 1 \tag{9}$$

Here, d is the spatial dimension, and the fourth time-averaged moment is defined similarly to the time-averaged MSD equation 2 (i.e., the power of the integrand is 4 instead of 2). For Brownian motion $G = 0$, whereas it deviates from zero for progressively non-Brownian diffusion.

Another useful tool to analyze measured stochastic data are different ratios of moments, such as $\langle r^4(t)\rangle/\langle r^2(t)\rangle^2$ for the time series $\mathbf{r}(t)$ or for the mean maximal excursions, $\mathbf{r}_{\mathrm{mme}}(t)$.[86] Figure 9 shows the moment ratios calculated from the mean

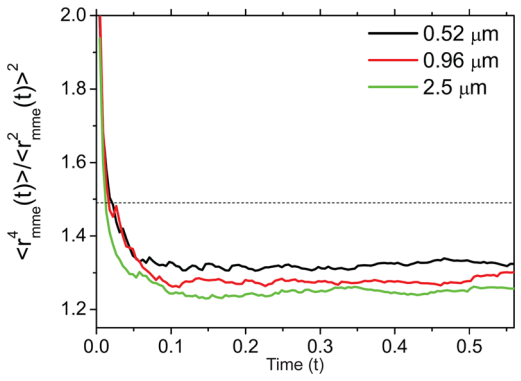

Figure 9. Moment ratios of the mean maximal excursion for video-tracked beads of various sizes in a micellar solution. The dotted line represents the critical value distinguishing a subdiffusive CTRW (above this value) from a subdiffusive FBM (below this value) motion. The different colors represent different bead diameters as explained in the legend. Reproduced with permission from ref 65. Copyright 2013 IOP Publishing Ltd.

maximal excursion of video tracked beads of various sizes immersed in aqueous solutions of wormlike micelles.[65] The horizontal dotted line in Figure 9 represents a critical value that can be used to distinguish CTRW processes (above) from FBM (below), see ref 86 for detailed information. Hence, using this analysis, it was determined clearly that the beads performed FBM motion in the viscoelastic solution.

2.5.2. Increment Velocity Correlation. A typical quantity accessible from experimental data is the position increment autocorrelation function, which is defined through

$$C_v^{(\epsilon)}(\tau) = \frac{1}{\epsilon^2}\langle[\mathbf{r}(\tau+\epsilon) - \mathbf{r}(\tau)][\mathbf{r}(\epsilon) - \mathbf{r}(0)]\rangle \tag{10}$$

and can be used as a tool to distinguish between different subdiffusion models.[63] Figure 10 shows the shape of the increment correlation function (eq 10) for CTRW and FBM processes.[87] For subdiffusive CTRW, $C_v^{(\epsilon)}(\tau)$ as a function of τ simply decays to zero within the resolution ϵ, as shown in the top panel. As soon as the CTRW is confined (e.g., in a potential well), the situation is quite different, as shown in the middle panel. Due to reflections at the flanks of a potential well, negative correlations emerge as the particle changes direction. As is also shown in the same panel, the emerging form resembles that of the overdamped behavior of FBM motion, where the negative values reflect the antipersistence of the motion.[87] The bottom panel shows $C_v^{(\epsilon)}(\tau)$ of a FBM together with experimental data of beads with various sizes recorded in a wormlike micellar solution.

2.5.3. Information from the Amplitude Scatter. The fluctuations of the time-averaged MSD from one trajectory to another can be quantified in terms of the probability density function $\phi_\alpha(\xi)$ of the dimensionless quantity $\xi = \overline{\delta^2(\Delta, T)}/\langle\overline{\delta^2(\Delta, T)}\rangle$. In fact, $\phi(\xi)$ is a reliable measure to distinguish different anomalous diffusion processes from one another, in particular, also for relatively short trajectories.[37,87,88] For a reproducible process, this distribution is very concentrated, becoming more and more narrow for increasing measurement time T. Deviations from this form are expected for processes such as subdiffusive CTRWs but also for relatively short trajectories. For example, for CTRW subdiffusion, the distribution $\phi(\xi)$ becomes quite broad and highly skewed, with a finite value at $\xi = 0$.[79,89] This reflects the possibility that the particle does not move at all during a finite observation period.

The centered variance $\mathrm{EB} = \langle\xi^2\rangle - 1$ of the distribution $\phi(\xi)$ is called the ergodicity breaking parameter and differs from zero for nonergodic processes.[37,79,87] In addition to all mentioned methods, there exist many more for the characterization of measured stochastic time series. These were recently summarized in refs 37 and 90. To guarantee a faithful interpretation of measured data, it is important to use several complementary analysis methods.

2.6. Active Motion in Biological Processes

Our description of anomalous diffusion has so far mostly concerned passive motion. However, several biological processes are active (e.g., mediated by molecular motors), converting biochemical energy into mechanical directed output. The underlying molecular mechanisms for active motion are discussed in a number of recent reviews (e.g., refs 91−94). Here, we discuss a few examples of numerical simulations, paralleled by experimental findings, with a focus on how to analyze such data. When the recorded data stems from observations of a larger cargo carried by a molecular motor, the data series will typically indicate anomalous diffusion,[95] including superdiffusion and directional persistence.[96,97] In particular, superdiffusive traces in living cells have been putatively associated with active motor motion.[8,98,99] However, sometimes directed motor motion can be masked and comprised by cargo size, linker elasticity, and loading force,

DOI: 10.1021/acs.chemrev.6b00638
Chem. Rev. 2017, 117, 4342−4375

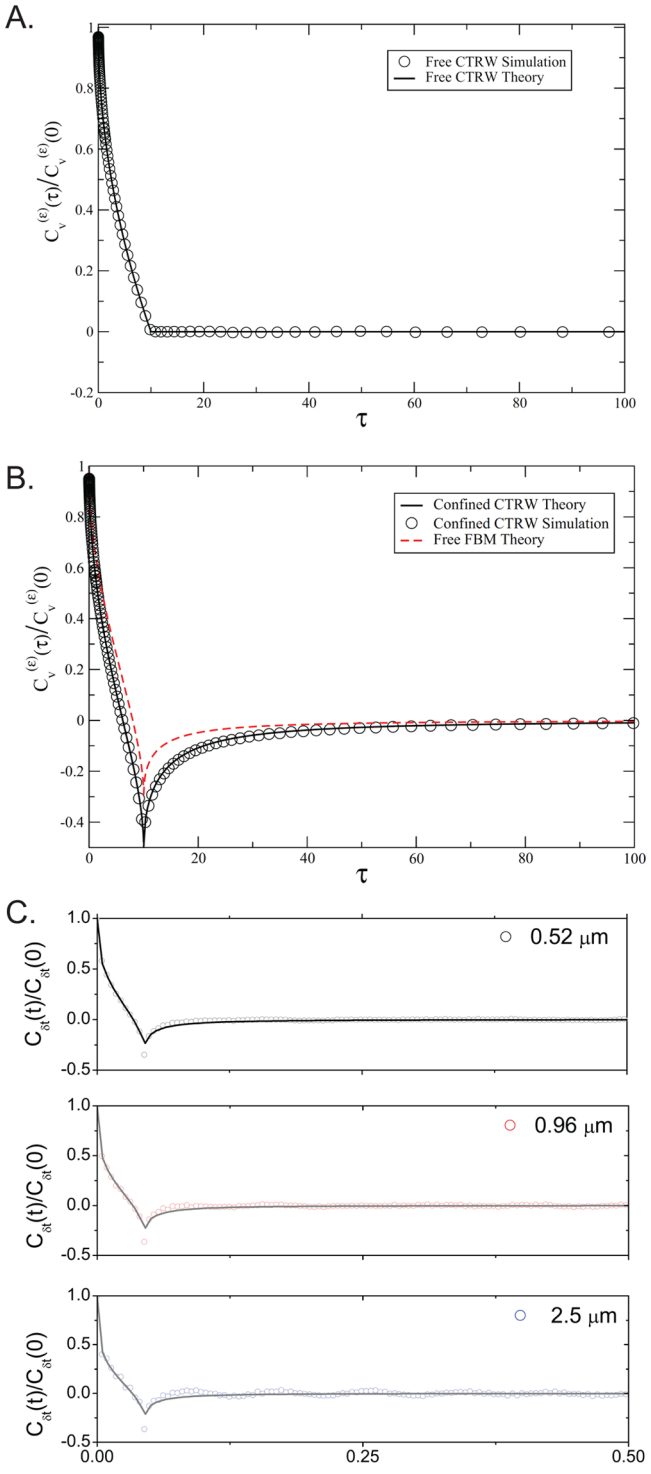

Figure 10. Increment correlation function for different processes. (A) $C_v^{(\epsilon)}(\tau)$ of a subdiffusive CTRW, showing that successive moves of the particle are completely decorrelated.[87] (B) When the same process is confined by an external potential, $C_v^{(\epsilon)}(\tau)$ overshoots to negative values. This behavior resembles that of the generalized Langevin equation or FBM.[87] Reproduced with permission from ref 87. Copyright 2011 Royal Society of Chemistry. (C) $C_v^{(\epsilon)}(\tau)$ of generalized Langevin equation motion compared to data measured for microbeads of different sizes in wormlike micellar solution.[65] Reproduced with permission from ref 65. Copyright 2013 IOP Publishing Ltd.

which might cause the motion to appear as passive anomalous diffusion.[95]

As with subdiffusive processes, a big challenge in active motion is to find the correct description of the underlying mechanism. For example, Chen et al.[100] used simple numerical models and experimentally recorded trajectories of fluorescently labeled endosomes in live mammalian cells to determine the parameter ranges for which the traces were better described by truncated Lévy walks than by Brownian transport. Even more authors have pointed to the need for development of new tools based on nonequilibrium statistical physics, allowing for a description of active processes in the framework of (passive) diffusion.[101] Bruno et al.[102] suggested a model that was shown useful for extracting step-sizes and dwell times from experimental trajectories of myosin-V driven organelles in living cells. As another example, Brunstein et al.[103] proposed a model that could determine distribution of velocities extracted from traces of experimental observations of Myosin-V driven melanosomes along microtubules in *Xenopus laevis*. Furthermore, several numerical models have been presented based on a tug-of-war scenario (see molecular description of tug-of-war mechanisms in section 5) that can be tuned to display multimodal velocity distributions similar to experimental data.[104−106] As these models attempt to describe the underlying kinetics of the cargo transport, the important conclusion put forward by Martinez et al.[107] that the cargo velocity is not directly indicative of the number of molecular motors involved in an active transport is worth bearing in mind.

The problem in separating the underlying motion of the motor complex from the thermal fluctuations of the cargo, originating from a floppy linkage between the observed cargo and the motor, were addressed in refs 95 and 108. In the latter, an algorithm based on Bayesian statistics reliably parsed cargo tracks into constant velocity segments given what was known about the noise stemming from the linkage.[108] The algorithm was applied to trajectories of lipid droplets along microtubules in wild-type Drosophila embryos, showing with statistical evidence that the tracked droplets separated into distinct populations around two preferred velocities. In a similar study, Gazzola et al.[109] developed a stochastic model for molecular motors stepping along microtubules including binding and unbinding to the cargo with parameters extracted from experimental observations of fluorescent adenovirus type 2 in HeLa cells. The six parameters of the model were inferred from the velocity and displacement distributions of segmented trajectories. These findings led the authors to suggest that bidirectional transport of human adenoviruses can be explained without explicit motor coordination and enabled the prediction of the number of motors active on the viral cargo during microtubule-dependent motions as well as the number of motor binding sites. In a more recent numerical model,[110] the cargo transport from a system with two identical molecular motors with floppy linkers to the cargo was investigated in detail, in a parametrically simple model. Furthermore, it was demonstrated that the model could be used to extract parameters involved in cargo transport by two such motors from experimental trajectories.

Ideally, comparison with experimental data should also identify if the model is relevant for the particular trajectory. For this purpose, Assmann et al.[111] addressed how trajectories with bidirectional character may be analyzed. Here, a series of statistical tools useful for analyzing and characterizing cargo trajectories were introduced, and it was demonstrated how the statistical properties of observed cargo trajectories could provide information on the motor proteins involved. Collective

DOI: 10.1021/acs.chemrev.6b00638
Chem. Rev. 2017, 117, 4342−4375

Table 1. Comparison of Different Light-Based Microscopy Techniques

	bright field	confocal	multiphoton	TIRF	light sheet	super-resolution
dye	staining	any	any	any	any	only certain fluorophores
optical sectioning	no	yes	yes	no	yes	yes
live-cell imaging	yes, but staining will compromise viability	yes	yes	yes, but only < ~300 nm from the glass surface	yes	STED is more invasive than PALM/STORM
multicolor	no, unless staining and killing the cell	yes	challenging	yes	yes	challenging
out-of-focus excitation	yes	limited by the pinhole	only very little	only very little	only very little	only very little
temporal resolution	ms-s	ns-s	ms-s	ms	ms	ms-min
spatial resolution (x,y)	> 250 nm	> 180 nm	> 300 nm	> 200 nm	> 500 nm	> 20 nm
illumination	wide field	point scanning	point scanning	evanescent field	light sheet	evanescent field for STORM/PALM, doughnut-shaped field for STED

action of molecular motors in a crowded environment was addressed most recently in refs 112 and 113.

3. HOW TO DETECT DYNAMICS INSIDE LIVING CELLS

Despite great technological achievements, in vivo imaging in combination with manipulation, in particular at the single molecule level, is a complicated task due to the difficulties related to the correct labeling of the relevant structures, the limited number of photons emitted, and potential autofluorescence from the cytoplasm. Also, the structures of interest may be so small that they are not distinguishable in normal optical microscopy where the resolution is limited by the diffractive nature of light.

The optical resolution limit was introduced by the physicist Ernst Abbe in 1873 and describes the distance, d, at which two pointlike objects are distinguishable in light microscopy:

$$d = \frac{\lambda}{2n \sin \theta} \tag{11}$$

Here, λ is the wavelength of the light, n is the index of refraction, θ is the half angle defining the cone of light exiting from the lens, and $n \sin \theta$ equals the numerical aperture (NA) of the objective. Thus, if more objects, for example, fluorescently labeled biomolecules, are within this distance (typically ~250 nm) of each other, their individual positions cannot be determined. Compared to the size of a cell, Abbe's diffraction limit is much smaller, but many cellular objects of interest, and distances between such objects, are smaller than d.

The image recorded by optical microscopy from a subdiffractive object is well-described by the point spread function, which consists of a central intensity peak surrounded by a series of higher-order diffraction patterns.[114] The central peak is known as the Airy disc and contains most of the photon distribution. The full width half-maximum (fwhm) of the Airy disc represents d from equation 11. With the development of single-molecule localization algorithms[13,115] and super-resolution microscopy techniques[14−17,116] Abbe's resolution limit has been bypassed. However, the application of super-resolution techniques is still somewhat limited due to technical and experimental demands that are not trivial to combine with single molecule manipulation, and also, so far only a limited number of fluorescent labels can be used for each super resolution technique.

Imaging of cells (in combination with force spectroscopy) is therefore still mostly based on conventional fluorescence light microscopy, as detailed in section 3.2. A variety of microscopy techniques offering different possibilities and trade-offs exist, as outlined in Table 1. A high resolution is achieved by collecting a sufficient number of photons from the emitting fluorophores. However, the overall photon count poses a trade-off on temporal resolution as more photons require longer measurement times. More photons can also be harvested by increasing excitation intensity, yet, this directly increases phototoxicity and bleaching of the sample.

The molecules or organelles of interest are often not visible without fluorescent labeling. Although some biomolecules exhibit intrinsic fluorescent properties, they do not display as good brightness as, for example, organic fluorophores, fluorescent proteins, quantum dots, or gold nanoparticles (AuNPs). The quality of a fluorophore is generally a product of high absorption cross section and quantum yield, chemical and fluorescent stability, high water solubility, and sufficient fluorescent-lifetime to prevent blinking and delay bleaching. Organic fluorophores come in basically any color in the visible spectrum. Also, with typical sizes of 200−1000 Da, they are much smaller than fluorescent proteins (20000−300000 Da), quantum dots, and AuNPs, where the latter two consist of hundred of thousands of heavy atoms. It is an advantage that fluorophores are small because they impose less steric hindrance. However, the process of labeling intracellular biomolecules with synthetic organic fluorophores can be challenging and is commonly done using antibody schemes. To reach their target, the fluorophores must be internalized through the highly nonpermeable cell membrane which can be a stressful process for the cell.

The discovery of genetically encoded fluorescent proteins that are either expressed alone or in fusion with other proteins helps overcome some of these obstacles. The challenges related to fluorescent proteins are instead that they have fairly low photon output and are less stable compared to organic fluorophores, quantum dots, and AuNPs. The selection of spectral regions for excitation is also limited, in particular in the red and near-infrared regime. This regime is of special interest as biological tissue does not absorb near-infrared light as well as visible light, hence, the penetration distance of near-infrared light is longer, and the sample is not damaged as much as by visible light.

Quantum dots are fluorescent semiconductor nanoparticles, with emission spectra inversely related to particle size. They usually consist of a CdSe or CdTe core surrounded by a ZnS shell that prevents quenching by water and enables conjugation.[117] Quantum dots have high extinction coefficients

DOI: 10.1021/acs.chemrev.6b00638
Chem. Rev. 2017, 117, 4342−4375

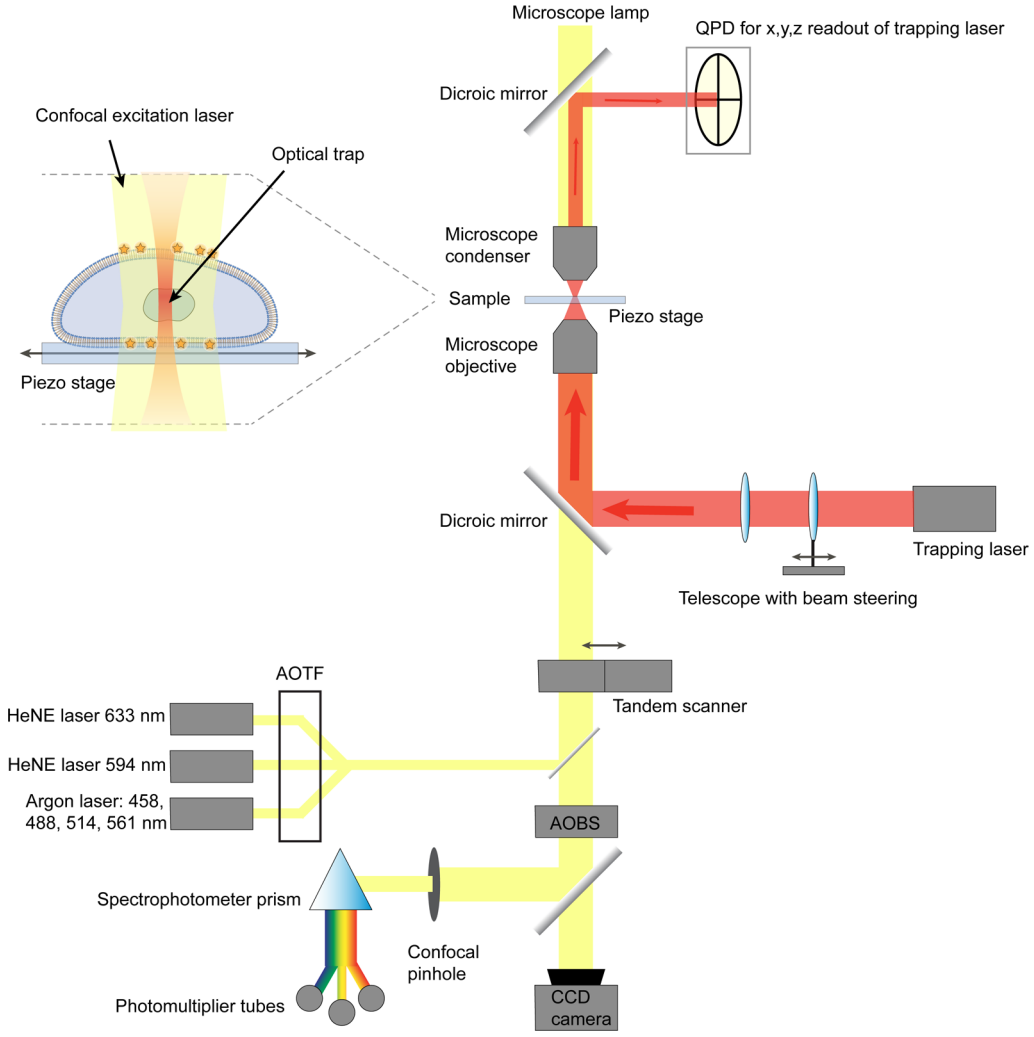

Figure 11. Illustration of how an optical trap can be implemented in a confocal microscope. This setup is similar to the one described in 2006 in ref 127. The trapping laser beam (red) is guided into the optical path of the confocal lasers by a dichroic mirror allowing visible lasers to pass but reflecting near infrared (NIR) light laser light. The signals from the confocal lasers are picked up by the AOBS and directed onto the photomultiplier tubes. The signal from the trapping laser is picked up by a quadrant photodiode (QPD) located close to the back focal plane, which allows for determining the 3D position of the trapped object. In this configuration, the confocal lasers and the optical trap can be steered independently (by the tandem scanner and the telescope, respectively).

and quantum yield, and they are extremely photostable wherefore they are easily visualized and localized in the cytoplasm of cells. Thus, quantum dots are attractive markers. However, as quantified above, they are several orders of magnitude larger than conventional fluorophores and impose larger steric hindrance. Also, their toxicity is currently under debate in literature.

Gold nanoparticles are not fluorescent; however, they reflect light in a certain spectrum very efficiently and can thus be detected (e.g., through confocal microscopy operated in the reflection mode). Gold nanoparticles, spheres, rods, or other shapes are quite attractive markers as they never bleach and can be conjugated through thiol chemistry to a number of biomolecules.

3.1. Transmitted Light Microscopy

In bright field microscopy, the sample is often illuminated from the top with a halogen lamp focused through a condenser before the sample plane and the transmitted light is collected by an objective. Köhler illumination produces both an extremely even illumination at the sample and excludes visualization of the light source in the final image. The image contrast is a consequence of absorption in the sample; the various specimen appear darker the more light they absorb. In living cells, the contrast is very low as most cellular material is transparent and colorless. Hence, it can be difficult to detect smaller structures, in particular, without staining. Unfortunately, staining often requires killing and fixing the cells, thus excluding dynamic investigations. Detection is commonly done with CCD or CMOS cameras with time resolutions up to kHz rates.[118,119] Bright field microscopy has often been combined with manipulation techniques. One example is with the use of optical tweezers for force calibration and quantification of viscoelastic properties of endogenous lipid granules inside the cytoplasm of yeast cells[120,121] or with magnetic tweezers using internalized magnetic beads in living macrophage.[122] The advantage of bright field microscopy is that it is simple to use and easy to implement with force spectroscopy techniques. The biggest disadvantage is that the contrast is rather low and staining includes killing the sample. Furthermore, out-of-focus

DOI: 10.1021/acs.chemrev.6b00638
Chem. Rev. 2017, 117, 4342−4375

structures induce significant blur in the images that limits the use for single molecule detection.

3.2. Fluorescence Microscopy

Fluorescence microscopy is based on excitation of fluorophores and detection of the emitted photons that have a red-shifted wavelength compared to the excitation wavelength. Commonly, the microscope is in an epifluorescent configuration where the light is focused through the objective onto the sample, and the emitted light is collected by the objective and passed onto the detector. Different wavelengths for illumination or detection can be separated by beam splitters, filters, or dichroic mirrors. The simplest form of fluorescence microscopy is wide field. Here, the entire sample is illuminated, typically with a xenon or mercury lamp, in a near-cylindrical volume. As all fluorophores are excited simultaneously, fluorescence from outside the focal plane also contributes to the collected emission spectra, leading to higher background and ultimately reducing single molecule detection capabilities significantly.

3.2.1. TIRF. Total internal reflection fluorescence (TIRF) microscopy can in principle be considered a wide field technique as a relatively large lateral plane is illuminated; however, only a small depth, typically up to ∼200 nm from the glass surface, is illuminated. In TIRF microscopy, the laser light irradiates a glass interface at an angle larger than the critical angle, thus leading to total internal reflection. This causes the presence of an evanescent wave that decays exponentially into the sample as a function of distance from the surface. Therefore, only fluorophores that reside within ∼200 nm from the glass surface experience the evanescent wave and may become excited. The restriction in illumination depth means that out-of-focus emission is significantly reduced and single molecules residing close to the surface can be more easily individually visualized. Also phototoxicity and bleaching are reduced, thus allowing longer imaging times. The main drawback of TIRF with respect to in vivo imaging is that only fluorophores located close to the glass surface can be studied (e.g., one can study membrane proteins and receptors in surface bound cells). TIRF microscopes have been combined with optical traps; however, to our knowledge they have so far only been reported for in vitro use.[123,124]

3.2.2. Confocal Microscopy. Confocal microscopy is a technique that has improved resolution and allows optical sectioning compared to wide field fluorescence microscopy. This is done by inserting a spatial pinhole in front of the detector, thus detecting light from only a small volume. Thereby, detection of emission from out-of-focus fluorophores is eliminated spatially before the detector. By axially controlling the focal plane, the sample can be imaged in different depths allowing 3D image reconstruction, which is very attractive for cell imaging. Spherical aberration, however, poses a significant barrier to how deep into tissue one can image in practice. Optimal cancellation of spherical aberration (e.g., by changing the index of refraction of the immersion media of the objective) allows for visualization as deep as hundreds of microns into the sample by simple confocal imaging.[125,126]

Confocal microscopes are typically equipped with a range of excitation lasers, thus providing a wide choice of fluorescent molecules with spectral properties spanning from UV to NIR wavelengths. If the sample contains multiple fluorophores with emission spectra that are well-separated, they can even be imaged simultaneously using acousto-optical beam splitters and rotating photomultiplier tubes. Some confocal microscopes can also be operated in reflection mode that allows for efficient visualization of, for example, AuNPs. The resolution of confocal microscopy is highly dependent on the size of the pinhole. Normally, the pinhole is set to the size of the Airy disc. Increasing the pinhole diameter allows more photons to be collected but causes detection of out-of-focus emitting fluorophores as the detection approaches a widefield configuration. On the other hand, squeezing the pinhole below the size of the Airy disc reduces the photon count. A drawback of confocal microscopy is that acquisition speeds are rather slow, as the entire sample volume must be raster-scanned with the point illumination source. The speed can be increased by scanning a smaller area and by scanning faster, however, with a trade-off on the photon count. Point illumination is also relatively phototoxic and may cause bleaching of fluorophores, even those beyond the focal plane. More sensitive detectors such as photomultiplier tubes or avalanche photodiodes can aid in preventing long exposure times or high excitation intensities and thereby decrease the amount of bleaching and phototoxicity.

As detailed in ref 127 and sketched in Figure 11, optical tweezers can relatively easily be implemented in a confocal microscope simply by guiding a trapping laser beam into the path of the confocal lasers. One beneficial detail about the setup sketched in Figure 11 is that the scanning confocal lasers can be moved independently by the tandem scanner from the trapping laser beam, which can be moved (in 3D) by the telescope. Also, the signals from the confocal and the trap can be independently picked up by the photomultiplier tubes and the quadrant photodiode (QPD), respectively. High quality and user-friendly optical tweezers implemented in a confocal microscope are now also commercially available (e.g., the C-Trap from Lumicks).

3.2.3. Multiphoton Microscopy. Multiphoton microscopy is somewhat similar to confocal microscopy in the sense that it also uses scanning illumination light to create an image and offers optical axial sectioning. The excitation scheme is, however, different as multiphoton microscopy involves excitation of fluorophores by the absorption of two or three photons simultaneously. As the energy is inversely proportional to the wavelength, two photons, each carrying half the energy needed for excitation, can excite a fluorophore. Hence, one usually uses near-infrared photons to excite fluorophores in the visible regime. For live cell imaging, this has the benefit that near-infrared photons can penetrate much deeper into biological material than visible light. As two-photon excitation is a nonlinear effect that requires simultaneous absorption of two photons, excitation only occurs in a very limited focal region, thus increasing the resolution. Often pulsed lasers are implemented to achieve not only spatial but also temporal focusing of the photon flux. Like in confocal microscopy, the emission spectra from different fluorophores can be efficiently separated by beam splitters and spectral filters and collected by sensitive detectors such as photomultiplier tubes. As the likelihood of simultaneous multiphoton absorption is fairly low and often requires a higher flux of photons for efficient emission, this technique is claimed to be relatively phototoxic to a living specimen. One advantage, however, is that outside the focal plane there is only a little photodamage.

3.2.4. Light-Sheet Microscopy. In light-sheet microscopy a thin sheet of light is created through the sample and the emitted fluorescence is detected by an objective oriented perpendicular to the light sheet. The light sheet can, for example, have a Gaussian, Bessel, or Airy beam profile, each

DOI: 10.1021/acs.chemrev.6b00638
Chem. Rev. 2017, 117, 4342−4375

with their specific advantages.[128] The Gaussian beam probably gives the optimal resolution; however, the Airy beam based light sheet provides nearly as good a resolution and has the additional advantage that the field of view is significantly larger than that provided by the other beam geometries. The Airy beam based light sheet microscope has a lateral extension of ~300 μm,[128] and also, less intensity is needed for the Airy beam light sheet compared to the other beam geometries, thus minimizing phototoxicity. The whole sample can be imaged in 3D by moving the sample through the light sheet. The emitted light can be collected in a wide-field fashion increasing the acquisition speed greatly compared to point illumination techniques. The phototoxicity is rather low for this type of microscopy, but the real advantage is the reachable depth. The combination of large penetration depth and little amount of phototoxicity makes light sheet microscopy ideal for imaging live organisms, and as an example, neuronal processes inside the brains of living larval zebrafish have been monitored.[129] Light-sheet microscopy provides image contrast comparable to TIRF, however, with a lower resolution, and can image up to 300 μm into the sample. Hence, whole living organisms can be visualized, even repeatedly, without signs of damage.[114] Most often, the objects of interest are embedded in an agarose gel while visualized by a light sheet microscope. Yang et al. recently demonstrated that tobacco plant cells and living *Spirobranchus lamarcki* larvae can also be held steady in an optical trap while being visualized by light sheet microscopy, thus eliminating the demand for the agarose matrix.[130]

3.2.5. Super-Resolution Microscopy. Over the past decades, several new light-based microscopy techniques have been developed to improve single molecule detection by breaking or bypassing the optical resolution beyond the Abbe limit. These new approaches are termed super-resolution microscopy and were awarded the Nobel Prize in Chemistry in 2014. Although super-resolution microscopy has not fully been realized in combination with force spectroscopy in living cells, here is a brief description of two of the major principal approaches within this class of microscopy.

In stimulated emission depletion (STED) microscopy, super resolution is achieved using patterned light that spatially confines the emission signal to an area much smaller than the classic point spread function.[14,15] Two excitation lasers are used; the first laser excites the fluorescent molecules from their dark states, the second laser (the STED laser) is red-shifted and kicks the electrons back into the ground state by stimulated emission without fluorescence. The STED laser has a doughnut shape, and only fluorophores in the zero intensity center emit. One important issue is the timing of the two laser pulses, the STED laser beam should arrive when the electron is in the excited state. Also, the wavelength of the STED beam should be in the tail of the emission spectrum of the dye without overlapping the absorption spectrum. Two of the fluorophores most often used for STED microscopy are Atto647N and Atto655; they are both excitable at 640 nm and optimally depleted by 750 and 780 nm, respectively.

The width of the zero intensity center sets the resolution of the image which can be improved by increasing the STED laser intensity. In practice, producing a good-quality zero intensity center of the STED laser requires extremely high laser intensities that are associated with phototoxicity for living cells. Also, acquisition is relatively time-consuming as the focal spot must be scanned through the entire sample volume to create the super resolution image. Furthermore, the choice of fluorescent molecules suitable is somewhat limited compared to conventional fluorescent-based microscopy techniques. In vivo STED has been used, for example, to investigate membrane lipid interactions with the cytoskeleton of living cells.[131] In vitro STED, in a linear configuration, has proven useful in combination with optical tweezers to investigate the dynamics of proteins on densely covered DNA.[132]

Stochastic optical reconstruction microscopy (STORM) and photo activated localization microscopy (PALM) are methods in which the image is reconstructed from thousands of images of spatially separated fluorescent molecules, which are excited in a stochastic manner between each image.[16,17] The idea is that the precise location of a single emitting fluorophore which is separated spatially from other fluorophores can be determined with a precision down to ~10 nm. The separation needs to be large enough that the two point-spread-functions (PSFs) do not overlap. Also, two molecules in close proximity can be spatially distinguished if their emission spectra do not overlap in time or in wavelength. In practice, the separation of identical fluorophores with overlapping PSFs can be achieved by stochastically activating a small subset of fluorophores in each image, thus lowering the likelihood that neighboring fluorescent molecules are emitting at the same time. Subsequently, the fluorophores are deactivated or bleached, and a new subset of fluorescent molecules stochastically activated. Thousands of individual images containing well-separated point-spread functions are then processed by fitting algorithms and their centroids combined to a super-resolved map of the sample. The localization accuracy of STORM/PALM is highly dependent on the number of photons collected from each fluorophore. More photons can be collected by increasing the excitation laser intensity; however, this will inevitably increase phototoxicity and bleaching. The photon count can also be improved by increasing acquisition time, but this is also a trade-off. The fluorophores used must be photoswitchable or photoactivatable and highly photostable to sustain multiple cycles of activation/deactivation.

As of now, super-resolution microscopy is limited to rather slow live cell processes and small imaging volumes. In the case of STORM related methods, the imaging volume is equal to the TIRF volume, hence, only within hundreds of nanometers from the coverslip. Furthermore, both above-mentioned techniques require fluorophores with special photochemical/physical characteristics which is a limitation in comparison to other microscopy techniques (e.g., confocal microscopy), where 3D live cell imaging is possible with essentially any fluorescent molecule and in multicolored combinations.

3.2.6. FRET. Förster resonance energy transfer (FRET) is based on a nonradiative energy transfer from an excited donor chromophore to a proximal acceptor chromophore that has a red-shifted excitation spectrum compared to the donor. FRET processes can be detected using any kind of fluorescence microscopy (e.g., wide-field or confocal). FRET efficiency is very sensitive to the distance between the FRET pairs, and the intensity of the emitted spectrum is used as a measure for distance between the fluorophores. FRET in living cells is challenged because of cellular autofluorescence and intracellular environmental factors such a pH and ion concentrations that fluorophores can be highly sensitive to. FRET pairs have also been used in molecular force spectroscopy where FRET intensity changes were used to measure local forces involved in, for example, cell adhesion and conformational changes.[133]

DOI: 10.1021/acs.chemrev.6b00638
Chem. Rev. 2017, 117, 4342−4375

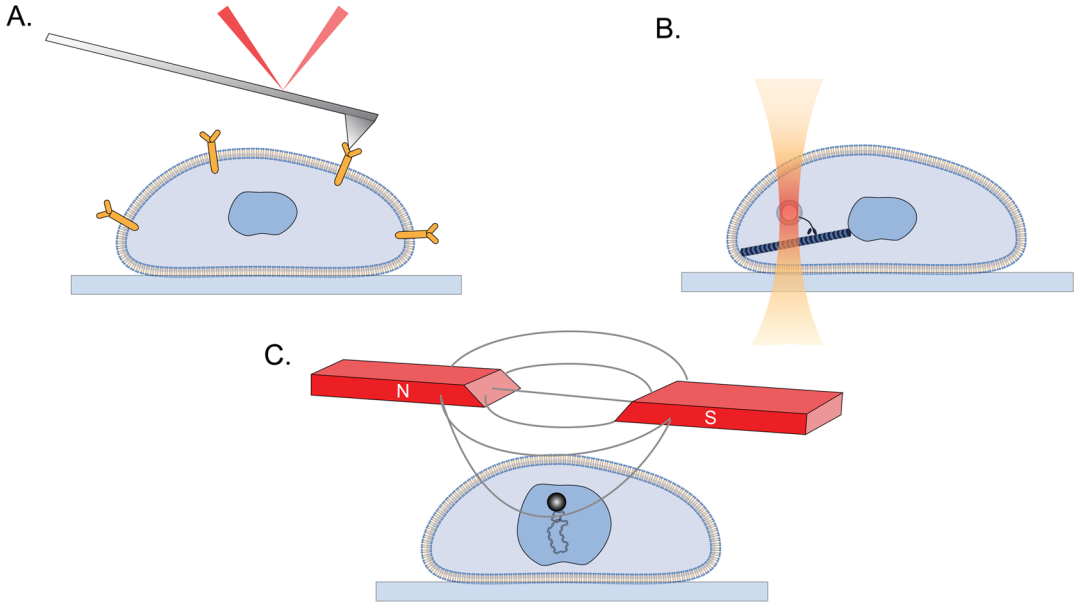

Figure 12. Sketches of the tools most commonly used for manipulation of single molecules or organelles in cells. (A) A tip attached to a cantilever of an atomic force microscope probes the adhesion of a surface receptor. The laser reflected off from the cantilever provides information about the bending of the cantilever. (B) An optical trap consisting of a single tightly focused laser beam traps a lipid granule that is being carried by the molecular motor dynein inside a living cell. (C) External magnets, forming magnetic tweezers, allow for the rotation of a magnetic probe attached to DNA inside the nucleus of a live cell.

3.3. Force-Sensing Fluorophores

As an alternative to techniques that measure forces mechanically, there exists fluorophores whose emission is correlated with the force applied to them. These force-sensing fluorophores, or fluorophore pairs, have their sensitivity in the pico-Newton range which is a relevant range for studying cellular processes. The emission of a fluorophore pair can vary as the distance between them is changed by local tension (e.g., if they are FRET pairs or if certain quenching/unquenching strategies are employed). For example, Grashoff et al. developed a vinculin-based tension sensor module that could measure the forces during cell adhesion and migration as the sensor module connects cell surface receptors to the actin cytoskeleton.[134] The module consisted of a nanospring inserted between the head and tail domains of vinculin and a FRET pair whose fluorescence decreased as the spring was stretched separating the fluorophores. Iwai et al. used green fluorescent proteins to detect strain between myosin II and F-actin in living cells.[135] Here, the module consisted of two green fluorescent proteins (GFPs) that were inserted between two motor domains of myosin II. In the absence of strain, the two GFPs were in direct contact providing a monomeric emission spectrum, whereas interactions with F-actin induced mechanical conformational changes provided a distinguishable emission spectrum. As a last example, Stabley et al. used a quenching-based tension sensor module to probe the forces involved in early stage receptor-mediated endocytosis.[136] The module was designed such that fluorophores were attached to the targeted ligand and linked via a polymer to a surface functionalized with quencher molecules. Cellular forces exerted onto the ligand via receptor−ligand interactions resulted in an extension of the linker which removed the fluorophores from the quenchers and increased the fluorescence intensity.

To use force-sensing molecules, many of the technical requirements are similar to those of mechanical force spectroscopy; the fluorescent molecule needs to be internalized without compromising the integrity of the cell, be stable inside the cell, localize specifically at its target site, and support a sufficient load. Importantly, the molecule into which the force sensing module is inserted needs to retain its biological function. Also, proper calibration of the probe's force sensitivity is necessary for reliable readouts. So far, many of these sensors lack single molecule sensitivity, and improving the spatial and temporal resolution is crucial; however, such improvements are likely to be realized in the future and will pave the way for exciting in vivo force measurements using force sensing fluorophores.

4. CELL AND SINGLE MOLECULE MANIPULATION

Most of the imaging techniques described in the preceding section work well in combination with the remarkable in vivo manipulation tools, which have been developed and refined within the last ∼30 years. In this section, the three most commonly used techniques for in vivo single molecule and single organelle manipulation are presented: the atomic force microscope (AFM), optical tweezers, and magnetic tweezers (sketched in Figure 12). The capability to perform quantitative measurements of the forces at play during dynamic processes inside living cells has gained much attention as the crucial role of force for cellular development and behavior is becoming more and more acknowledged in the literature.[137] Selected examples of exciting research performed with these techniques are provided in section 5 of this review.

4.1. Challenge of Measuring Forces in Vivo

In vivo, it cannot be ignored that the individual molecules and organelles are present in a matrix, be it the cytoplasm, the membrane or the nucleus, and the physical properties of this matrix, as well as the interaction between the matrix and the individual molecules and organelles, are highly relevant to uncover. Therefore, much effort has been put into determining the material properties of the living cell, both by early magnetic

DOI: 10.1021/acs.chemrev.6b00638
Chem. Rev. 2017, 117, 4342−4375

methods,[138] by magnetic tweezers,[122,139,140] and by optical tweezers.[23,121]

Although the force exerted by these tools in theory can be calculated directly, in a real experiment there are typically many unknown parameters, for instance the material properties inside the cell. Therefore, in order to make quantitative force measurements, the techniques need to be calibrated. There are several ways to perform such a calibration, but all three techniques can be calibrated by observing the thermal fluctuations of the manipulated objects (or of the AFM cantilever) around an equilibrium position. To a first, and often very good, approximation, the force F exerted by the manipulation tool is Hookean (i.e., the restoring force scales linearly with the distance from equilibrium, x). The force is written as $F = -kx$, and the associated Hookean trapping potential is harmonic. If the motion takes place in a purely viscous fluid, the thermal fluctuations are well-described by simple Brownian diffusion. Simple Brownian diffusion at absolute temperature T in a harmonic trapping potential would then result in the following relation between position fluctuations and the spring constant, or trapping stiffness, k:

$$\langle x^2 \rangle - \langle x \rangle^2 = \frac{k_B T}{k} \tag{12}$$

Hence, by recording the handle's positions, k can be determined through calibration and finally the force acting on a trapped particle can be found. However, the cell cytoplasm is not a purely viscous fluid, and calibration of manipulation techniques inside the cytoplasm is significantly more cumbersome than in a viscous fluid.

4.2. Handles

Normally in force spectroscopy techniques, the investigated biomolecule is attached to a handle through which the force is applied and measured. Ideally, the handle should be attached in a one-to-one ratio and in a way that does not interfere with the biological system. Manipulation and force-sensing on the surface of cells can readily be done using most techniques by, for example, attaching the handle to cell surface receptors. Probing intracellular biomolecules, however, necessitates bringing the handle inside the cell which can be complicated or highly invasive. For example, an AFM transduces force through a tip that needs to be mechanically connected to the cantilever and therefore cannot reach the inside of the cell without penetrating the cell wall. In contrast, optical and magnetic tweezers operate by exerting forces onto the handles by externally applied fields which readily penetrate into the cell with only little physiological damage provided the correct choice of, for example, laser wavelength, power, and irradiation time.[141,142] As detailed later, optical tweezers can manipulate objects endogenously present inside living cells, but often, and always for magnetic tweezers, there is a need to insert handles into the living system of interest. Also, biocompatibility and cytotoxicity of the handle are crucial concerns that should be addressed when designing the experiment.

4.2.1. Internalizing Handles. Different strategies can be employed for internalizing nonendogenous handles as, for example, polystyrene, metallic, or magnetic particles. One option is to take advantage of the cell's own pathway for intracellular uptake of nutrients, signaling molecules, and receptors. This pathway is known as the endocytotic pathway and can facilitate the uptake of particles ranging in size from nanometers to microns, corresponding well with the size range that can be trapped both by optical and magnetic tweezers. The simplest way of triggering endocytotic uptake is by adding the particles to the cell medium. When the particles come into contact with the outer membrane, either by nonspecific adhesion or receptor recognition, the plasma membrane invaginates thus forming a lipid vesicle around the particles, called an endosome. After internalization, particle-loaded endosomes often enter the intracellular trafficking pathway leading to fusion with lysosomes.[143] These are essentially degradative compartments with low pH and various enzymes responsible for digesting the content. If the endocytosed particles should be used as handles, one should either be aware that they will reside inside a vesicle, or they must be released from the endosomes or lysosomes. Also, endocytosed particles will enter the endocytotic pathway, and if any other locations should be probed, the particle must literally be dragged through the crowded cell (by means of the tweezers) to the position of interest. Some strategies for endosomal release are based on conjugating the particles with cell-penetrating peptides[143,144] while others employ the heating capabilities of metallic nanoparticles to melt and permeate the lipid membrane of the endosomes.[145]

As a rule of thumb, the rate of endocytosis is inversely related to particle size and for most cell types effective uptake takes place if the handles are smaller than ∼100 nm.[143,146] For this reason, the use of metallic nanoparticles and quantum dots as handles is attractive as they are smaller while still easier to stably trap and visualize. Care should be taken though if metallic nanoparticles are used as they can heat their surroundings substantially in the power regime used for optical trapping.[147] In contrast, quantum dots and magnetic particles do not heat significantly in electromagnetic fields.[148] Another factor affecting the endocytotic efficiency is surface charge[149] that can readily be adjusted by correct surface functionalization by neutralizing molecules (see discussion in section 4.2.2).

Micropipetting is a delivery method that in principle enables delivery of particles anywhere in the cytosol.[144,150] Here, the handles are injected by penetrating the cell wall with a fine-tipped microcapillary (diameter of 0.2−0.5 μm) in femtoliters volumes.[144,150] The injection is conducted while visualizing the cell in a microscope to guide the microcapillary insertion. Although this technique offers control over the handle distribution inside the cell, it includes penetrating the cell wall which can have consequences for the cell viability. Furthermore, a successful injection is highly dependent on cell morphology, substrate adhesion, and the thickness/mechanical properties of the cell wall. Another method to deliver femtoliter volumes of particles to specific cells is by encapsulating the particles in a vesicle, and through hot-nanoparticle-mediated fusion deliver the particles to the cells of interest.[151]

Handles can also be inserted by electroporation that uses an electric pulse to temporarily create pores in the cell wall. This technique provides a fairly homogeneous distribution of the handles inside the cell and is well-suited for delivering a large amount of handles.[144] Photoporation is yet another technique where the handles are optically injected. It uses a tightly focused laser beam to create multiple submicron holes in the cell wall through which the surrounding medium containing the handles can enter the cell in volumes of femtoliters.[152] Endocytosis and electroporation enable delivery to many cells simultaneously, whereas micropipetting, photoporation, and hot nanoparticle mediated fusion enable delivery of handles to a

DOI: 10.1021/acs.chemrev.6b00638
Chem. Rev. 2017, 117, 4342−4375

specific cell in a controlled fashion. Another important consideration is that, except for endocytosis, all techniques are fairly invasive and require recovery of the cell wall as it might otherwise be compromised.

4.2.2. Reducing Unspecific Bindings and Probe Contamination. A huge challenge when conducting force spectroscopy inside cells is that the handle is constantly exposed to unspecific bindings and contaminations. For example, the handle can be attached to multiple molecules simultaneously, to multiple sites on the molecule of interest, or to a molecule not of interest. The most common way to deal with unspecific bindings is by using adhesion of inert molecules that passivate the surface of the handle. Proteins such as bovine serum albumin and α-casein are very efficient at suppressing unspecific bindings, but also nonionic surfactants such as polyethylene glycol (PEG) have been successfully used. Reducing unspecific bindings is a key element in collecting trustworthy data, but in most intracellular experiments, it will be impossible to completely eliminate them. Often, the measurements curve will bear signs of whether single or multiple molecules were manipulated, but under all circumstances, intelligent and reliable control experiments are absolutely crucial.

Ideally in force spectroscopy, the handle and the molecule of interest are specifically attached. That is, the experiment is designed such that the handle carries a characteristic signature that the molecule recognizes and binds specifically to. This strategy is often facilitated by means of conjugation schemes such as receptor−ligand or antibody−antigen bindings, where one component is attached on the handle and the other at a specific location on the probed molecule. Specificity can be increased by reducing the number of conjugates available on the handle and on the probed molecule, thus increasing the likelihood of one-to-one binding. Preferentially, the bonds between the handle and the molecule should be strong enough to support the highest force applied by the force spectroscopy technique, or at least comparable to it. Popular bonds for specific conjugations involving beads are the biotin−streptavidin bond, which has nearly the same strength as a covalent bond, or the antibody−antigen pair, digoxigenin-antidigoxigenin. Proteins are often attached via histidines and reactive cysteine residues.

4.3. Atomic Force Microscopy

The AFM was invented ∼40 years ago.[9] Its principle of action is similar to the scanning tunneling microscope (STM) in the sense that both rely on a cantilever with a very sharp tip moving above a surface of interest, approaching or possibly attaching to a molecule of interest, as illustrated in Figure 12A. If the cantilever tip firmly attaches to a molecule, the cantilever bends slightly, and this bending can be measured by a laser reflected off the back side of the cantilever. The AFM can be used for scanning a surface but also as a force-transducer to directly probe the elastic response or adhesional properties of a whole cell stuck to a glass surface, or of a single molecule extracted from a cell. The force-range that one may investigate with an AFM is determined by the physical properties of the cantilever, and much effort has been put into refining AFM for investigations on cells.[153]

The AFM works well both in gaseous and aqueous environments. The typical force-range is the pN to nN regime and in vivo AFM has been used to study the deformability of cell surfaces,[154−156] adhesive forces between cells or surfaces and cells,[157] and also adhesion forces of single molecules.[158]

For force spectroscopy with a cantilever based technique, like AFM, the cantilever would a priori be positioned outside the cell in the surrounding medium, which is commonly a viscous liquid like an aqueous medium. Hence, the force calibration can be based on thermal fluctuations in a normal viscous fluid as alluded to in section 4.1. Therefore, force calibration is relatively straightforward and not hampered by unknown viscoelastic characteristics of the cell interior.

During the development of AFM functioning in biocompatible aqueous environments, an alternative method relying on a soft probe rather than a sharp tip at the edge of the cantilever was also developed.[159] This technique is known as the biomembrane force probe (BFP) and works by having a handle, a microscopic sphere, glued to a lipid vesicle held under controlled tension by a micropipette. The BFP has a wide force-range of 0.1−1000 pN, which is enabled by the versatility in the choice of vesicle size, vesicle membrane composition, and properties of the micropipette. One drawback of the BFP is that the technique turned out to be somewhat inaccurate in force determinations. Recently, a combination of single molecule fluorescence detection and the BFP method was demonstrated.[160]

If either AFM or BFP is used to measure the rupture force of a bond, then one should be aware that the measured force is highly dependent on the loading rate (the increase of force per unit time). The so-called Bell-Evans relation between the loading rate, ν, and the rupture force, F, is as follows:[161]

$$\nu = \nu_0 \exp\left(\frac{F x_\beta}{k_B T}\right) \tag{13}$$

where x_β is a length over which the force, F, is applied and ν_0 is a constant. From this expression, for example, the force at zero loading rate can be extracted.

4.3.1. AFM Tips. In the AFM, force sensing is mediated by a tip that is mechanically connected to the cantilever. For this reason, AFM is not considered a contact-free technique. Hence, AFM and related techniques mainly probe biological systems on the outside of the cell by, for example, stretching bonds or mapping out surfaces, as membrane penetration can be fatal for the cell. The simplest way to probe a biological system using AFM is by nonspecific attachment. However, as the cantilever is often much larger than the probed molecule, it can be difficult to distinguish whether it is attached (i) to the correct molecule, (ii) at the correct location on the molecule, and (iii) to one or multiple sites on the molecule. As discussed in the previous subsection 4.2.2, nonspecific attachments can be suppressed by passivating the tip with surface neutralizing proteins or polymers. If the attachment is specific with conjugation schemes such as streptavidin−biotin bonds, so-called molecular handles, it is important to take their mechanical contribution into account. A possible solution to address whether multiple or unspecific molecules are attached to the tip is by using a linker with a compliance signature that can confirm if the linker was correctly attached.[162] For example, the probed molecule can be linked with a DNA strand displaying a characteristic overstretching transition at 65 pN.[163]

4.4. Optical Tweezers

In the simplest implementation, optical tweezers are formed by tightly focusing a single laser beam with a Gaussian intensity profile. The first publication demonstrating how radiation

DOI: 10.1021/acs.chemrev.6b00638
Chem. Rev. 2017, 117, 4342−4375

pressure from a continuous laser can be used to accelerate and trap micron-sized particles was published as early as 1970 by Arthur Ashkin, the father of optical tweezers.[5] In later investigations, Ashkin and co-workers proved optical trapping to be extremely versatile, also for manipulating living cells which appeared to stay viable in optical traps based on near-infrared lasers.[6−8] As detailed in section 5, optical tweezers have found widespread use for probing biological specimen, both in vivo and in vitro, at the single molecule to whole cell level. With a wise choice of wavelength in the near-infrared regime and limited laser powers and exposure times, optical tweezers appear to be nearly noninvasive.[141,142]

Even without focusing, light with a propagation direction, z, and an intensity profile, $I(x,y)$, narrowly centered around the z-axis ($x = 0$, $y = 0$, z) will, through the interaction between the electrically induced dipole and the electrical field from the light beam, attract permanent or inducible dipoles. Hence, if a particle is made of dielectric material with refractive index larger than that of the surrounding medium then the particle will be drawn toward the most intense part of the laser beam.

For most of the published in vitro applications of optical tweezers, the dielectric material trapped would be a polystyrene or a silica microsphere, but an entire cell is also a (complicated) dielectric object and can similarly be optically manipulated. As explained quantitatively below, an appropriate intensity profile can create an attractive potential in the (x, y)-plane for the dielectric material. In order to enable manipulation also in the direction of propagation, here the z-axis, an intensity gradient in the z-direction is required. Figure 12B shows an example of an optical trap, formed by focusing a laser beam with a Gaussian intensity profile in the axial direction. The optical trap is in this example used to manipulate a cargo transported along microtubules inside a living cell.

If the dielectric object is small compared to the wavelength of the light, the induced dipole moment of the dielectric object, $\mathbf{p}$, can be considered a point dipole and is proportional to the electric field, $\mathbf{E}$, with which it interacts. The dipole, $\mathbf{p}$, and the interaction potential created by the optical trap, $V_{\mathrm{dip}}^{\mathrm{OT}}$, are related through the following expression:

$$\mathbf{p} = \alpha\mathbf{E};\ V_{\mathrm{dip}}^{\mathrm{OT}} = -\frac{1}{2}\langle\mathbf{p}\cdot\mathbf{E}\rangle = -\frac{1}{2}\alpha\mathbf{E}^2 \tag{14}$$

where α is the polarizability of the object. The force acting on the dipole is then given as

$$\mathbf{F}_{\mathrm{dip}}^{\mathrm{OT}} = -\nabla V_{\mathrm{dip}}^{\mathrm{OT}} = \frac{\alpha}{2}\nabla\mathbf{E}^2 \tag{15}$$

The polarizability, α, is related to the relative index of refraction $m \equiv n_{\mathrm{object}}/n_{\mathrm{medium}}$, where n_{medium} and n_{object} are the refractive indices of the medium and the object, respectively. The polarizability is positive when $m > 1$, or $n_{\mathrm{object}} > n_{\mathrm{medium}}$, and as a result, the force points in the direction of increasing light intensity.

If the dielectric object is large compared to the wavelength of the light, the object can no longer be considered a point dipole and a ray-optics picture better describes the situation. Conservation of momentum leads to the conclusion that the object is attracted by the highest light intensity if $n_{\mathrm{object}} > n_{\mathrm{medium}}$, and 3D trapping is possible with a single tightly focused Gaussian beam.

Often the wavelength of the trapping laser beam is on the same order as the dimension of the trapped object. In this case, force calculations are not as straightforward as in the two regimes outlined above, but ref 164 devises how to calculate the trapping forces in any regime. In practice, however, the force in a real experiment is found by calibrating the optical trap as described in section 4.4.2 below.

4.4.1. Handles for Optical Tweezers. The force that can be exerted by an optical trap on a trapped object, the handle, correlates with the size and polarizability of the particle. Figure 13 shows some of the most typical handles used for in vivo

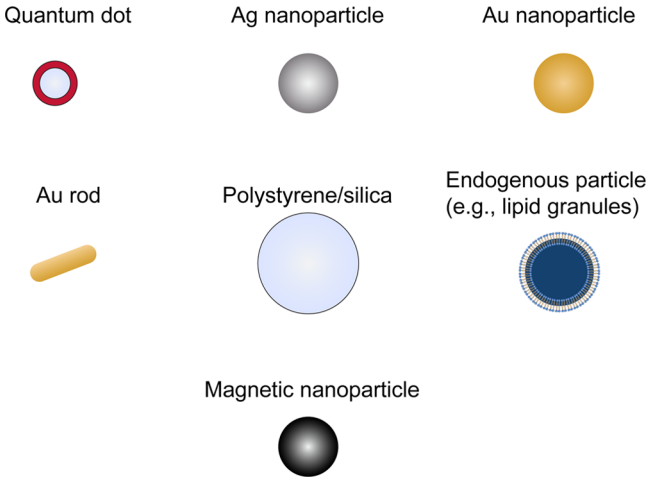

Figure 13. Handles most commonly used for in vivo single molecule manipulation techniques inside living cells. For optical tweezers there exists a variety of handles from large micron-sized dielectric beads to small metallic and semiconductor nanoparticles as well as naturally occurring lipid granules and organelles. In contrast, magnetic tweezers can only grap and manipulate magnetizable objects.

manipulation with optical tweezers. Dielectric particles like the popular polystyrene and silica beads can be stably trapped in sizes ranging from ∼200 nm to several microns,[164] and polystyrene microscopic particles trapped at normal laser powers typically heat less than a couple of degrees Celsius.[165] Metallic nanoparticles with diameters as small as 10 nm can be trapped individually by a single laser beam,[166,167] even gold nanorods, which align with the polarization of the trapping laser beam.[168] One should, however, be aware that metallic nanoparticles have a large absorption cross section, even in the near-infrared, hence, these particles may heat substantially, up to hundreds of degrees Celsius, while irradiated.[147] This heating of trapped metallic nanoparticles can, however, also be used in an advantageous manner (e.g., for photothermal treatment of cancer).[169] In addition, metallic nanoparticles have very high luminescence and no photobleaching, hence, they are excellent for visualization. Metallic nanoparticles are commercially available in a good quality in sizes ranging from 5−250 nm, and gold nanoparticles even offer easy surface modifications by thiol-chemistry. One should be aware, though, that silver nanoparticles can be cytotoxic due to their oxidative nature[170] and that the synthesis of gold nanorods involves high concentrations of cytotoxic surfactants.

Another nanoparticle that can be used both as a force-transducing handle for optical trapping and for visualization is a quantum dot.[171,172] Quantum dots typically have overall diameters of 2−30 nm.[171,173] Notably, their trapping strengths do not simply correlate with size but are comparable to trapping strengths reported for metallic nanoparticles.[171,172] Because of their fluorescent properties, quantum dots are easily

DOI: 10.1021/acs.chemrev.6b00638
Chem. Rev. 2017, 117, 4342−4375

visualized and localized in the cytoplasm of cells, a task that can be challenging with other nonfluorescent handles. In addition, the trapping laser can act simultaneously as a source of two-photon excitation for the quantum dot, hence a second excitation source becomes unnecessary for visualization.[171]

What really separates optical tweezers from other force spectroscopy techniques is the capability of trapping any object that has an index of refraction mismatch compared to the surrounding medium. Simply speaking, any structure that can be distinguished in bright field microscopy can also be trapped. Therefore, optical tweezers are capable of trapping endogenous lipid granules and organelles.[174,175] These endogenous handles are highly attractive for intracellular force spectroscopy because they are a natural part of many cellular processes such as transport by molecular motors[174] that thereby can be directly studied with minimal perturbation of the system. Also the lipid granules are excellent probes for studying microrheological properties of the cytoplasm, as detailed in section 5.

4.4.2. Quantitative in Vivo Force Measurements Using Optical Tweezers. Several methods have been proposed in literature to quantify forces inside living cells. The simplest assumption is that the force exerted by an optical trap on a handle inside a cell would be the same as the force exerted on a handle of similar size, shape, and optical properties, in a viscous liquid of similar refractive properties as the cell cytoplasm.[174,176−178] This approach assumes that the cytoplasm behaves as a purely viscous fluid and one should thus be able to employ the same techniques for quantitative force calibration that have become standard for calibration in simple fluids within the optical tweezers community.[179−182]

It is, however, a fact that the cytoplasm of a living cell is not purely viscous. For this reason, it is not completely correct to use the same calibration methods as in a purely viscous fluid. To quantify forces inside a living cell for which numerous parameters are unknown, the optical trap needs to be calibrated in situ. One method proposed for in situ calibration consists of a combination of passive and active measurements, as detailed below and in refs 120, 183, 184. A similar approach assumes a typical and plausible model for the cytoplasm characteristics,[185] however, by imposing a particular model for the viscoelastic nature of the cytoplasm, fewer free parameters can be extracted from the experimental data.[185]

In the following, we detail the steps in the measurement protocol for the active-passive calibration method suggested in refs 120, 183, and 184, for which the experimental setup is sketched in Figure 14. For the passive calibration measurement, the positions visited during the thermal fluctuations of several handles are recorded, Fourier-transformed, and the average power spectrum, $P(\omega)$, of the different measurements is calculated.

The first active measurements, referred to as active force calibration, drives the system by oscillating the sample stage sinusoidally with respect to the laser with driving frequency ω and amplitude A_S. The positions of the stage, $x_S(t) = A_S \sin(\omega t + \phi_S)$, and the handle, $x_P^{dr}(t) = A_P \sin(\omega t + \phi_P)$, are recorded simultaneously. The amplitude and phase of the handle's movement can be extracted from the recorded position by fitting the relaxation spectrum $\tilde{R}(\omega)$ to the Fourier transformed experimental data:

$$\tilde{R}(\omega) = \frac{A_P}{\omega A_S}(\sin \Delta\phi - i \cos \Delta\phi) \tag{16}$$

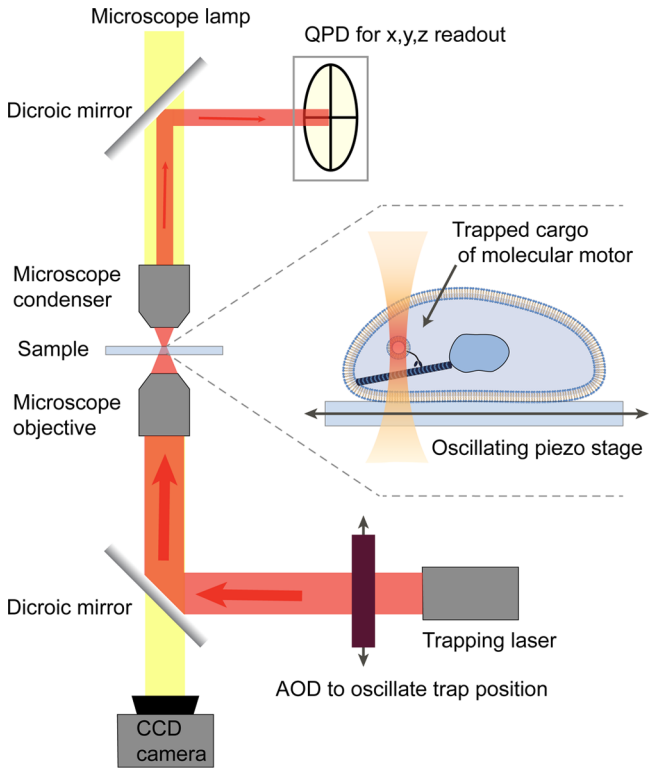

Figure 14. Sketch of an optical tweezers setup that enables calibration and quantitative force measurements, also within a live cell. The calibration is based on (i) observation of thermally induced (passive) fluctuations of the handle in the trap and (ii) observation of the response of the handle when either the trap or the stage is oscillated at fixed frequency and small amplitude.

Here $\Delta\phi$ stands for the phase difference and is given by

$$\Delta\phi = \phi_P - \phi_S \tag{17}$$

To directly translate the voltage output of the QPD to SI units, another step, direct positional calibration, is needed. A conversion factor $\beta = \frac{x_{SI}}{x_V}$, relating the position (x) measured in SI units (meters) to the position measured in volts, is determined by separately recording the oscillations by a QPD and by a CCD camera and comparing the amplitudes of the movement from a sinusoidal fit to the experimental data.

To correctly determine the conversion factor β, a pixel size calibration has to be performed to relate pixel size of the CCD camera to SI units. This is achieved by moving a bead, which is stuck to the bottom of a sample chamber, in both lateral and axial direction in predefined steps, while imaging with a CCD. The movement in lateral and axial direction can either be tracked by using software packages like "Video Spot Tracker" or by turning the images into binary images, where the bead is depicted as a white ring on black background. The position of the center of the ring can be interpreted as the bead's lateral position, while the ring's diameter can related to the axial position.[186] By plotting the linear and axial displacement in pixels as a function of displacement in nm, the effective pixel size in nm per pixel can be extracted by a linear fit.

The last active measurement, phase correction calibration, determines the time delay of the acquisition card used for simultaneous readout of the QPD signal and the stage positions. Determining the time delay is necessary, as it otherwise causes systematic errors. When purchasing a data

DOI: 10.1021/acs.chemrev.6b00638
Chem. Rev. 2017, 117, 4342−4375

acquisition card, this fact should be taken into account and a card with fast readout should be chosen. Since the QPD signal is delayed compared to the sample stage position, the phase difference given in equation 17 must be corrected for the delay: $\Delta\phi^{corr} = \Delta\phi - \Delta\phi^{delay}$. This delay calibration only needs to be performed once for a given acquisition card. The time delay is found by oscillating a stuck bead and tracking the position of the bead by a QPD and simultaneously recording the stage position. The phase difference, $\Delta\phi^{delay}$, is determined by extracting the phase of the movement by fitting the bead and stage data with a sinusoidal function.

The trap stiffness, k, can be calculated by using the information gained from the calibration steps. For example when the experiment is performed with stage driving, k is given by the following equation, for each value of the driving frequencies ω:

$$k = \frac{2k_BT}{P(\omega)}\frac{A_P}{\omega}\sin\Delta\phi \tag{18}$$

When the trap stiffness k is found, the value can be used to calculate the elastic modulus $G(\omega)$, which characterizes the viscoelastic properties of the cells' cytoplasm:

$$G(\omega) = \frac{i\omega}{6\pi r}k\frac{\tilde{R}(\omega)}{1 - i\omega\tilde{R}(\omega)} \tag{19}$$

where r is the radius of the handle, which can be extracted from CCD images.

When applying the active-passive calibration method, care must be taken while choosing the oscillation amplitude and frequency. Even though a larger amplitude will lead to a better signal-to-noise ratio, the excursion of the handle must not exceed the harmonic trapping potential of the optical tweezers nor the linear regime of the QPD, in which the distance the handle has moved is proportional to the voltage signal of the QPD. Also, the oscillation amplitude should be small enough to not interfere with the viscoelastic medium (i.e., the cell cytoplasm). Most importantly, the theory on which this calibration method is built is only valid for small excursions, which limits the amplitude size. Choosing the amplitude to be about half the width of the trap $(k_BT/k)^{1/2}$, will ensure that the above-mentioned conditions are met.

The active−passive calibration method assumes that the optically trapped handle is not affected by active processes. That active processes do not contribute may be checked by observing that the value of k returned by equation 18 is constant and independent of the driving frequency. If k varies with driving frequency (more than the experimental error) in a certain frequency range then this is an indication that active biological processes take place at those frequencies wherefore these frequencies should be avoided. The frequency range available when oscillating the stage is limited. To reach higher frequencies, one can instead oscillate the optical trap, as also indicated in Figure 14. Additionally, when oscillating the optical trap, direct positional calibration can be omitted, as the conversion factor β can be directly deducted from the oscillation amplitude.

Further details of the calibration methods may be found in refs 184 and 185, and a detailed step-by-step guide to the active−passive calibration method can be found in ref 187.

4.5. Magnetic Tweezers

Magnetic tweezers rely on the interaction between a magnetic field and a permanent magnet or a magnetized object and are capable of inducing torque on biological molecules attached to the handle.[188−191] The force-range for magnetic tweezers are on the order of tens of fN to tens of pN. Similar to optical tweezers, one may understand the functioning of the magnetic tweezers as a result of a dipole-field interaction, in this case between an object of magnetic dipole moment μ and a magnetic field, $\mathbf{B}$. Here, the interaction can be described by the interaction potential, V_{dip}^{MT} and the force $\mathbf{F}_{dip}^{MT}$,

$$V_{dip}^{MT} = -\boldsymbol{\mu}\cdot\mathbf{B};\ \mathbf{F}_{dip}^{MT} = -\nabla V_{dip}^{MT} \tag{20}$$

For a permanent magnetic dipole, the force is simply proportional to the gradient of the magnetic field whereas for, for example, a paramagnetic bead which has a dipole moment that depends on the magnetic field, the final expression for the magnetic force is more involved. An experiment where magnetic tweezers rotate double-stranded DNA within the cell nucleus is illustrated in Figure 12C.

For magnetic tweezers acting in a normal viscous fluid, the force is also typically determined from an analysis of Brownian fluctuations of the magnetic handle, which is attached to the molecule of interest (e.g., to a single DNA tether). Hence, it is assumed that the recorded positions of the bead represent positions that are distributed according to the potential energy landscape created by the magnetic force acting on the handle and the forces resulting from DNA's linear and torsional elasticity. For small extensions of the DNA, l, its linear elasticity is well-described by a Hookean spring. Therefore, the longitudinal and transverse fluctuations of the handle may be characterized by effective trap stiffness', $k_{\parallel}$, and $k_{\perp}$, related by the expressions[189]

$$\begin{aligned}\langle z^2\rangle - \langle z\rangle^2 &= \frac{k_BT}{k_{\parallel}} = \frac{k_BT}{\partial F_{dip,z}^{MT}/\partial z}\\ \langle x^2\rangle - \langle x\rangle^2 &= \frac{k_BT}{k_{\perp}} = \frac{k_BT}{F_{dip,z}^{MT}/l}\end{aligned} \tag{21}$$

These spring constants can then be used to determine the force and torque acting on the handle.

4.5.1. Handles for Magnetic Tweezers. Magnetic tweezers require a handle which is either a permanent magnet or a magnetizable object (see Figure 13). Since there do not exist any cellular magnetic structures, in vivo application of magnetic tweezers requires the internalization of a handle which is typically done either by means of endocytosis or microinjection. Superparamagnetic beads come in sizes ranging from ∼500 nm to 5 μm. They are normally composed of a porous matrix sphere in which 10−20 nm magnetic nanoparticles (e.g., iron oxide nanoparticles) are embedded. The sphere is typically enclosed in a polystyrene or silica shell to protect the encapsulated magnetic nanoparticles and to provide a surface for modifications. Cobalt and nickel are also highly magnetic materials but are toxic and therefore not applicable for live cell experiments.

4.6. Alternative Methods Holding Promise for Future in Vivo Manipulation

In this section, we outline a couple of methods that have not yet been demonstrated for in vivo manipulation of single molecules or organelles, but which do hold promise for future in vivo exploration.

4.6.1. Acoustic Force Spectroscopy. Acoustic manipulation of entire cells is a well-founded technique[192] that has

DOI: 10.1021/acs.chemrev.6b00638
Chem. Rev. 2017, 117, 4342−4375

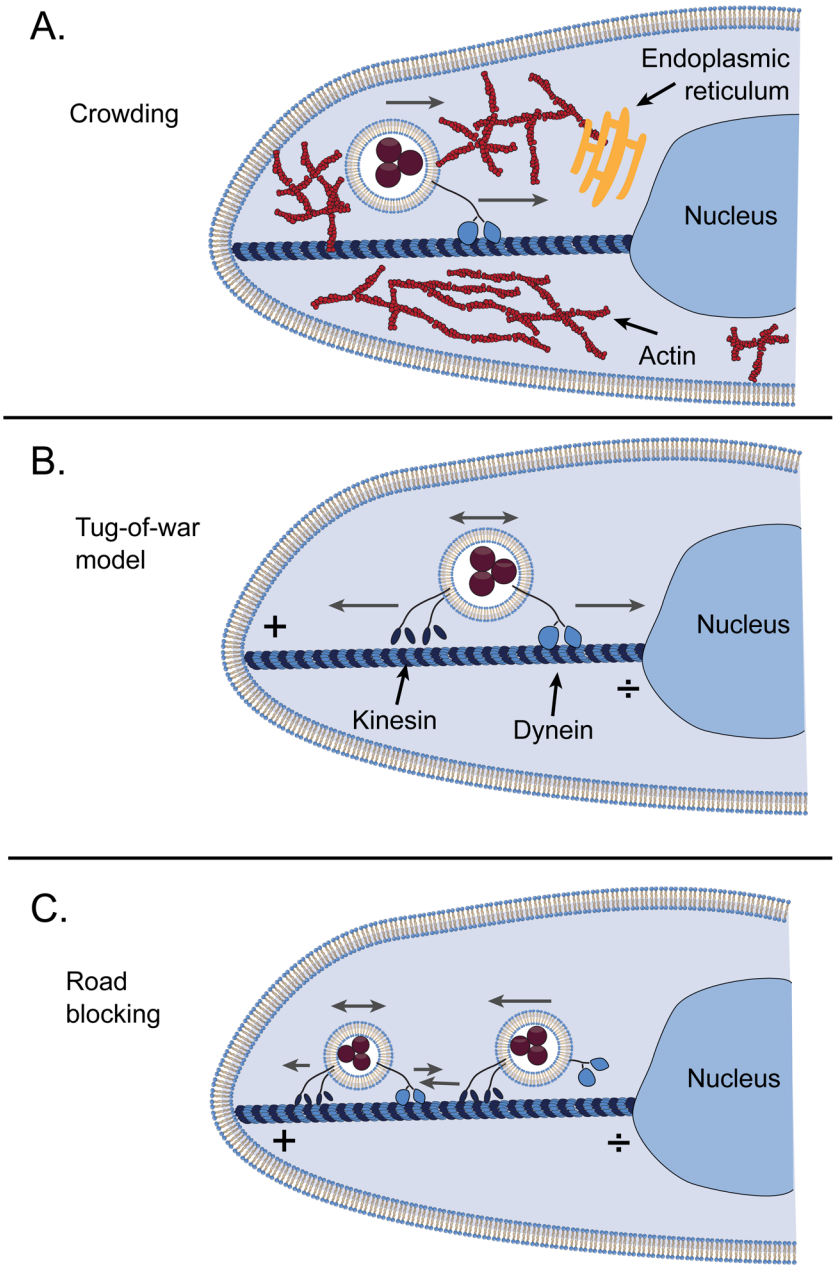

Figure 15. Illustration of different types of molecular motor motion in the complex intracellular environment. (A) The cytoplasm is highly crowded due to the presence of, for example, cytoskeletal elements, organelles such as the large nucleus, and proteins. (B) Different molecular motors performing "tug-of-war". In this model, different motors, possibly moving in opposite directions, are attached to the cargo and the observed motion of the cargo is the sum of the action of all motors involved. (C) The presence of a road block on the track, for instance on a microtubules bundle, can make transportation dynamics even more complex.

demonstrated its use for rapid sorting and storage of cells suspended in an aqueous medium.[193] Also, the ability to use an acoustic force to perform quantitative high-throughput in vitro single molecule force spectroscopy and manipulation has been demonstrated.[194] Acoustic manipulations of single molecules within a cell have yet to be accomplished. However, if proper handles can be introduced into the cell and if reliable methods can be developed to calculate the acoustic forces inside living cells, such manipulations could be realized. The acoustic radiation force depends on the relative density and the relative speed of sound between the object to manipulate and the surrounding medium.[195] For very small objects, acoustic streaming forces dominate over the acoustic radiation force[196] and could therefore be important for internalized, small handles. The parameter dependence of the acoustic forces indicate that handles made out of hard materials (metals, silica) may be useful for acoustic manipulation also inside living cells.

4.6.2. Optical Stretchers and Other Tools for Cell Mechanics Investigations. Optical stretchers are composed of two counterpropagating laser beams[197,198] and are conveniently applied for investigations of whole cells that have a liquid medium as their natural surrounding. For a soft object of refractive index larger than the surrounding medium, like a cell in an aqueous medium, the two counter-propagating laser beams tend to stretch the cell along the direction of propagation of the two lasers. As recently reviewed by Yang et

DOI: 10.1021/acs.chemrev.6b00638
Chem. Rev. 2017, 117, 4342−4375

al.,[199] optical stretchers have become an interesting tool in connection with investigations of mechanical properties of, for example, cancer cells and stem cells. In connection with single molecule investigations inside living cells, the benefit of the optical stretcher setup would be that a single cell may be held and controlled while in solution, and one could imagine combining the optical stretcher with force-sensing fluorophore modalities or with one of the single molecule tools for manipulation discussed above. Although believed to be feasible, to our knowledge, so far no single molecules inside cells have been investigated in a cell held (maybe even stretched) by optical stretchers.

Finally, embedding single cells in a biomimetic, soft matrix with magnetic tracer particles allows for 3D force mapping.[200] This method is particularly relevant for cells for which the natural environment are other surrounding cells or a specific matrix. Also, this 3D force mapping method could in principle be combined with single molecule fluorescence detection.

4.7. Comparisons

The single molecule manipulation methods described above allow for quantitative force spectroscopy, either at the surface of, or inside, a living cell. With the massive development the research community has witnessed for single molecule force spectroscopy in vitro, a similarly interesting future may be expected for the investigations in vivo. One task still remaining for the community, both in vitro and in vivo, however, is to make cross-technique calibrations to ensure that the force measured by, say, optical tweezers, is indeed the same as returned by an AFM or by force-sensing fluorophore modalities.

5. OBSERVED DYNAMICS OF ORGANELLES AND SINGLE MOLECULES IN VIVO

Taking advantage of the overwhelming technical development described in sections 3 and 4 with respect to manipulation and detection, also inside living cells, there has been great progress in uncovering the fundamental molecular processes as well as in mapping out the landscape inside living cells and organisms. In parallel with this, progress in theoretical understanding of the dynamics of life processes, as described in section 2, helps us understand the underlying mechanisms. In this section, recent experimental progress regarding the dynamics inside living cells is reviewed, starting with outlining our current understanding of the matrix into which the molecules and organelles move, namely the highly crowded cellular cytoplasm. After this, we review recent results on the dynamics of molecules and organelles inside living cells and organisms.

5.1. Exploring Movement in the Crowded Cytoplasm

The cytoplasm, as sketched in Figure 15A, is highly crowded, and the density of organelles, biopolymers, and membraneous structures is high. Also, the large nucleus poses a significant obstacle for dynamics within the cytoplasm. Inside the cell, diffusion is probably the most normal mode of transportation; however, there exist many active and specific transport routes. For instance, transport by molecular motors along microtubules or transport across the nuclear membrane by specific channels. The cytoplasm displays both viscous and elastic properties, and these vary spatially in a highly inhomogeneous manner and may depend on the crowdedness of, for example, cytoskeletal elements.

5.1.1. External Objects As Tracers. When single particle tracking methods based on enhanced video microscopy reached a sufficiently technical level, the interest of researchers quickly focused on characterizing the complex cytoplasm. One of the first reports on this was by Caspi et al.[201] who let fibroblasts engulf micron-sized polystyrene particles and then followed the motion of these particles by video microscopy. They found that the particles predominantly performed subdiffusion with a scaling exponent of $\alpha \approx 0.75$ at short times. This exponent is consistent with observations in passive networks of semiflexible biopolymers. The study by Caspi was followed by numerous other studies using endocytosed video-tracked particles to probe the cytoplasm. For instance Weiss et al. observed subdiffusion of fluorescently labeled dextran probes of different size in living HeLa cells, with α values ranging from 0.74 to 0.87.[202] As mentioned in section 4, cells also endocytose gold nanoparticles in a certain size range, and these were found to perform anomalous diffusion in both the cytoplasm and nucleoplasm, with $\alpha \approx 0.48-0.70$, in HeLa, HepG2, and THLE cells.[203] These reported scaling exponents are reasonable in agreement, despite the variety of cell types probed. One should, however, be aware that experiments relying on endocytosed particles have a limitation; they only probe the endocytotic pathway. The dynamics of this pathway have also been studied: endosomes loaded with magnetic nanoparticles were shown to perform subdiffusion with $\alpha \approx 0.40$ in intact PC3 tumor cells, with $\alpha \approx 0.49$ in cells with disrupted microtubules, and $\alpha \approx 0.56$ with disrupted actin filaments.[98] The infectious pathway of single fluorescently labeled adeno-associated viruses has been investigated, and scaling exponents ranging between $0.5 < \alpha < 0.9$ were reported.[204]

5.1.2. Endogeneous Tracers. Most, maybe all, cells have lipid reservoirs which are termed lipid granules and which appear as 300−500 nm dark spots in bright field microscopy. As these are optically much denser than the cell cytoplasm and the nucleus, they can be used both as tracer particles in image-based tracking and as handles for optical trapping. Lipid granules are occasionally grabbed and moved by molecular motors along their tracks and are therefore great handles for studying the motion of kinesin and dynein inside living cells,[205,206] as detailed below in the Molecular Motors subsection.

Lipid granules have also been used as handles to probe the viscoelastic properties of living cells. One of the first examples of this was published in 2004,[121] where naturally occurring lipid granules were tracked inside living yeast cells using both video tracking and optical tweezers. With appropriate detection mechanisms, optical tweezers have a significantly better time and temporal resolution than video-based tracking, and by combining these techniques the viscoelastic properties of the cytoplasm was probed at time scales ranging from 10 μs to 100 s. The cytoplasm was found to be subdiffusive at short time scales with a scaling exponent of ∼0.75, whereas different types of anomalous diffusion was found at longer time scales,[121] signifying the different biological processes taking place. Later, the same model system showed that the viscoelastic properties of the cytoplasm changed during the cell cycle[207] and that the system even exhibited weak ergodicity breaking at the shortest observed time scales.[64] Recently, lipid granules have been shown to behave quite differently in another model system, namely the *A. castellani* amoeba. In this system, some granules were observed to be superdiffusive with $\alpha \approx 1.79$ due to cytoplasmic streaming, while treatment with the chemicals latrunculin and nocadozole lowered the exponent to $\alpha \approx 1.53$

DOI: 10.1021/acs.chemrev.6b00638
Chem. Rev. 2017, 117, 4342−4375

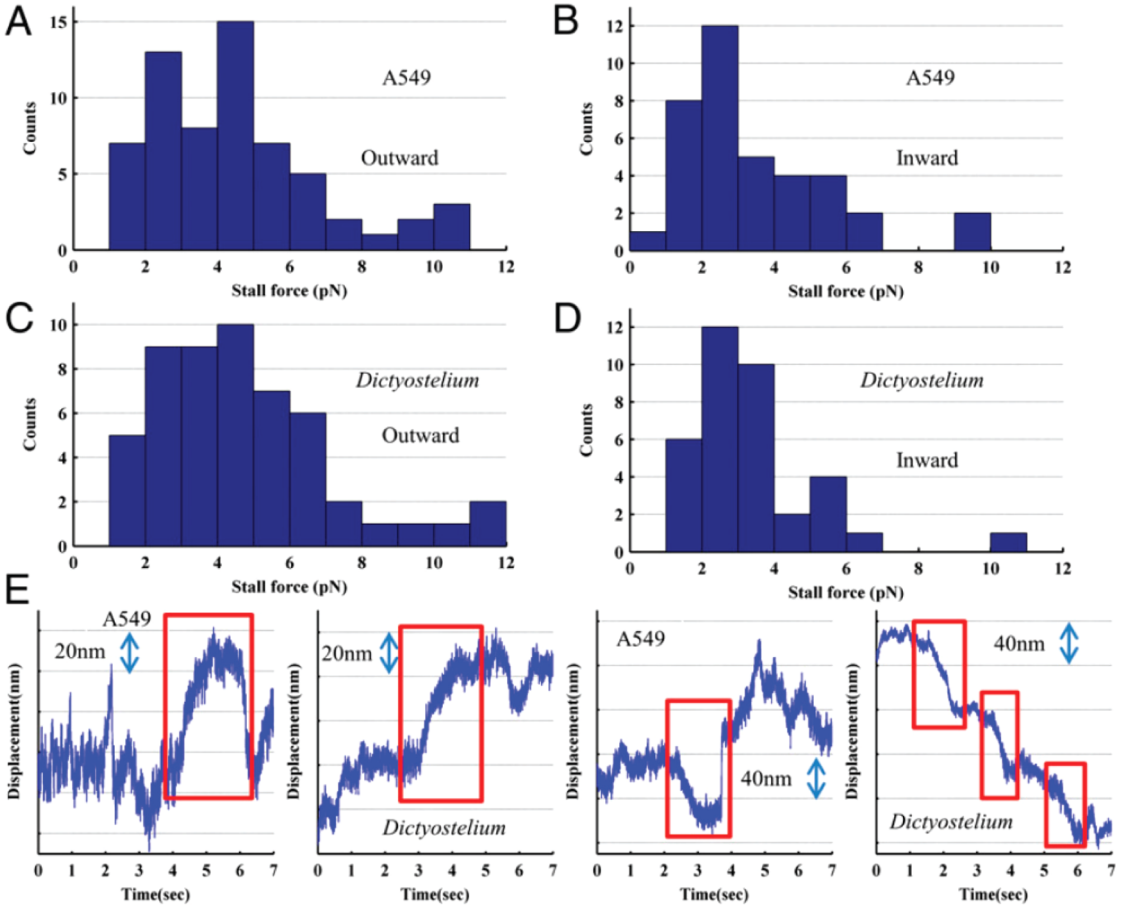

Figure 16. Tug-of-war between kinesin and dynein during in vivo transportation of lipid granules along microtubules in (A and B) A549 human cancer cells and (C and D) during the transportation of endocytosed latex beads in Dictyostelium. (A and B) Stall force histograms of (A) outward and (B) inward cargo movement in A549 cells. (C and D) Stall force histograms of (C) outward and (D) inward cargo movement in Dictyostelium. (E) Examples of cargo traces showing periods of active motion in both directions interrupted by stalls. Reproduced with permission from ref 215. Copyright 2013 National Academy of Sciences.

and 1.60, respectively.[208] If the amoeba was treated with blebbistatin, the lipid granules were almost stalled with $\alpha \approx 0.13$.[208]

5.1.3. Diffusion of Single Molecules. With appropriate labeling, even the motion of individual molecules can be tracked inside living cells. For instance, Golding and Cox reported the subdiffusion of fluorescently tagged mRNA in *E. coli* with $\alpha \approx 0.77$ and showed that this value does not significantly change when the measurements are performed in mutants lacking the cytoskeletal proteins MReB and FtsZ. Moreover, they reported discontinuous motion with periods of almost localized motion and fast jumps.[209] Observation in live *E. coli* of RNA molecules with tandem hairpins bound by GFP indicated a value $\alpha = 0.71$, which was unaffected by different biological perturbations, as reported by Weber et al.[63] Motion of single molecules has also been investigated in eukaryotic cells. One such example is the motion of different modifications of HIV-1 integrase labeled with enhanced GFP molecules in HeLa cells. These enzymes were shown to exhibit subdiffusion with α values ranging from 0.59 to 0.94.[210]

5.1.4. In Vitro Comparisons. Even though single molecules in vitro lack their natural environment, it still makes sense to study their diffusive properties in vitro as this can help identify the essential components giving rise to the in vivo observations. One must be aware though that in vitro there is no metabolism, hence, the only energy present for driving the motion is typically thermal diffusion (unless, for example, ATP is added to a sample containing ATP consuming enzymes). One example of in vitro studies of protein diffusion was carried out by Banks and Fradin who demonstrated that proteins subdiffuse in crowded solutions of polymeric dextran. They observed α values systematically varying from 1 in dilute solution down to 0.75 at higher dextran concentrations.[211] Later, Szymanski and Weiss reported anomalous diffusion of fluorescently labeled aptoferritin in 20% (weight) solutions of dextran with a consistent α value of $\approx$0.8.[67] Also, the diffusion of larger tracer particles has been investigated in vitro. Fluorescently coated microscopic particles were shown to exhibit anomalous diffusion in lysozyme protein solutions with α varying from one to 0.45 with increasing lysozyme concentration.[212] Also, Jeon et al. proved anomalous diffusion of submicron-sized polystyrene beads in micellar solution with α values around the remarkably low value of 0.3.[65]

5.2. Molecular Motors

Molecular motors are individual molecules which perform a biased movement, most often in a linear or rotary fashion, while consuming energy, and the dynamics of such molecular machines have been observed and measured in vivo.[23,213,214] Molecular motors have different processivety; that is, the number of steps taken before the motor dissociates from its trail differs from one motor to another and may also differ from

DOI: 10.1021/acs.chemrev.6b00638
Chem. Rev. 2017, 117, 4342−4375

in vivo to in vitro conditions. The motion of cargo carried by a motor in a linear fashion will be superdiffusive. This has been observed in a variety of living eukaryotic cells[8,98,99,121,201,206] represented by scaling exponents typically in the range of α = 1.3−1.5. Besides pure superdiffusion, intermittent Lévy walk-like superdiffusion with a power law run length distribution has been observed for molecular motors in mammalian epithelium cells.[100]

5.2.1. Kinesin and Dynein. Kinesin and dynein are the molecular motors responsible for transport along microtubules. Most kinesins move their cargo toward the plus end of microtubules, whereas dynein moves in the opposite direction, toward the minus end of microtubules (see Figure 15). They are relatively processive motors taking hundreds of steps before disengaging, and they often carry cargo, for instance lipid granules, which is directly visible even in bright field microscopy and can be directly manipulated by an optical trap. For these reasons, kinesins and dyneins are among the best-studied molecular motors, also in vivo.[214] Both in vitro and in vivo, the step size of microtubule associating kinesins and dyneins has been shown to be 8 nm, consistent with the size of the tubulin monomer.

The first measurement of molecular transport along microtubules mediated by kinesin and dynein was conducted by Ashkin and co-workers who used optical tweezers to trap a mitochondrion moving along microtubules inside a living giant amoeba *Reticulomyxa*.[8] Here, the maximum force exerted by a single motor was estimated to be ∼4 pN. A few years later, optical tweezers were used to observe retrograde transport of vesicles along microtubules inside *Drosophila* embryos,[205,206] that were interpreted as dynein movement. From the measurements, the force needed for stalling an individual dynein was estimated to be 1.1 pN.

Similarly, motion of kinesins were observed in *Drosophila* using optical tweezers as measurement device and transported lipid granules as tracers.[205] The stall force was here found to be ∼2.4 pN, which is significantly lower than the value measured in vitro for single kinesin molecules, 5−7 pN.[205,215] In addition, the kinesins were observed to stay on the track for shorter distances in vivo than in vitro and their velocities were also lower than those measured in vitro.[205]

In a study by Kural et al.,[216] it was suggested that multiple kinesins or dyneins work together in organelle transport along microtubules. They claimed that the motors do not work against each other but act in a concerted fashion and manage to produce speeds in vivo that are up to 10 times faster than in vitro speeds. In recent years, it has become more and more clear that the regulation and action of kinesins and dyneins in vivo is anything but simple. Typically several dyneins and kinesins are attached to the same cargo, and the dynamics are regulated in a complex "tug-of-war" manner (illustrated in Figure 15B), where dyneins pull the cargo toward the minus end while kinesins simultaneously pull the cargo toward the plus end.[214,215] Also, it appears that synergistic collaboration between kinesins and dyneins is required for intracellular bidirectional transport,[217] thus signifying complex regulation mechanisms that are not yet fully understood. The engagement of different motors on the same cargo may also assist transportation across road-blocks as for example microtubule intersections[214] (see road-blocking illustrated in Figure 15C). Blehm et al. investigated the complex transport of lipid granules inside living cells (*Dictyostelium discoideum* and A549 cells) by optically trapping the granules.[215] They found plus-end directed stall forces of 2−7 pN and minus-end directed stall forces of 2−3 pN, which is higher than the stall force of a single dynein. Hence, the authors concluded that for transport of lipid granules along microtubules, dyneins are probably also engaged during plus-end directed motion during which they pull in the opposite direction of the kinesins. In the minus-end directed motion, their results were consistent with several dyneins pulling in concerto on the cargo. Typical traces and stall force histograms from ref 215 are shown in Figure 16. In literature, there are quite a large number of reports of stall forces of kinesin and dynein in vivo, probably the largest force reported is 60 pN.[218] This comes from an experiment where the stall force was measured in an indirect manner by attaching a bead from the outside to a membrane protein of a *Chlamydomonas* flagella, that is anticipated to be moved by kinesins and dyneins. A force of 60 pN would require at least 10 motors to synchronize, which has not been reported in other studies. The variety in stall forces probably reflects that the motors act in a complex fashion but also calls for a critical evaluation of the calibration procedures involved in the different measurements. In vivo calibration of manipulation techniques, as reviewed in section 4, is not trivial and still cross-calibrations between the different modalities are called for.

To further complicate the picture, there exist "hand-over" mechanisms between motors for transport across the entire cell.[219] For instance, the kinesin-II and OSM-3 motors (both kinesin-2 types) have different functions but have recently been shown to cooperate for efficient cargo import and transport along cilia inside *C. Elegans*.[220] Interestingly, the motors distribute the work; kinesin-II which is slower and less processive than OSM-3, functions as an import motor of intraflagellar transport (IFT) trains through the ciliary base. At the "handover-zone" OSM-3 replaces kinesin-II and functions as a long-range transport motor that carries the IFT train to the ciliary tip. In vitro kinesin-II generates runs of ∼0.2 μm at a speed of ∼0.5 μm/s, whereas OSM-3 runs longer and faster (∼2 μm at a speed of ∼1.5 μm/s). When the two motors operate together in vivo, they move at an intermediate speed of ∼0.7 μm/s. However, in this study it was shown that as the OSM-3 takes over the cargo from kinesin-II, the speed accelerated, thus overall making the transport more efficient.

5.2.2. Myosin. Myosin V is another example where there is a discrepancy between in vitro and in vivo observations. In vitro, myosin V was found to move significantly slower than suggested by observations of organelles transported by myosin V in vivo. To study the gap between these findings, single myosin V molecules were labeled with quantum dots and tracked inside living HeLa cells.[21] The investigators did indeed find a difference both in the velocities and in the processivity of the motor: the in vitro velocity of a myosin V molecule was (500 ± 30) nm/s, whereas it was (710 ± 50) nm/s in vivo. Also, myosin V appeared to stay on track for longer in vivo, (2.2 ± 0.2) μm, than in vitro, (1.3 ± 0.2) μm. The longer processivity in vivo may be explained by the fact that the escape time in aqueous medium is much shorter than the binding time. Hence, if the motor unbinds in water, chances are it will fall off and disappear. In contrast, due to the more crowded environment of the living cell (see Figure 15), the escape time is longer and the myosin motor has a larger chance of rebinding. The fact that the velocity inside the crowded cytoplasm is higher than in the aqueous environment seems counterintuitive and could be due to the lack of optimization of the in vitro assay.[21] The counterintuitive effect of macro-

DOI: 10.1021/acs.chemrev.6b00638
Chem. Rev. 2017, 117, 4342−4375

molecular crowding on processes has also been reported in Morelli et al.[221]

Interestingly, myosins are often present on organelles which are transported by kinesin and dynein, and their purpose in this context is under debate.[214] It might be that myosins assist organelle docking or pausing at the right location,[222] or maybe myosin allows for grabbing onto passing actin cables whereby the transported organelle may switch from microtubule to actin-based transportation.

5.3. Dynamics in the Membranes of Living Cells

Living cells are encapsulated in membranes. The cell membrane is not merely an envelope for the cytoplasm, it actively participates in maintaining the development and life of the cell. Also, the membrane has a critical function in communication with the extra-cellular environment. Here, we discuss both the dynamics of the lipids within the membrane and the dynamics of proteins located in the membranes, including the dynamics of raftlike structures possibly containing both lipids and proteins, as observed, for example, in epidermal cells in living zebrafish embryos.[223] Certain proteins located on or in the outer surface of the living cell are crucial for cell−cell and cell−substrate adhesion, as also discussed here.

5.3.1. Dynamics of Membrane Lipid Molecules. In the simplest case, a membrane consists of molecules of one type of lipid compound and the dynamics depend both on the temperature and on the observation time scale. At a temperature above the phase transition temperature, the lipids are in a liquid phase. At extremely short times (up to 10 ns), the dynamics of lipids in this state are expected to exhibit anomalous diffusion with $\alpha \approx 0.65$; and after ∼10 ns, the diffusion will be normal with an exponent of $\alpha = 1$.[68,69,224,225] At temperatures below the phase transition temperature, the lipids enter an ordered phase. Through simulations, Jeon et al. showed that in this regime and at extremely short times (up to 10 ns) the lipids exhibited anomalous diffusion with an exponent of $\alpha \approx 0.16$, wherafter it crossed over to $\alpha \approx 0.59$, which characterized motion up to the longest simulations times of 10^2 nsec.[69]

The situation becomes more complex when other molecules (e.g., cholesterols) are embedded in the membrane. Simulations have shown that the motion of a mixture of phospholipid molecules and cholesterol in the liquid ordered phase is subdiffusive with a scaling exponent of $\alpha \approx 0.82$, even for time scales beyond 10 ns. If additional disorder is added, for instance in the form of much bigger and significantly less mobile membrane proteins, anomalous diffusion was shown to persist beyond 10^4 nsec and both lipid and protein diffusion was non-Gaussian and had a distinct distribution of mobilities.[70,71] Membranes can include raftlike structures of lipids and proteins, as illustrated in Figure 17. Munguira et al. reported that diffusion properties of membranes are domain-dependent such that Brownian motion, anomalous diffusion, and glasslike properties may coexist in a single membrane bilayer.[226]

5.3.2. Dynamics of Membrane Proteins. Closely connected to the dynamics of the membrane itself is the dynamics of proteins embedded in the membrane (see Figure 17). The first single-molecule observation of lateral protein movement in the membrane of living cells was carried out by Edidin et al.[227] Here, a gold nanoparticle was attached to the protein complex of interest and dragged through the membrane using optical tweezers. In the experiment, the distance the gold nanoparticle could be dragged through the membrane without escaping the trap was measured and designated as the "barrier-free path".[227] This experiment, along with notable experiments from the Kusumi group,[228] led to the hypothesis that the cellular membrane is compartmentalized by cytoskeletal elements connected to the membrane, and that proteins in the membrane are typically "fenced" by such compartment structures or tethered by the structures, as illustrated in Figure 17.

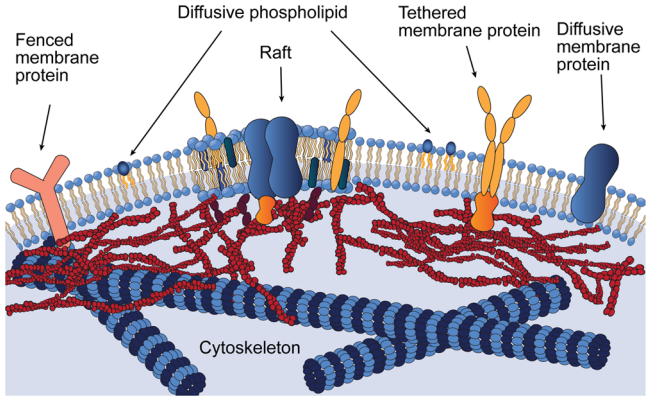

Figure 17. Illustration of membrane-related dynamics (i.e., diffusive motion of phospholipids) and the motion of membrane proteins which perform anomalous diffusion, for example, because they are tethered to cytoskeletal elements or confined.

The prokaryotic membrane is significantly different from the eukaryotic membrane. In addition to the innermost bilayer, the prokaryotic cell wall also consists of a peptidoglycan layer and an outer lipo-poly saccharide coat. The first experiments demonstrating how a single membrane protein moves in the membrane of a living prokaryotic cell was published in 2002. Here, the Brownian motion of a single lambda receptor in the cell wall of *Escherichia coli* was monitored by weak optical tweezers using specifically attached polystyrene beads as handles.[229] This type of experiment had the advantage that the protein dynamics were probed in the local natural environment without dragging it through potential obstacles that it normally might not pass. The motion of the lambda receptor was shown to be diffusive, with a larger diffusion constant than typically observed for protein motion in eukaryotic membranes, meanwhile having an elastic response due to cell wall tethering.[229] Interestingly, the motion was shown to be strongly dependent on the bacterial metabolism[229−231] (i.e., the motion contained an active component which required a fully functional metabolism).

Particle tracking was applied for studying the motion of individual DC-SIGN receptors, labeled with quantum dots, in the membrane of Chinese hamster ovary cells.[81] Overall, these receptors perform subdiffusion with $\alpha \approx 0.82-0.85$, however, with the observation that they also undergo changes of diffusivity. In addition, the motion of the receptors exhibited weak ergodicity breaking and aging, thus supporting the view of the cell membrane as being highly dynamic and diverse.

By tracking individual potassium channels in the plasma membrane of human kidney cells, it was demonstrated that such channels exhibit anomalous diffusion at time scales up to hundreds of seconds.[53] The channels exhibit both ergodic and nonergodic behavior, with the nonergodic process being regulated by transient binding to the actin cytoskeleton.

DOI: 10.1021/acs.chemrev.6b00638
Chem. Rev. 2017, 117, 4342−4375

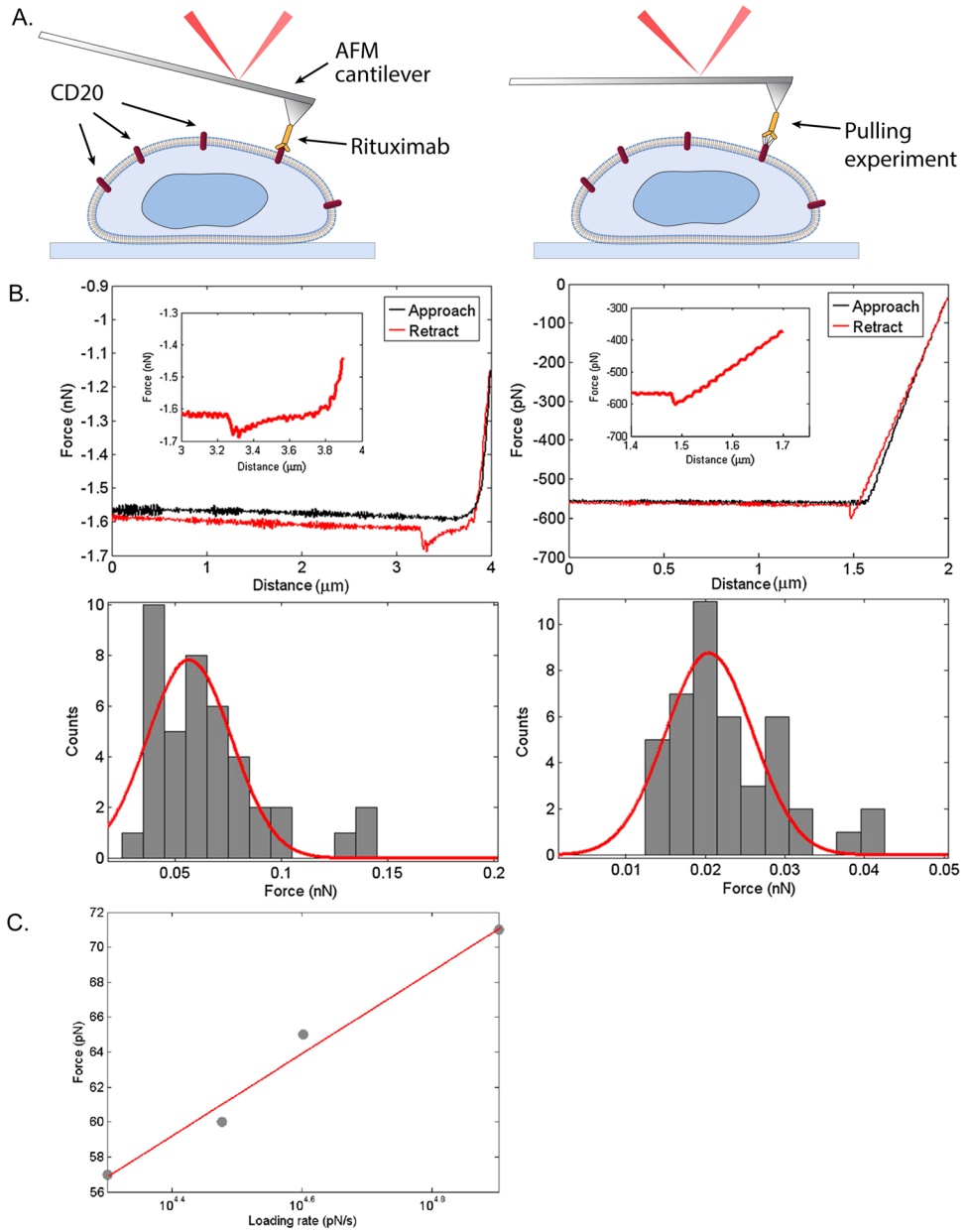

Figure 18. AFM force measurements of the binding between the CD20 receptor expressed in the outer surface of lymphoma cancer cells and the cancer drug Rituximab. (A) Illustrations of how an AFM cantilever coated with Rituximab approaches a cell and binds specifically to a CD20 receptor. Thereafter, the tip is retracted and the bond between CD20 and Rituximab is stretched and finally broken. (B) An example of force–distance curves and rupture force histograms of measurements from a lymphoma cell expressing the CD20 receptor (left) and a control cell that does not express the CD20 receptor (right). The bond breaks at the most negative point in the retraction curve (red), and it requires a higher force to break specific CD20-rituximab bond than nonspecific attachment. (C) Semilogarithmic plot of Rituximab-CD20 rupture force as a function of loading rate, the linear relation confirms the Bell-Evans model equation 13. B–C are reproduced with permission from ref 233. Copyright 2013 Wiley-Blackwell.

5.4. Adhesion

Cell–cell and cell–substrate adhesion has predominantly been studied by AFM, as the forces involved are typically too large to be probed by other manipulation techniques. AFM has the additional advantage that it can also be used to scan surfaces. Hence, within the same experiment, the surface of a cell can be mapped out and force spectroscopy of selected regions can be performed. For a recent overview of AFM, in particular in relation to cell surface mapping and single molecule force spectroscopy, see ref 232. Adhesion of living cells has been studied on the single molecule level using AFMs. One example regards the marine mussel, whose survival is dependent on a firm adhesion. The bond responsible for mussel adhesion, dopa, was studied on a single molecule level using AFM revealing a surprisingly strong, yet fully reversible noncovalent interaction.[158] AFM is particularly well-suited for studying molecular and cellular binding forces, one example of this is an investigation of the binding force between a single receptor expressed in the outer cell wall of lymphoma cancer cells, CD20/ROR1, and the cancer drug targeting this receptor, rituximab.[233] Figure 18A shows a sketch of the experimental setup for measuring adhesion between CD20 and rituximab, and Figure 18B, left panel, shows typical force–distance graphs

DOI: 10.1021/acs.chemrev.6b00638
Chem. Rev. 2017, 117, 4342–4375

upon approach (black) and retraction (red) of a rituximab-coated tip to or from a CD20 expressing cell. The dip in the retraction graph signifies the breakage of the CD20-rituximab bond, the breakage force can be read off directly as ~0.07 nN. For comparison, the right panel of Figure 18B shows a similar event from a cell that does not express CD20. The histograms shown in Figure 18 demonstrate a significant difference between the nonspecific bindings probed in the control cells and the CD20-rituximab binding probed in the CD20 expressing cells. In the latter, there is, of course, a fraction of nonspecific bonds probed. As explained in section 4.3, the rupture force depends on the loading rate (how quickly the cantilever is retracted). Figure 18C shows a plot of obtained rupture forces as a function of the logarithm of the loading rate. This relation is linear, as expected from the Bell-Evans model, equation 13. The kind of investigations demonstrated in ref 233 can be used to probe whether cancer cells from a specific B-cell lymphoma patient will bind well to the cancer drug, and hence, paves the way for personalized cancer treatments.

5.5. Nerves

The development of the central nervous system is a delicate process where differentiation of precursor stem cells results in fully functional nerve cells, which must migrate and create long axons and finer-branched dendrites. In the central nervous system, glial cells exist alongside the neurons; these glial cells may serve as a scaffold for the neurons. With the use of scanning force microscopy, bulk rheology, and optical stretchers, it was found that, compared to most other eukaryotic cells, both neurons and glial cells are very soft.[234] Interestingly, glial cells are even softer than the neighboring neurons and could serve as a protective cushioning or as a soft substrate guiding neurite growth. In a recent publication, a research collaboration[235] made a beautiful experiment where they used AFM-based sensing to investigate the mechanisms behind axon growth in *Xenopus* embryos. The AFM cantilever was placed inside the brain of the living embryo (underneath the skin), and it was found that the axons grew toward the tissue's softer side. These results were reproduced in vitro in the complete absence of chemical gradients. Also, by immunocytochemical manipulation of a mechanically activated cation channel, the authors proved that the sensing of substrate stiffness is mediated by mechanosensitive ion channels.[235]

5.6. Chromosomes

Chromosomes exist in the nuclei of eukaryotic cells and freely floating in prokaryotic cells' cytoplasm. Eukaryotic chromosomes consist of tightly packaged DNA wrapped around protein complexes, called nucleosomes, which regulate transcription. Chromosomes are made from a complex of DNA, protein, and RNA called chromatin which display several organization levels spanning from the 2 nm diameter of the DNA double helix to micrometer structures.[236] The dynamics of chromosomal loci has been investigated by fluorescent labeling, and they have been shown to exhibit anomalous subdiffusion with $\alpha \approx 0.5$.[236] Another study returned $\alpha \approx 0.39$, and this relatively small exponent is attributed to the relaxation of the Rouse modes of the DNA chain.[63] Fluorescently labeled telomeres, the extremities of individual chromosomes, were shown to diffuse anomalously with $\alpha \approx 0.32$ in human U2OS cancer cells.[66,237]

The mechanical properties of chromatin fibers, and how these relate to chromosome orientation during the cell division cycle, was investigated in vivo using glass microneedles as early as 1969,[4] and in 1979 this pioneering work was followed by a similar study using glass microneedles to force-manipulate chromosomes inside living spermatocytes.[238] They found that chromosomes are individually anchored to the spindle by fibers connecting the kinetochores to the spindle poles.[238]

In vitro, optical tweezer experiments have been useful for mapping out the structure of chromatin fibers[239] and for increasing the understanding of the association between DNA and nucleosomes.[240,241] In vivo, there still does not exist direct quantitive measurements of the mechanical properties of chromatin, although some aspects of mechanical stability can be inferred from observing the thermal fluctuations.[242]

5.7. Bacterial Flagella

Motile bacteria are often propelled by a flagella, a corkscrewlike structure which is attached to a rotary motor driven by a transmembrane proton gradient. In 1989 Block et al.[243] showed that optical tweezers were strong enough to overcome the torque generated by the flagellar motor of a living bacterium attached to a glass surface, and by using the tweezers, the authors were able to determine the torsional compliance of two different bacterial types.[243] Also, optical tweezers have proven useful for quantifying the run-tumble dynamics mediated by the flagellar determined motion of *E. coli*[244] and *Vibrio alginolyticus*.[245] In addition, the motion of the bacterial flagella was used as a measure to investigate whether optical trapping of individual *E. coli* at specific wavelengths and laser powers influenced the viability of the bacteria.[141] These results, as well as results monitoring the ability of different types of bacteria to maintain a proton gradient across the cell wall during trapping,[142] showed that bacteria can remain physiologically fully competent while in an optical trap provided that the correct wavelength (e.g., 1064 nm) is used and that laser power and irradiation period is kept relatively low.

6. SUMMARY AND OUTLOOK

The rapid and impressive progress within the development of techniques capable of monitoring life processes down to the single molecule level has led to fundamentally new insights into the functioning of single molecules and organelles. Looking back on the last couple of decades, it is, however, evident that there has been significantly more progress in vitro than in vivo. In vitro one can isolate the influence of a single or very few parameters, thus making interpretation of the experiments relatively easy. In vivo, the environment is exceedingly complex and we might only be aware of a small fraction of the players participating in a given life process.

The most widely used techniques for monitoring dynamics in vivo are optical tweezers, magnetic tweezers, and AFMs, which all have pros and cons in relation to in vivo experimentation. The magnetic tweezers are probably the least invasive; however, they require insertion of a magnetic probe as no naturally occurring object can be magnetically manipulated. Usage of AFM is beneficial for probing adhesion and properties of the outer surface and proteins located therein. An AFM cannot, however, reach inside the cell without penetrating the cell membrane, a rather invasive event. Optical tweezers can be nearly noninvasive and can reach and operate deep inside living cells and whole organisms. It is possible, but not trivial, to perform reliable force-calibration inside a living cell and thereby perform absolute force measurements (e.g., of the action of molecular motors in vivo).

DOI: 10.1021/acs.chemrev.6b00638
Chem. Rev. 2017, 117, 4342−4375

In parallel with the experimental developments, the theoretical understanding of the dynamical processes inside living cells has made huge leaps forward. There now exists relevant and successful models for describing various forms for normal and anomalous diffusive processes inside living cells. These models pinpoint the relevant and fundamental parameters responsible for life dynamics and helps understand and predict the processes.

Despite the challenges that exist for reliable probing of in vivo dynamics, there has been significant progress over the past decade, for instance in unraveling the complex interplay of kinesins and dyneins during microtubules associated transportation and in mapping out the viscoelastic landscape inside living cells. The field of in vivo investigations at the single molecule to whole cell level holds great potential for the future. We foresee that within the near future, focus will also be directed toward understanding the role of mechanics and dynamics for lineage specification of stem cells and for embryonic development. Through recent technological progress, it has now proven possible to manipulate inside whole living organisms (e.g., optical manipulation inside developing zebrafish embryos[246] and AFM manipulation inside the brains of developing larvae).[235] As stem cells have the potential to develop into any specialized cell of the organism, they can be considered "the holy grail" for regenerative medicine, and understanding the molecular and mechanical mechanisms at play during differentiation holds the key to understanding and controlling this important process. On the basis of the remarkable in vivo achievements described in this review, there is hope that the future will bring new knowledge on the dark matter of biology and on the basic mechanisms governing life.

AUTHOR INFORMATION

Corresponding Author

*E-mail: oddershede@nbi.dk.

ORCID

Lene B. Oddershede: 0000-0003-2923-2844

Notes

The authors declare no competing financial interest.

Biographies

Kamilla Norregaard is a postdoctoral fellow at Cluster for Molecular Imaging, Department of Biomedical Science, University of Copenhagen, Denmark, with a Ph.D. degree from the Niels Bohr Institute, University of Copenhagen. Her current research interests include plasmonic heating of nanoparticles and their use for photothermal therapy and medical nuclear imaging based evaluation of treatment efficacy.

Ralf Metzler is a Professor of Theoretical Physics at the University of Potsdam, Germany. He previously held faculty positions at the Technical University of Munich, the University of Ottowa, and NORDITA, Copenhagen. He is well-known for his work on anomalous diffusion and the modelling of dynamic effects in biological systems such as molecular regulation and transport mechanisms in cells.

Christine Ritter is a Ph.D. student at the Niels Bohr Institute, University of Copenhagen. She is affiliated with the StemPhys Center of Excellence and works with a focus on quantifying the changes in cellular viscoelastic properties as stem cells undergo differentiation.

Kirstine Berg-Sørensen is Associate Professor and Head of Studies at the Technical University of Denmark. She is well-known for her work on data analysis tools to quantify optical trapping experiments, and her current research interests include optical methods for investigations of fluidic flow and applications in connection with medical questions.

Lene Broeng Oddershede is a Professor of Experimental Physics at the Niels Bohr Institute, University of Copenhagen, Denmark. She is also Center Leader for StemPhys Center of Excellence. She is well-known for her work on optical manipulation and nanophotonics, especially related to living systems ranging from the single molecule to whole cell level.

ACKNOWLEDGMENTS

The authors acknowledge financial support from the Danish National Research Foundation, grant DNRF116 (StemPhys), and from the Novo Nordisk Foundation, grant NNFOC150011361 (LANTERN).

REFERENCES

(1) Wang, M. D.; Schnitzer, M. J.; Yin, H.; Landick, R.; Gelles, J.; Block, S. M. Force and velocity measures for single molecule of RNA polymerase. *Science* **1998**, *282*, 902−907.

(2) Abbondanzieri, E. A.; Greenleaf, W. J.; Shaevitz, J. W.; Landick, R.; Block, S. M. Direct observation of base-pair stepping by RNA polymerase. *Nature* **2005**, *438*, 460−465.

(3) Wen, J.-D.; Lancaster, L.; Hodges, C.; Zeri, A.-C.; Yoshimura, S. H.; Noller, H. F.; Bustamante, C.; Tinoco, I. Following translation by single ribosomes one codon at a time. *Nature* **2008**, *452*, 598−603.

(4) Nicklas, R. B.; Koch, C. A. Chromosome micromanipulation. 3. Spindle fiber tension and the reorientation of mal-oriented chromosomes. *J. Cell Biol.* **1969**, *43*, 40−50.

(5) Ashkin, A. Acceleration and trapping of particles by radiation pressure. *Phys. Rev. Lett.* **1970**, *24*, 156−159.

(6) Ashkin, A.; Dziedzic, J. M.; Yamane, T. Optical trapping and manipulation of single cells using infrared laser beams. *Nature* **1987**, *330*, 769−771.

(7) Ashkin, A.; Dziedzic, J. M. Internal cell manipulation using infrared laser traps. *Proc. Natl. Acad. Sci. U. S. A.* **1989**, *86*, 7914−7918.

(8) Ashkin, A.; Schütze, K.; Dziedzic, J. M.; Euteneuer, U.; Schliwa, M. Force generation of organelle transport measured in vivo by an infrared laser trap. *Nature* **1990**, *348*, 346−348.

(9) Binnig, G.; Quate, C. F.; Gerber, Ch. Atomic force microscope. *Phys. Rev. Lett.* **1986**, *56*, 930−933.

(10) Muller, D. J.; Helenius, J.; Alsteens, D.; Dufrene, Y. F. Force probing surfaces of living cells to molecular resolution. *Nat. Chem. Biol.* **2009**, *5*, 383−390.

(11) Amblard, F.; Yurke, B.; Pargellis, A.; Leibler, S. A magnetic manipulator for studying local rheology and micromechanical properties of biological systems. *Rev. Sci. Instrum.* **1996**, *67*, 818−827.

(12) De Vlaminck, I.; Dekker, C. Recent advances in magnetic tweezers. *Annu. Rev. Biophys.* **2012**, *41*, 453−472.

(13) Gelles, J.; Schnapp, B. J.; Sheetz, M. P. Tracking kinesin-driven movements with nanometre-scale precision. *Nature* **1988**, *331*, 450−453.

(14) Hell, S. W.; Wichmann, J. Breaking the diffraction resolution limit by stimulated emission: stimulated-emission-depletion fluorescence microscopy. *Opt. Lett.* **1994**, *19*, 780−782.

(15) Klar, T. A.; Jakobs, S.; Dyba, M.; Egner, A.; Hell, S. W. Fluorescence microscopy with diffraction resolution barrier broken by stimulated emission. *Proc. Natl. Acad. Sci. U. S. A.* **2000**, *97*, 8206−8210.

(16) Rust, M. J.; Bates, M.; Zhuang, X. W. Sub-diffraction-limit imaging by stochastic optical reconstruction microscopy (STORM). *Nat. Methods* **2006**, *3*, 793−795.

(17) Betzig, E.; Patterson, G. H.; Sougrat, R.; Lindwasser, O. W.; Olenych, S.; Bonifacino, J. S.; Davidson, M. W.; Lippincott-Schwartz,

DOI: 10.1021/acs.chemrev.6b00638
Chem. Rev. 2017, 117, 4342−4375

J.; Hess, H. F. Imaging intracellular fluorescent proteins at nanometer resolution. *Science* **2006**, *313*, 1642−1645.
(18) Schnitzer, M. J.; Block, S. M. Kinesin hydrolyses one ATP per 8-nm step. *Nature* **1997**, *388*, 386−390.
(19) Wuite, G. J.; Smith, S. B.; Young, M.; Keller, D.; Bustamante, C. Single-molecule studies of the effect of template tension on T7 DNA polymerase activity. *Nature* **2000**, *404*, 103−106.
(20) Sørensen, M. A.; Pedersen, S. Absolute in vivo translation rates of individual codons in Escherichia coli. The two glutamic acid codons GAA and GAG are translated with a threefold difference in rate. *J. Mol. Biol.* **1991**, *222*, 265−280.
(21) Pierobon, P.; Achouri, S.; Courty, S.; Dunn, A. R.; Spudich, J. A.; Dahan, M.; Cappello, G. Velocity, processivity, and individual steps of single myosin V molecules in live cells. *Biophys. J.* **2009**, *96*, 4268−4275.
(22) Ross, J. L. The dark matter of biology. *Biophys. J.* **2016**, *111*, 909−916.
(23) Oddershede, L. B. Force probing of individual molecules inside the living cell is now a reality. *Nat. Chem. Biol.* **2012**, *8*, 879−886.
(24) Ingenhousz, J. *Nouvelles Expériences et Observations sur Divers Objets de Physique*; T. Barrois le jeune: Paris, 1785.
(25) Brown, R. On the existence of active molecules in organic and inorganic bodies. *Philos. Mag.* **1828**, *4*, 161−173.
(26) Rigler, R.; Elson, E. L. *Fluorescence Correlation Spectroscopy: Theory and Applications*; Springer: Berlin, 2001.
(27) Axelrod, D.; Koppel, D. E.; Schlessinger, J.; Elson, E.; Webb, W. W. Mobility measurement by analysis of fluorescence photobleaching recovery kinetics. *Biophys. J.* **1976**, *16*, 1055−1069.
(28) Bräuchle, C.; Lamb, D.; Michaelis, J. *Single Particle Tracking and Single Molecule Energy Transfer*; Wiley-VCH: Weinheim, Germany, 2012.
(29) Di Rienzo, C.; Piazza, V.; Gratton, E.; Beltram, F.; Cardarelli, F. Probing short-range protein Brownian motion in the cytoplasm of living cells. *Nat. Commun.* **2014**, *5*, 5891.
(30) Honigmann, A.; Mueller, V.; Hell, S. W.; Eggeling, C. STED microscopy detects and quantifies liquid phase separation in lipid membranes using a new far-red emitting fluorescent phosphoglycerolipid analogue. *Faraday Discuss.* **2013**, *161*, 77−89.
(31) Gouy, M. Notes on Brownian motion. *J. Phys. Theor. Appl.* **1888**, *7*, 561−565.
(32) Perrin, J. Brownian movement to molecular agitation. *Compt. Rend.* **1908**, *146*, 967−970.
(33) Nordlund, I. New determination of the Avogadro constant from the Brownian motion of small spheres of mercury suspended in water. *Z. Phys. Chem.* **1914**, *87*, 40−62.
(34) Einstein, A. In *Investigations on the theory of the Brownian movement*; Fürth, R., Ed.; Dover: New York, 1956.
(35) von Smoluchowski, M. The kinetic theory of Brownian molecular motion and suspensions. *Ann. Phys.* **1906**, *21*, 756−780.
(36) Barkai, E.; Garini, Y.; Metzler, R. Strange kinetics of single molecules in living cells. *Phys. Today* **2012**, *65*, 29−35.
(37) Metzler, R.; Jeon, J.-H.; Cherstvy, A. G.; Barkai, E. Anomalous diffusion models and their properties: non-stationarity, non-ergodicity, and ageing at the centenary of single particle tracking. *Phys. Chem. Chem. Phys.* **2014**, *16*, 24128−64.
(38) Saxton, M. J.; Jacobson, K. SINGLE-PARTICLE TRACKING: Applications to membrane dynamics. *Annu. Rev. Biophys. Biomol. Struct.* **1997**, *26*, 373−399.
(39) Höfling, F.; Franosch, T. Anomalous transport in the crowded world of biological cells. *Rep. Prog. Phys.* **2013**, *76*, 046602.
(40) Metzler, R.; Klafter, J. The random walk's guide to anomalous diffusion: a fractional dynamics approach. *Phys. Rep.* **2000**, *339*, 1−77.
(41) Leijnse, N.; Jeon, J. H.; Loft, S.; Metzler, R.; Oddershede, L. B. Diffusion inside living human cells. *Eur. Phys. J.: Spec. Top.* **2012**, *204*, 75−84.
(42) Pearson, K. The problem of a random walk. *Nature* **1905**, *72*, 294−294.
(43) van Kampen, N. G. *Stochastic Processes in Physics and Chemistry*; North Holland: Amsterdam, 1981.
(44) Risken, H. *The Fokker-Planck Equation*; Springer Verlag: Heidelberg, 1989.
(45) Montroll, E. W. Random walks on lattices. III. Calculation of first-passage times with application to exciton trapping on photosynthetic units. *J. Math. Phys.* **1969**, *10*, 753−765.
(46) Scher, H.; Montroll, E. W. Anomalous transit-time dispersion in amorphous solids. *Phys. Rev. B* **1975**, *12*, 2455−2477.
(47) Shlesinger, M. F. Asymptotic solutions of continuous-time random walks. *J. Stat. Phys.* **1974**, *10*, 421−434.
(48) Hughes, B. *Random Walks and Random Environments, Vol 1: Random Walks*; Oxford University Press: Oxford, 1995.
(49) Klafter, J.; Blumen, A.; Shlesinger, M. F. Stochastic pathway to anomalous diffusion. *Phys. Rev. A: At., Mol., Opt. Phys.* **1987**, *35*, 3081−3085.
(50) Bouchaud, J.-P.; Georges, A. Anomalous diffusion in disordered media: Statistical mechanisms, models and physical applications. *Phys. Rep.* **1990**, *195*, 127−293.
(51) Wong, I. Y.; Gardel, M. L.; Reichman, D. R.; Weeks, E. R.; Valentine, M. T.; Bausch, A. R.; Weitz, D. A. Anomalous diffusion probes microstructure dynamics of entangled F-actin networks. *Phys. Rev. Lett.* **2004**, *92*, 178101−1.
(52) Xu, Q.; Feng, L.; Sha, R.; Seeman, N. C.; Chaikin, P. M. Subdiffusion of a sticky particle on a surface. *Phys. Rev. Lett.* **2011**, *106*, 228102.
(53) Weigel, A. V.; Simon, B.; Tamkun, M. M.; Krapf, D. Ergodic and nonergodic processes coexist in the plasma membrane as observed by single-molecule tracking. *Proc. Natl. Acad. Sci. U. S. A.* **2011**, *108*, 6438−6443.
(54) Jeon, J.-H.; Barkai, E.; Metzler, R. Noisy continuous time random walks. *J. Chem. Phys.* **2013**, *139*, 121916.
(55) Mandelbrot, B. B. *The Fractal Geometry of Nature*; Freeman: New York, 1982.
(56) Kubo, R. The fluctuation-dissipation theorem. *Rep. Prog. Phys.* **1966**, *29*, 255−284.
(57) Hänggi, P. Correlation functions and masterequations of generalized (non-Markovian) Langevin equations. *Z. Phys. B: Condens. Matter Quanta* **1978**, *31*, 407−416.
(58) Hanggi, P.; Mojtabai, F. Thermally activated escape rate in presence of long-time memory. *Phys. Rev. A: At., Mol., Opt. Phys.* **1982**, *26*, 1168−1170.
(59) Lutz, E. Fractional Langevin equation. *Phys. Rev. E: Stat. Phys., Plasmas, Fluids, Relat. Interdiscip. Top.* **2001**, *64*, 051106.
(60) Goychuk, I. Viscoelastic Subdiffusion: Generalized Langevin Equation Approach. *Adv. Chem. Phys.* **2012**, 187−253.
(61) Kneller, G. R. Communication: A scaling approach to anomalous diffusion. *J. Chem. Phys.* **2014**, *141*, 041105.
(62) Kou, S. C. Stochastic modeling in nanoscale biophysics: Subdiffusion within proteins. *Ann. Appl. Stat.* **2008**, *2*, 501−535.
(63) Weber, S. C.; Spakowitz, A. J.; Theriot, J. A. Bacterial chromosomal loci move subdiffusively through a viscoelastic cytoplasm. *Phys. Rev. Lett.* **2010**, *104*, 238102.
(64) Jeon, J.-H.; Tejedor, V.; Burov, S.; Barkai, E.; Selhuber-Unkel, C.; Berg-Sørensen, K.; Oddershede, L.; Metzler, R. In Vivo Anomalous Diffusion and Weak Ergodicity Breaking of Lipid Granules. *Phys. Rev. Lett.* **2011**, *106*, 048103.
(65) Jeon, J.-H.; Leijnse, N.; Oddershede, L. B.; Metzler, R. Anomalous diffusion and power-law relaxation of the time averaged mean squared displacement in worm-like micellar solutions. *New J. Phys.* **2013**, *15*, 045011.
(66) Bronstein, I.; Israel, Y.; Kepten, E.; Mai, S.; Shav-Tal, Y.; Barkai, E.; Garini, Y. Transient Anomalous Diffusion of Telomeres in the Nucleus of Mammalian Cells. *Phys. Rev. Lett.* **2009**, *103*, 018102.
(67) Szymanski, J.; Weiss, M. Elucidating the origin of anomalous diffusion in crowded fluids. *Phys. Rev. Lett.* **2009**, *103*, 038102.
(68) Kneller, G. R.; Baczynski, K.; Pasenkiewicz-Gierula, M. Communication: Consistent picture of lateral subdiffusion in lipid bilayers: Molecular dynamics simulation and exact results. *J. Chem. Phys.* **2011**, *135*, 141105.

DOI: 10.1021/acs.chemrev.6b00638
Chem. Rev. 2017, 117, 4342−4375

(69) Jeon, J. H.; Monne, H. M. S.; Javanainen, M.; Metzler, R. Anomalous diffusion of phospholipids and cholesterols in a lipid bilayer and its origins. *Phys. Rev. Lett.* **2012**, *109*, 188103.
(70) Jeon, J.-H.; Javanainen, M.; Martinez-Seara, H.; Metzler, R.; Vattulainen, I. Protein crowding in lipid bilayers gives rise to non-Gaussian anomalous lateral diffusion of phospholipids and proteins. *Phys. Rev. X* **2016**, *6*, 021006.
(71) Javanainen, M.; Hammaren, H.; Monticelli, L.; Jeon, J.-H.; Miettinen, M. S.; Martinez-Seara, H.; Metzler, R.; Vattulainen, I. Anomalous and normal diffusion of proteins and lipids in crowded lipid membranes. *Faraday Discuss.* **2013**, *161*, 397−417.
(72) Lim, S. C.; Muniandy, S. V. Self-similar Gaussian processes for modeling anomalous diffusion. *Phys. Rev. E: Stat. Phys., Plasmas, Fluids, Relat. Interdiscip. Top.* **2002**, *66*, 021114.
(73) Jeon, J.-H.; Chechkin, A. V.; Metzler, R. Scaled Brownian motion: a paradoxical process with a time dependent diffusivity for the description of anomalous diffusion. *Phys. Chem. Chem. Phys.* **2014**, *16*, 15811−7.
(74) Metzler, R.; Jeon, J.-H.; Cherstvy, A. Non-Brownian diffusion in lipid membranes: Experiments and simulations. *Biochim. Biophys. Acta, Biomembr.* **2016**, *1858*, 2451−2467.
(75) Sokolov, I. M. Models of anomalous diffusion in crowded environments. *Soft Matter* **2012**, *8*, 9043.
(76) Deng, W.; Barkai, E. Ergodic properties of fractional Brownian-Langevin motion. *Phys. Rev. E* **2009**, *79*, 011112.
(77) Jeon, J.-H.; Metzler, R. Inequivalence of time and ensemble averages in ergodic systems: Exponential versus power-law relaxation in confinement. *Phys. Rev. E* **2012**, *85*, 021147.
(78) Kursawe, J.; Schulz, J.; Metzler, R. Transient ageing in fractional Brownian and Langevin equation motion. *Phys. Rev. E* **2013**, *88*, 062124.
(79) He, Y.; Burov, S.; Metzler, R.; Barkai, E. Random time-scale invariant diffusion and transport coefficients. *Phys. Rev. Lett.* **2008**, *101*, 058101.
(80) Tabei, S. M.; Burov, S.; Kim, H. Y.; Kuznetsov, A.; Huynh, T.; Jureller, J.; Philipson, L. H.; Dinner, a. R.; Scherer, N. F. Intracellular transport of insulin granules is a subordinated random walk. *Proc. Natl. Acad. Sci. U. S. A.* **2013**, *110*, 4911−4916.
(81) Manzo, C.; Torreno-Pina, J. a.; Massignan, P.; Lapeyre, G. J.; Lewenstein, M.; Parajo, M. F. G. Weak ergodicity breaking of receptor motion in living cells stemming from random diffusivity. *Phys. Rev. X* **2014**, *5*, 011021.
(82) Barkai, E. Aging in subdiffusion generated by a deterministic dynamical system. *Phys. Rev. Lett.* **2003**, *90*, 104101.
(83) Schulz, J. H. P.; Barkai, E.; Metzler, R. Aging effects and population splitting in single-particle trajectory averages. *Phys. Rev. Lett.* **2013**, *110*, 02602.
(84) Schulz, J. H. P.; Barkai, E.; Metzler, R. Aging renewal theory and application to random walks. *Phys. Rev. X* **2014**, *4*, 011028.
(85) Hu, X.; Hong, L.; Dean Smith, M.; Neusius, T.; Cheng, X.; Smith, J. C. The dynamics of single protein molecules is non-equilibrium and self-similar over thirteen decades in time. *Nat. Phys.* **2015**, *12*, 171−174.
(86) Tejedor, V.; Metzler, R. Anomalous diffusion in correlated continuous time random walks. *J. Phys. A: Math. Theor.* **2010**, *43*, 082002.
(87) Burov, S.; Jeon, J.-H.; Metzler, R.; Barkai, E. Single particle tracking in systems showing anomalous diffusion: the role of weak ergodicity breaking. *Phys. Chem. Chem. Phys.* **2011**, *13*, 1800.
(88) Jeon, J.-H.; Metzler, R. Analysis of short subdiffusive time series: scatter of the time-averaged mean-squared displacement. *J. Phys. A: Math. Theor.* **2010**, *43*, 252001.
(89) Sokolov, I. M.; Heinsalu, E.; Hänggi, P.; Goychuk, I. Universal fluctuations in subdiffusive transport. *Europhys. Lett.* **2009**, *86*, 30009.
(90) Meroz, Y.; Sokolov, I. M. A toolbox for determining subdiffusive mechanisms. *Phys. Rep.* **2015**, *573*, 1−29.
(91) Gross, S. P.; Vershinin, M.; Shubeita, G. T. Cargo transport: Two motors are sometimes better than one. *Curr. Biol.* **2007**, *17*, R478−R486.
(92) Mallik, R.; Gross, S. P. Intracellular transport: How do motors work together? *Curr. Biol.* **2009**, *19*, R416−R418.
(93) Barlan, K.; Rossow, M. J.; Gelfand, V. I. The journey of the organelle: Teamwork and regulation in intracellular transport. *Curr. Opin. Cell Biol.* **2013**, *25*, 483−488.
(94) Mallik, R.; Rai, A. K.; Barak, P.; Rai, A.; Kunwar, A. Teamwork in microtubule motors. *Trends Cell Biol.* **2013**, *23*, 575−582.
(95) Goychuk, I.; Kharchenko, V. O.; Metzler, R. Molecular motors pulling cargos in the viscoelastic cytosol: how power strokes beat subdiffusion. *Phys. Chem. Chem. Phys.* **2014**, *16*, 16524−16535.
(96) Despósito, M. A.; Pallavicini, C.; Levi, V.; Bruno, L. Active transport in complex media: Relationship between persistence and superdiffusion. *Phys. A* **2011**, *390*, 1026−1032.
(97) Röding, M.; Guo, M.; Weitz, D. A.; Rudemo, M.; Särkkä, A. Identifying directional persistence in intracellular particle motion using Hidden Markov Models. *Math. Biosci.* **2014**, *248*, 140−145.
(98) Robert, D.; Nguyen, T. H.; Gallet, F.; Wilhelm, C. In vivo determination of fluctuating forces during endosome trafficking using a combination of active and passive microrheology. *PLoS One* **2010**, *5*, e10046.
(99) Gal, N.; Weihs, D. Experimental evidence of strong anomalous diffusion in living cells. *Phys. Rev. E* **2010**, *81*, 020903.
(100) Chen, K.; Wang, B.; Granick, S. Memoryless self-reinforcing directionality in endosomal active transport within living cells. *Nat. Mater.* **2015**, *14*, 589−593.
(101) Shinkai, S.; Togashi, Y. Energetics of single active diffusion trajectories. *Europhys. Lett.* **2014**, *105*, 30002.
(102) Bruno, A.; Bruno, L.; Levi, V. Extracting the stepping dynamics of molecular motors in living cells from trajectories of single particles. *Cell Biochem. Biophys.* **2013**, *65*, 1−11.
(103) Brunstein, M.; Bruno, L.; Desposito, M.; Levi, V. Anomalous dynamics of melanosomes driven by myosin-V in Xenopus laevis melanophores. *Biophys. J.* **2009**, *97*, 1548−1557.
(104) Zhang, Y.; Fisher, M. E. Dynamics of the tug-of-war model for cellular transport. *Phys. Rev. E* **2010**, *82*, 1−14.
(105) Bouzat, S.; Levi, V.; Bruno, L. Transport properties of melanosomes along Microtubules interpreted by a tug-of-war model with loose mechanical coupling. *PLoS One* **2012**, *7*, e43599.
(106) Zhang, Y. Cargo transportation by two species of motor protein. *Phys. Rev. E* **2013**, *87*, 1−10.
(107) Martinez, J. E.; Vershinin, M. D.; Shubeita, G. T.; Gross, S. P. On the use of in vivo cargo velocity as a biophysical marker. *Biochem. Biophys. Res. Commun.* **2007**, *353*, 835−840.
(108) Petrov, D. Y.; Mallik, R.; Shubeita, G. T.; Vershinin, M.; Gross, S. P.; Yu, C. C. Studying molecular motor-based cargo transport: what is real and what is noise? *Biophys. J.* **2007**, *92*, 2953−2963.
(109) Gazzola, M.; Burckhardt, C. J.; Bayati, B.; Engelke, M.; Greber, U. F.; Koumoutsakos, P. A stochastic model for microtubule motors describes the in vivo cytoplasmic transport of human adenovirus. *PLoS Comput. Biol.* **2009**, *5*, No. e1000623.
(110) Keller, C.; Berger, F.; Liepelt, S.; Lipowsky, R. Network complexity and parametric simplicity for cargo transport by two molecular motors. *J. Stat. Phys.* **2013**, *150*, 205−234.
(111) Assmann, M.-A.; Lenz, P. Characterization of bidirectional molecular motor-assisted transport models. *Phys. Biol.* **2013**, *10*, 016003.
(112) Ciandrini, L.; Romano, M. C.; Parmeggiani, A. Stepping and crowding of molecular motors: statistical kinetics from an exclusion process perspective. *Biophys. J.* **2014**, *107*, 1176−84.
(113) Khan, M.; Mason, T. G. Local collective motion analysis for multi-probe dynamic imaging and microrheology. *J. Phys.: Condens. Matter* **2016**, *28*, 305201.
(114) Liu, Z.; Lavis, L. D.; Betzig, E. Imaging live-cell dynamics and structure at the single-molecule level. *Mol. Cell* **2015**, *58*, 644−659.
(115) Mortensen, K. I.; Churchman, L. S.; Spudich, J. a.; Flyvbjerg, H. Optimized localization analysis for single-molecule tracking and super-resolution microscopy. *Nat. Methods* **2010**, *7*, 377−381.

DOI: 10.1021/acs.chemrev.6b00638
Chem. Rev. 2017, 117, 4342−4375

(116) Schermelleh, L.; Heintzmann, R.; Leonhardt, H. A guide to super-resolution fluorescence microscopy. *J. Cell Biol.* **2010**, *190*, 165−175.
(117) Giepmans, B. N. G.; Adams, S. R.; Ellisman, M. H.; Tsien, R. Y. The fluorescent toolbox for assessing protein location and function. *Science* **2006**, *312*, 217−224.
(118) Otto, O.; Czerwinski, F.; Gornall, J. L.; Stober, G.; Oddershede, L. B.; Seidel, R.; Keyser, U. F. Real-time particle tracking at 10,000 fps using optical fiber illumination. *Opt. Express* **2010**, *18*, 22722−22733.
(119) Huhle, A.; Klaue, D.; Brutzer, H.; Daldrop, P.; Joo, S.; Otto, O.; Keyser, U. F.; Seidel, R. Camera-based three-dimensional real-time particle tracking at kHz rates and Ångström accuracy. *Nat. Commun.* **2015**, *6*, 5885.
(120) Mas, J.; Richardson, A. C.; Reihani, S. N. S.; Oddershede, L. B.; Berg-Sørensen, K. Quantitative determination of optical trapping strength and viscoelastic moduli inside living cells. *Phys. Biol.* **2013**, *10*, 046006.
(121) Tolic-Nørrelykke, I. M.; Munteanu, E. L.; Thon, G.; Oddershede, L.; Berg-Sørensen, K. Anomalous diffusion in living yeast cells. *Phys. Rev. Lett.* **2004**, *93*, 078102.
(122) Bausch, A. R.; Möller, W.; Sackmann, E. Measurement of local viscoelasticity and forces in living cells by magnetic tweezers. *Biophys. J.* **1999**, *76*, 573−579.
(123) Lang, M. J.; Fordyce, P. M.; Block, S. M. Combined optical trapping and single-molecule fluorescence. *J. Biol.* **2003**, *2*, 6.
(124) Lee, J. Y.; Wang, F.; Fazio, T.; Wind, S.; Greene, E. C. Measuring intermolecular rupture forces with a combined TIRF-optical trap microscope and DNA curtains. *Biochem. Biophys. Res. Commun.* **2012**, *426*, 565−570.
(125) Reihani, S. N. S.; Oddershede, L. B. Optimizing immersion media refractive index improves optical trapping by compensating spherical aberrations. *Opt. Lett.* **2007**, *32*, 1998−2000.
(126) Reihani, S. N. S.; Oddershede, L. B. Confocal microscopy of thick specimens. *J. Biomed. Opt.* **2009**, *14*, 030513.
(127) Richardson, A. C.; Reihani, N.; Oddershede, L. B. Combining confocal microscopy with precise force-scope optical tweezers. *Proc. SPIE* **2006**, 632628.
(128) Vettenburg, T.; Dalgarno, H. I. C.; Nylk, J.; Coll-Lladó, C.; Ferrier, D. E. K.; Cižmár, T.; Gunn-Moore, F. J.; Dholakia, K. Light-sheet microscopy using an Airy beam. *Nat. Methods* **2014**, *11*, 541−4.
(129) Ahrens, M. B.; Orger, M. B.; Robson, D. N.; Li, J. M.; Keller, P. J. Whole-brain functional imaging at cellular resolution using light-sheet microscopy. *Nat. Methods* **2013**, *10*, 413−420.
(130) Yang, Z.; Piksarv, P.; Ferrier, D. E.; Gunn-Moore, F. J.; Dholakia, K. Macro-optical trapping for sample confinement in light sheet microscopy. *Biomed. Opt. Express* **2015**, *6*, 2778−2785.
(131) Mueller, V.; Ringemann, C.; Honigmann, A.; Schwarzmann, G.; Medda, R.; Leutenegger, M.; Polyakova, S.; Belov, V. N.; Hell, S. W.; Eggeling, C. STED nanoscopy reveals molecular details of cholesterol- and cytoskeleton-modulated lipid interactions in living cells. *Biophys. J.* **2011**, *101*, 1651−1660.
(132) Heller, I.; Sitters, G.; Broekmans, O. D.; Farge, G.; Menges, C.; Wende, W.; Hell, S. W.; Peterman, E. J. G.; Wuite, G. J. L. STED nanoscopy combined with optical tweezers reveals protein dynamics on densely covered DNA. *Nat. Methods* **2013**, *10*, 910−6.
(133) Cost, A.-L.; Ringer, P.; Chrostek-Grashoff, A.; Grashoff, C. How to measure molecular forces in cells: A guide to evaluating genetically-encoded FRET-based tension sensors. *Cell. Mol. Bioeng.* **2015**, *8*, 96−105.
(134) Grashoff, C.; Hoffman, B. D.; Brenner, M. D.; Zhou, R.; Parsons, M.; Yang, M. T.; McLean, M. A.; Sligar, S. G.; Chen, C. S.; Ha, T.; et al. Measuring mechanical tension across vinculin reveals regulation of focal adhesion dynamics. *Nature* **2010**, *466*, 263−6.
(135) Iwai, S.; Uyeda, T. Q. P. Visualizing myosin-actin interaction with a genetically-encoded fluorescent strain sensor. *Proc. Natl. Acad. Sci. U. S. A.* **2008**, *105*, 16882−16887.
(136) Stabley, D. R.; Jurchenko, C.; Marshall, S. S.; Salaita, K. S. Visualizing mechanical tension across membrane receptors with a fluorescent sensor. *Nat. Methods* **2011**, *9*, 64−67.
(137) Yusko, E. C.; Asbury, C. L. Force is a signal that cells cannot ignore. *Mol. Biol. Cell* **2014**, *25*, 3717−25.
(138) Crick, F.; Hughes, A. The physical properties of cytoplasm. *Exp. Cell Res.* **1950**, *1*, 37−80.
(139) Alenghat, F. J.; Fabry, B.; Tsai, K. Y.; Goldmann, W. H.; Ingber, D. E. Analysis of cell mechanics in single vinculin-deficient cells using a magnetic tweezer. *Biochem. Biophys. Res. Commun.* **2000**, *277*, 93−9.
(140) Robert, D.; Aubertin, K.; Bacri, J. C.; Wilhelm, C. Magnetic nanomanipulations inside living cells compared with passive tracking of nanoprobes to get consensus for intracellular mechanics. *Phys. Rev. E* **2012**, *85*, 1−9.
(141) Neuman, K. C.; Chadd, E. H.; Liou, G. F.; Bergman, K.; Block, S. M. Characterization of photodamage to Escherichia coli in optical traps. *Biophys. J.* **1999**, *77*, 2856−63.
(142) Rasmussen, M. B.; Oddershede, L. B.; Siegumfeldt, H. Optical tweezers cause physiological damage to Escherichia coli and Listeria bacteria. *Appl. Environ. Microbiol.* **2008**, *74*, 2441−2446.
(143) Iversen, T.-G.; Skotland, T.; Sandvig, K. Endocytosis and intracellular transport of nanoparticles: Present knowledge and need for future studies. *Nano Today* **2011**, *6*, 176−185.
(144) Delehanty, J. B.; Mattoussi, H.; Medintz, I. L. Delivering quantum dots into cells: Strategies, progress and remaining issues. *Anal. Bioanal. Chem.* **2009**, *393*, 1091−1105.
(145) Huschka, R.; Neumann, O.; Barhoumi, A.; Halas, N. J. Visualizing light-triggered release of molecules inside living cells. *Nano Lett.* **2010**, *10*, 4117−4122.
(146) Chithrani, B. D.; Ghazani, A. A.; Chan, W. C. W. Determining the size and shape dependence of gold nanoparticle uptake into mammalian cells. *Nano Lett.* **2006**, *6*, 662−668.
(147) Bendix, P. M.; Reihani, S. N.; Oddershede, L. B. Direct measurements of heating by electromagnetically trapped gold nanoparticles on supported lipid bilayers. *ACS Nano* **2010**, *4*, 2256−2262.
(148) Neuman, K. K. C.; Nagy, A. Single-molecule force spectroscopy: optical tweezers, magnetic tweezers and atomic force microscopy. *Nat. Methods* **2008**, *5*, 491−505.
(149) Blanco, E.; Shen, H.; Ferrari, M. Principles of nanoparticle design for overcoming biological barriers to drug delivery. *Nat. Biotechnol.* **2015**, *33*, 941−951.
(150) Zhang, Y.; Yu, L. C. Single-cell microinjection technology in cell biology. *BioEssays* **2008**, *30*, 606−610.
(151) Rørvig-Lund, A.; Bahadori, A.; Semsey, S.; Bendix, P. M.; Oddershede, L. B. Vesicle fusion triggered by optically heated gold nanoparticles. *Nano Lett.* **2015**, *15*, 4183−4188.
(152) Marchington, R. F.; Arita, Y.; Tsampoula, X.; Gunn-Moore, F. J.; Dholakia, K. Optical injection of mammalian cells using a microfluidic platform. *Biomed. Opt. Express* **2010**, *1*, 527−536.
(153) Guillaume-Gentil, O.; Potthoff, E.; Ossola, D.; Franz, C. M.; Zambelli, T.; Vorholt, J. A. Force-controlled manipulation of single cells: From AFM to FluidFM. *Trends Biotechnol.* **2014**, *32*, 381−388.
(154) Alcaraz, J.; Buscemi, L.; Grabulosa, M.; Trepat, X.; Fabry, B.; Farré, R.; Navajas, D. Microrheology of human lung epithelial cells measured by atomic force microscopy. *Biophys. J.* **2003**, *84*, 2071−9.
(155) Cai, P.; Mizutani, Y.; Tsuchiya, M.; Maloney, J. M.; Fabry, B.; Van Vliet, K. J.; Okajima, T. Quantifying cell-to-cell variation in power-law rheology. *Biophys. J.* **2013**, *105*, 1093−1102.
(156) Hecht, F. M.; Rheinlaender, J.; Schierbaum, N.; Goldmann, W. H.; Fabry, B.; Schäffer, T. E. Imaging viscoelastic properties of live cells by AFM: power-law rheology on the nanoscale. *Soft Matter* **2015**, *11*, 4584−4591.
(157) Dufrêne, Y. F. Atomic force microscopy in microbiology: New structural and functional insights into the microbial cell surface. *mBio* **2014**, *5*, No. e01363.

DOI: 10.1021/acs.chemrev.6b00638
Chem. Rev. 2017, 117, 4342−4375

(158) Lee, H.; Scherer, N. F.; Messersmith, P. B. Single-molecule mechanics of mussel adhesion. *Proc. Natl. Acad. Sci. U. S. A.* **2006**, *103*, 12999−13003.
(159) Evans, E.; Ritchie, K.; Merkel, R. Sensitive force technique to probe molecular adhesion and structural linkages at biological interfaces. *Biophys. J.* **1995**, *68*, 2580−7.
(160) Chen, Y.; Liu, B.; Ju, L.; Hong, J.; Ji, Q.; Chen, W.; Zhu, C. Fluorescence biomembrane force probe: Concurrent quantitation of receptor-ligand kinetics and binding-induced intracellular signaling on a single cell. *J. Visualized Exp.* **2015**, *102*, 27−29.
(161) Merkel, R.; Nassoy, P.; Leung, A.; Ritchie, K.; Evans, E. Energy landscapes of receptor-ligand bonds explored with dynamic force spectroscopy. *Nature* **1999**, *397*, 50−53.
(162) Valle, F.; Zuccheri, G.; Bergia, A.; Ayres, L.; Rowan, A. E.; Nolte, R. J. M.; Samorì, B. A polymeric molecular "Handle" for multiple AFM-based single-molecule force measurements. *Angew. Chem., Int. Ed.* **2008**, *47*, 2431−2434.
(163) Smith, S. B.; Cui, Y.; Bustamante, C. Overstretching B-DNA: The elastic response of individual double-stranded and single- stranded DNA molecules. *Science* **1996**, *271*, 795−799.
(164) Rohrbach, A. Stiffness of optical traps: Quantitative agreement between experiment and electromagnetic theory. *Phys. Rev. Lett.* **2005**, *95*, 1−4.
(165) Peterman, E. J. G.; Gittes, F.; Schmidt, C. F. Laser-induced heating in optical traps. *Biophys. J.* **2003**, *84*, 1308−16.
(166) Svoboda, K.; Block, S. M. Optical trapping of metallic Rayleigh particles. *Opt. Lett.* **1994**, *19*, 930.
(167) Hansen, P. M.; Bhatia, V. K.; Harrit, N.; Oddershede, L. Expanding the optical trapping range of gold nanoparticles. *Nano Lett.* **2005**, *5*, 1937−1942.
(168) Selhuber-Unkel, C.; Zins, I.; Schubert, O.; Sönnichsen, C.; Oddershede, L. B. Quantitative optical trapping of single gold nanorods. *Nano Lett.* **2008**, *8*, 2998−3003.
(169) Jørgensen, J. T.; Nørregaard, K.; Tian, P.; Bendix, P. M.; Kjaer, A.; Oddershede, L. B. Single particle and PET-based platform for identifying optimal plasmonic nano-heaters for photothermal cancer therapy. *Sci. Rep.* **2016**, *6*, 30076.
(170) Johnston, H. J.; Hutchison, G. R.; Christensen, F. M.; Peters, S.; Hankin, S.; Stone, V. A review of the in vivo and in vitro toxicity of silver and gold particulates: Particle attributes and biological mechanisms responsible for the observed toxicity. *Crit. Rev. Toxicol.* **2010**, *40*, 328−346.
(171) Jauffred, L.; Richardson, A. C.; Oddershede, L. B. Three-dimensional optical control of individual quantum dots. *Nano Lett.* **2008**, *8*, 3376−3380.
(172) Jauffred, L.; Oddershede, L. B. Two-photon quantum dot excitation during optical trapping. *Nano Lett.* **2010**, *10*, 1927−1930.
(173) Jensen, R. A.; Huang, I.-C.; Chen, O.; Choy, J. T.; Bischof, T. S.; Lončar, M.; Bawendi, M. G. Optical trapping and two-photon excitation of colloidal quantum dots using Bowtie apertures. *ACS Photonics* **2016**, *3*, 423−427.
(174) Shubeita, G. T.; Tran, S. L.; Xu, J.; Vershinin, M.; Cermelli, S.; Cotton, S. L.; Welte, M. A.; Gross, S. P. Consequences of motor copy number on the intracellular transport of Kinesin-1-driven lipid droplets. *Cell* **2008**, *135*, 1098−1107.
(175) Sacconi, L.; Tolić-Nørrelykke, I. M.; Stringari, C.; Antolini, R.; Pavone, F. S. Optical micromanipulations inside yeast cells. *Appl. Opt.* **2005**, *44*, 2001−7.
(176) Sims, P. A.; Xie, X. S. Probing dynein and kinesin stepping with mechanical manipulation in a living cell. *ChemPhysChem* **2009**, *10*, 1511−1516.
(177) Leidel, C.; Longoria, R. A.; Gutierrez, F. M.; Shubeita, G. T. Measuring molecular motor forces in VIVO: Implications for tug-of-war models of bidirectional transport. *Biophys. J.* **2012**, *103*, 492−500.
(178) Rai, A. K.; Rai, A.; Ramaiya, A. J.; Jha, R.; Mallik, R. Molecular adaptations allow dynein to generate large collective forces inside cells. *Cell* **2013**, *152*, 172−182.
(179) Gittes, F.; Schmidt, C. F. *Methods in Cell Biology*; Elsevier: Waltham, MA, 1997; Vol. *55*, Chapter 8, pp 129−156.
(180) Berg-Sorensen, K.; Flyvbjerg, H. Power spectrum analysis for optical tweezers. *Rev. Sci. Instrum.* **2004**, *75*, 594−612.
(181) Tolic-Norrelykke, S. F.; Schaeffer, E.; Howard, J.; Pavone, F. S.; Juelicher, F.; Flyvbjerg, H. Calibration of optical tweezers with positional detection in the back focal plane. *Rev. Sci. Instrum.* **2006**, *77*, 103101.
(182) Andersson, M.; Czerwinski, F.; Oddershede, L. B. Optimizing active and passive calibration of optical tweezers. *J. Opt.* **2011**, *13*, 044020.
(183) Fischer, M.; Berg-Sørensen, K. Calibration of trapping force and response function of optical tweezers in viscoelastic media. *J. Opt. A: Pure Appl. Opt.* **2007**, *9*, S239−S250.
(184) Fischer, M.; Richardson, A. C.; Reihani, S. N. S.; Oddershede, L. B.; Berg-Sørensen, K. Active-passive calibration of optical tweezers in viscoelastic media. *Rev. Sci. Instrum.* **2010**, *81*, No. 015103.
(185) Hendricks, A. G.; Holzbaur, E. L. F.; Goldman, Y. E. Force measurements on cargoes in living cells reveal collective dynamics of microtubule motors. *Proc. Natl. Acad. Sci. U. S. A.* **2012**, *109*, 18447−52.
(186) Richardson, A. C.; Reihani, S. N. S.; Oddershede, L. B. Non-harmonic potential of a single beam optical trap Abstract. *Opt. Express* **2008**, *16*, 15709−15717.
(187) Ritter, C.; Mas, J.; Oddershede, L. B.; Berg-Sørensen, K. In *Optical Tweezers*; Gennerich, A., Ed.; Springer: Berlin, 2016; Chapter 20.
(188) Strick, T. R.; Allemand, J. F.; Bensimon, D.; Bensimon, A.; Croquette, V. The elasticity of a single supercoiled DNA molecule. *Science* **1996**, *271*, 1835−1837.
(189) Strick, T. R.; Allemand, J. F.; Bensimon, D.; Croquette, V. Behavior of supercoiled DNA. *Biophys. J.* **1998**, *74*, 2016−28.
(190) Haber, C.; Wirtz, D. Magnetic tweezers for DNA micro-manipulation. *Rev. Sci. Instrum.* **2000**, *71*, 4561.
(191) Gosse, C.; Croquette, V. Magnetic tweezers: micromanipulation and force measurement at the molecular level. *Biophys. J.* **2002**, *82*, 3314−3329.
(192) Bruus, H.; Dual, J.; Hawkes, J.; Hill, M.; Laurell, T.; Nilsson, J.; Radel, S.; Sadhal, S.; Wiklund, M. Forthcoming Lab on a Chip tutorial series on acoustofluidics: acoustofluidics-exploiting ultrasonic standing wave forces and acoustic streaming in microfluidic systems for cell and particle manipulation. *Lab Chip* **2011**, *11*, 3579−80.
(193) Laurell, T.; Lenshof, A. *Microscale Acoustofluidics*; Royal Society of Chemistry: London, 2014; pp P001−574.
(194) Sitters, G.; Kamsma, D.; Thalhammer, G.; Ritsch-Marte, M.; Peterman, E. J. G.; Wuite, G. J. L. Acoustic force spectroscopy. *Nat. Methods* **2014**, *12*, 47−50.
(195) Bruus, H. Acoustofluidics 7: The acoustic radiation force on small particles. *Lab Chip* **2012**, *12*, 1014−21.
(196) Antfolk, M.; Muller, P. B.; Augustsson, P.; Bruus, H.; Laurell, T. Focusing of sub-micrometer particles and bacteria enabled by two-dimensional acoustophoresis. *Lab Chip* **2014**, *14*, 2791−9.
(197) Guck, J.; Ananthakrishnan, R.; Mahmood, H.; Moon, T. J.; Cunningham, C. C.; Käs, J. The optical stretcher: a novel laser tool to micromanipulate cells. *Biophys. J.* **2001**, *81*, 767−784.
(198) Guck, J.; Schinkinger, S.; Lincoln, B.; Wottawah, F.; Ebert, S.; Romeyke, M.; Lenz, D.; Erickson, H. M.; Ananthakrishnan, R.; Mitchell, D.; et al. Optical deformability as an inherent cell marker for testing malignant transformation and metastatic competence. *Biophys. J.* **2005**, *88*, 3689−3698.
(199) Yang, T.; Bragheri, F.; Minzioni, P. A comprehensive review of optical stretcher for cell mechanical characterization at single-cell level. *Micromachines* **2016**, *7*, 90.
(200) Steinwachs, J.; Metzner, C.; Skodzek, K.; Lang, N.; Thievessen, I.; Mark, C.; Münster, S.; Aifantis, K. E.; Fabry, B. Three-dimensional force microscopy of cells in biopolymer networks. *Nat. Methods* **2015**, *13*, 171−176.
(201) Caspi, a.; Granek, R.; Elbaum, M. Enhanced diffusion in active intracellular transport. *Phys. Rev. Lett.* **2000**, *85*, 5655−5658.

DOI: 10.1021/acs.chemrev.6b00638
Chem. Rev. 2017, 117, 4342−4375

(202) Weiss, M.; Elsner, M.; Kartberg, F.; Nilsson, T. Anomalous subdiffusion is a measure for cytoplasmic crowding in living cells. *Biophys. J.* **2004**, *87*, 3518−24.
(203) Guigas, G.; Kalla, C.; Weiss, M. Probing the nanoscale viscoelasticity of intracellular fluids in living cells. *Biophys. J.* **2007**, *93*, 316−23.
(204) Seisenberger, G.; Ried, M. U.; Endress, T.; Büning, H.; Hallek, M.; Bräuchle, C. Real-time single-molecule imaging of the infection pathway of an adeno-associated virus. *Science* **2001**, *294*, 1929−1932.
(205) Welte, M. A.; Gross, S. P.; Postner, M.; Block, S. M.; Wieschaus, E. F. Developmental regulation of vesicle transport in Drosophila embryos: Forces and kinetics. *Cell* **1998**, *92*, 547−557.
(206) Gross, S. P.; Welte, M. A.; Block, S. M.; Wieschaus, E. F. Dynein-mediated cargo transport in vivo: A switch controls travel distance. *J. Cell Biol.* **2000**, *148*, 945−955.
(207) Selhuber-Unkel, C.; Yde, P.; Berg-Sørensen, K.; Oddershede, L. B. Variety in intracellular diffusion during the cell cycle. *Phys. Biol.* **2009**, *6*, 025015.
(208) Reverey, J. F.; Jeon, J.-H.; Bao, H.; Leippe, M.; Metzler, R.; Selhuber-Unkel, C. Superdiffusion dominates intracellular particle motion in the supercrowded cytoplasm of pathogenic Acanthamoeba castellanii. *Sci. Rep.* **2015**, *5*, 11690.
(209) Golding, I.; Cox, E. C. Physical nature of bacterial cytoplasm. *Phys. Rev. Lett.* **2006**, *96*, 098102.
(210) Vercammen, J.; Martens, G.; Engelborghs, Y. *Fluorescence of Supermolecules, Polymers, and Nanosystems*; Springer Series on Fluorescence, 2007; p 323.
(211) Banks, D. S.; Fradin, C. Anomalous diffusion of proteins due to molecular crowding. *Biophys. J.* **2005**, *89*, 2960−2971.
(212) Pan, W.; Filobelo, L.; Pham, N. D. Q.; Galkin, O.; Uzunova, V. V.; Vekilov, P. G. Viscoelasticity in homogeneous protein solutions. *Phys. Rev. Lett.* **2009**, *102*, 058101.
(213) Norregaard, K.; Jauffred, L.; Berg-Sørensen, K.; Oddershede, L. B. Optical manipulation of single molecules in the living cell. *Phys. Chem. Chem. Phys.* **2014**, *16*, 12614−24.
(214) Blehm, B. H.; Selvin, P. R. Single-molecule fluorescence and in vivo optical traps: How multiple dyneins and kinesins interact. *Chem. Rev.* **2014**, *114*, 3335−3352.
(215) Blehm, B. H.; Schroer, T. A.; Trybus, K. M.; Chemla, Y. R.; Selvin, P. R. Correction for Blehm et al., In vivo optical trapping indicates kinesin's stall force is reduced by dynein during intracellular transport. *Proc. Natl. Acad. Sci. U. S. A.* **2013**, *110*, 9613−9613.
(216) Kural, C. Kinesin and dynein move a peroxisome in vivo: A tug-of-war or coordinated movement? *Science* **2005**, *308*, 1469−1472.
(217) Ally, S.; Larson, A. G.; Barlan, K.; Rice, S. E.; Gelfand, V. I. Opposite-polarity motors activate one another to trigger cargo transport in live cells. *J. Cell Biol.* **2009**, *187*, 1071−1082.
(218) Laib, J. A.; Marin, J. A.; Bloodgood, R. A.; Guilford, W. H. The reciprocal coordination and mechanics of molecular motors in living cells. *Proc. Natl. Acad. Sci. U. S. A.* **2009**, *106*, 3190−5.
(219) Schuster, M.; Kilaru, S.; Fink, G.; Collemare, J.; Roger, Y.; Steinberg, G. Kinesin-3 and dynein cooperate in long-range retrograde endosome motility along a nonuniform microtubule array. *Mol. Biol. Cell* **2011**, *22*, 3645−3657.
(220) Prevo, B.; Mangeol, P.; Oswald, F.; Scholey, J. M.; Peterman, E. J. G. Functional differentiation of cooperating kinesin-2 motors orchestrates cargo import and transport in C. elegans cilia. *Nat. Cell Biol.* **2015**, *17*, 1536−45.
(221) Morelli, M. J.; Allen, R. J.; Rein Ten Wolde, P. Effects of macromolecular crowding on genetic networks. *Biophys. J.* **2011**, *101*, 2882−2891.
(222) Pathak, D.; Sepp, K. J.; Hollenbeck, P. J. Evidence that myosin activity opposes microtubule-based axonal transport of mitochondria. *J. Neurosci.* **2010**, *30*, 8984−8992.
(223) Schaaf, M. J. M.; Koopmans, W. J. A.; Meckel, T.; Van Noort, J.; Snaar-Jagalska, B. E.; Schmidt, T. S.; Spaink, H. P. Single-molecule microscopy reveals membrane microdomain organization of cells in a living vertebrate. *Biophys. J.* **2009**, *97*, 1206−1214.
(224) Stachura, S.; Kneller, G. R. Anomalous lateral diffusion in lipid bilayers observed by molecular dynamics simulations with atomistic and coarse-grained force fields. *Mol. Simul.* **2014**, *40*, 245−250.
(225) Akimoto, T.; Yamamoto, E.; Yasuoka, K.; Hirano, Y.; Yasui, M. Non-Gaussian fluctuations resulting from power-law trapping in a lipid bilayer. *Phys. Rev. Lett.* **2011**, *107*, 178103.
(226) Munguira, I.; Casuso, I.; Takahashi, H.; Rico, F.; Miyagi, A.; Chami, M.; Scheuring, S. Glasslike membrane protein diffusion in a crowded membrane. *ACS Nano* **2016**, *10*, 2584−2590.
(227) Edidin, M.; Kuo, S. C.; Sheetz, M. P. Lateral movements of membrane glycoproteins restricted by dynamic cytoplasmic barriers. *Science* **1991**, *254*, 1379−82.
(228) Sako, Y.; Kusumi, A. Barriers for lateral diffusion of transferrin receptor in the plasma membrane as characterized by receptor dragging by laser tweezers: Fence versus tether. *J. Cell Biol.* **1995**, *129*, 1559−1574.
(229) Oddershede, L.; Dreyer, J. K.; Grego, S.; Brown, S.; Berg-Sørensen, K. The motion of a single molecule, the lambda-receptor, in the bacterial outer membrane. *Biophys. J.* **2002**, *83*, 3152−3161.
(230) Winther, T.; Xu, L.; Berg-Sørensen, K.; Brown, S.; Oddershede, L. B. Effect of energy metabolism on protein motility in the bacterial outer membrane. *Biophys. J.* **2009**, *97*, 1305−1312.
(231) Winther, T.; Oddershede, L. B. Effect of antibiotics and antimicrobial peptides on single protein motility. *Curr. Pharm. Biotechnol.* **2009**, *10*, 486−493.
(232) Li, Q.; Zhang, T.; Pan, Y.; Ciacchi, L. C.; Xu, B.; Wei, G. AFM-based force spectroscopy for bioimaging and biosensing. *RSC Adv.* **2016**, *6*, 12893−12912.
(233) Li, M.; Xiao, X.; Liu, L.; Xi, N.; Wang, Y.; Dong, Z.; Zhang, W. Atomic force microscopy study of the antigen-antibody binding force on patient cancer cells based on ROR1 fluorescence recognition. *J. Mol. Recognit.* **2013**, *26*, 432−438.
(234) Lu, Y.-B.; Franze, K.; Seifert, G.; Steinhäuser, C.; Kirchhoff, F.; Wolburg, H.; Guck, J.; Janmey, P.; Wei, E.-Q.; Käs, J.; et al. Viscoelastic properties of individual glial cells and neurons in the CNS. *Proc. Natl. Acad. Sci. U. S. A.* **2006**, *103*, 17759−64.
(235) Koser, D. E.; Thompson, A. J.; Foster, S. K.; Dwivedy, A.; Pillai, E. K.; Sheridan, G. K.; Svoboda, H.; Viana, M.; Costa, L. d. F.; Guck, J.; et al. Mechanosensing is critical for axon growth in the developing brain. *Nat. Neurosci.* **2016**, *19*, 1592−1598.
(236) Lebeaupin, T.; Sellou, H.; Timinszky, G.; Huet, S. Chromatin dynamics at DNA breaks: what, how and why? *AIMS Biophysics* **2015**, *2*, 458−475.
(237) Burnecki, K.; Kepten, E.; Janczura, J.; Bronshtein, I.; Garini, Y.; Weron, A. Universal algorithm for identification of fractional Brownian motion. A case of telomere subdiffusion. *Biophys. J.* **2012**, *103*, 1839−1847.
(238) Begg, D. A. Micromanipulation studies of chromosome movement. II. Birefringent chromosomal fibers and the mechanical attachment of chromosomes to the spindle. *J. Cell Biol.* **1979**, *82*, 542−554.
(239) Bennink, M. L.; Leuba, S. H.; Leno, G. H.; Zlatanova, J.; de Grooth, B. G.; Greve, J. Unfolding individual nucleosomes by stretching single chromatin fibers with optical tweezers. *Nat. Struct. Biol.* **2001**, *8*, 606−610.
(240) Brower-Toland, B. D.; Smith, C. L.; Yeh, R. C.; Lis, J. T.; Peterson, C. L.; Wang, M. D. Mechanical disruption of individual nucleosomes reveals a reversible multistage release of DNA. *Proc. Natl. Acad. Sci. U. S. A.* **2002**, *99*, 1960−5.
(241) Chien, F.-T.; van Noort, J. 10 years of tension on chromatin: Results from single molecule force spectroscopy. *Curr. Pharm. Biotechnol.* **2009**, *10*, 474−85.
(242) Poirier, M. G.; Eroglu, S.; Marko, J. F. The bending rigidity of mitotic chromosomes. *Mol. Biol. Cell* **2002**, *13*, 2170−2179.
(243) Block, S. M.; Blair, D. F.; Berg, H. C. Compliance of bacterial flagella measured with optical tweezers. *Nature* **1989**, *338*, 514−518.
(244) Min, T. L.; Mears, P. J.; Chubiz, L. M.; Rao, C. V.; Golding, I.; Chemla, Y. R. High-resolution, long-term characterization of bacterial motility using optical tweezers. *Nat. Methods* **2009**, *6*, 831−835.

DOI: 10.1021/acs.chemrev.6b00638
Chem. Rev. 2017, 117, 4342−4375

(245) Altindal, T.; Chattopadhyay, S.; Wu, X.-L. Bacterial chemotaxis in an optical trap. *PLoS One* **2011**, *6*, e18231.
(246) Johansen, P. L.; Fenaroli, F.; Evensen, L.; Griffiths, G.; Koster, G. Optical micromanipulation of nanoparticles and cells inside living zebrafish. *Nat. Commun.* **2016**, *7*, No. 10974.

DOI: 10.1021/acs.chemrev.6b00638
Chem. Rev. 2017, 117, 4342−4375